Energetic Swarm Control with Application to Multiple Vehicle Systems

Sivaram Wijenddra

A Thesis

in

The Department

of

Mechanical and Industrial Engineering

Presented in Partial Fulfillment of the Requirements

for the Degree of Master of Applied Science (Mechanical Engineering) at

Concordia University

Montreal, Quebec, Canada

June 2010

Your file Votre référence
ISBN: 978-0-494-71034-0
Our file Notre référence
ISBN: 978-0-494-71034-0

This Page will be replaced by the signature page for master's thesis from the graduate school

ABSTRACT

Energetic Swarm Control with Application to Multiple Vehicle Systems

Sivaram Wijenddra

Control and coordination of multiple vehicle systems has been a very active area of research in recent years. Recent advancements in computation, communication, and mechatronics have allowed the development of large groups of vehicles, often referred to as swarms, in order to accomplish complex missions over large areas with redundant fault tolerant capabilities. Existing swarm control work has addressed swarm aggregation, foraging swarms, swarm formation, and swarms that track and enclose targets. Energetic swarm control is another significant recent contribution to the swarm control literature. It allows the control of the internal kinetic energy and potential kinetic energy of the swarm system in order to achieve tasks such as sweeping an area, patrolling, and area coverage. This thesis involves the application of energetic swarm control to wheeled mobile robots. A lower level control layer for wheeled mobile robots, based on feedback linearization, is developed and combined with a higher level particle based energetic swarm controller. Furthermore, input saturation constraints are addressed using a suitable control allocation approach. An experimentally verified model of a wheeled mobile robot is developed and used to demonstrate the capabilities of the new energetic swarm control approach for wheeled mobile robots.

Acknowledgements

I would like to thank Dr. Brandon Gordon, my supervisor, for his valuable guidance and encouragement through out the research. I am grateful to him in learning control systems engineering, gaining many programming skills along with the practical knowledge that few had the privilege to get all in one academic place.

I would like to thank Reza Pedrami wholeheartedly for his help towards understanding his PhD work and getting enough background in energetic swarm to do research thereafter. He is so much eager to share his knowledge and to help others as much as possible whenever needed.

I would like to thank my friends Yan Zhao, Hojjat Izadi, Ali Azimi, Fei Yang, Hongan Wang, Tong Li, Farid Sharifi and Mostafa Mirzaii with whom I shared my joy and sorrow, pleasure and pain over the last three years and built a friendly atmosphere in the office.

Also, my special thanks go to Sabesan Selvadurai and Balasubramanian Esakki for their continuous help, support and encouragement to finish the thesis.

Further, I can not explain in words the support and help provided my parents, brother and sister. I will be always in debt for their never ending love and encouragement to finish the thesis and without their help this thesis wouldn't have been finished at all. Finally, I thank all those who have helped me to finish the thesis. God bless all.

Dedication

To my family, Tony Sivasothy and those who have helped me

Table of Contents

List of Figures

List of Tables

Nomenclature

WMR	Wheeled Mobile Robot
MIMO	Multi input multi output system
RC	Radio Controlled
CIS	Control and Information System
IC	Initial Condition
M	The number of members in the swarm
t	Time concerned with the state
$\mathbf{x}_i$	Position vector of the i^{th} member in the swarm
$\mathbf{v}_i$	Velocity vector of the i^{th} member in the swarm
m_i	Mass of the i^{th} member in the swarm
$\mathbf{u}_i$	Control input for the i^{th} member in the swarm
h_i	Control coefficient for the i^{th} member in the swarm
b_i	Coefficient of viscous damping of the i^{th} member in the swarm
$\mathbf{d}_i(t)$	Bounded disturbance on the i^{th} member in the swarm
β_i	The upper bound of the disturbance on the i^{th} member in the swarm
$\mathbf{u}_i^{ext}$	External input on the i^{th} member in the swarm
$\mathbf{u}_i^{in}$	Internal input on the i^{th} member in the swarm
$\mathbf{g}(\cdot)$	Attraction repulsion function between each member in swarm
A	Positive constant related to the attraction term in $\mathbf{g}(\cdot)$

B	Positive constant related to the repulsion term in $\mathbf{g}(\cdot)$
$\bar{\mathbf{x}}$	Swarm centre
$\bar{\mathbf{v}}$	Swarm centre velocity
$\overline{\omega}_i$	Positive coefficient associated with swarm centre
T	Swarm temperature
E_k	Weighted kinetic energy
E_b	Weighted bulk kinetic energy
$\widetilde{\omega}_i$	Positive coefficient associated with swarm kinetic energies
J	Swarm potential
ρ	Swarm size
α_i	Connection weight in swarm potential function
$\widetilde{\mathbf{x}}$	Tracking error of swarm centre
$\bar{\mathbf{s}}$	Sliding surface for swarm centre tracking
$\bar{\mathbf{x}}_{des}$	Desired swarm centre
$\bar{\boldsymbol{\lambda}}$	Positive constant vector associated with sliding surface of swarm centre tracking
$\boldsymbol{\upsilon}_c$	Virtual controller for swarm centre tracking
$\mathbf{k}_c$	Vector of positive constant gain terms
η_c	Positive constant relating to sliding surface of swarm centre
$sat(\cdot)$	Saturation function
$\boldsymbol{\varepsilon}_c$	Thickness of the boundary layer for swarm centre tracking

T_{des}	Desired swarm temperature
s_T	Sliding surface for swarm temperature
ϖ	Coefficient associated with virtual controller of swarm temperature
σ, γ, ψ	Parameters associated with virtual controller of swarm temperature
ς	Parameters associated with virtual controller of swarm centre
υ_T	Virtual controller for swarm temperature
k_T	Positive constant associated with swarm temperature
η_T	Positive constant associated with swarm temperature
ε_T	Thickness of the boundary layer for swarm temperature tracking
s_J	Sliding surface for swarm potential
J_{des}	Desired swarm potential
λ_J	Positive constant associated with swarm potential
$\tilde{\xi}, \chi$	Parameters associated with virtual controller of swarm potential
υ_J	Virtual Controller for swarm potential
k_J	Positive constant associated with swarm potential
η_J	Positive constant associated with swarm potential
ε_J	Thickness of the boundary layer for swarm potential tracking
n_o	Number of outputs of energetic swarm
n_i	Number of inputs of energetic swarm
$\mathbf{I}$	Identity matrix
$\mathbf{B}_c$	Control effectiveness matrix associated with swarm centre tracking

$\mathbf{B}_T$	Control effectiveness vector associated with temperature tracking
$\mathbf{B}_J$	Control effectiveness vector associated with potential tracking
$\mathbf{B}$	Control effectiveness matrix associated with control allocation
$\mathbf{u}$	Actual input vector associated with control allocation
$\mathbf{v}$	Virtual input vector associated with control allocation
$\mathbf{W}$	Weighting matrix associated with control allocation
w_{ij}	Weighting coefficient of weighting matrix $\mathbf{W}$
$\mathbf{u}_i^{ext}{}_{\min}$	Lower saturation limit of input $\mathbf{u}_i^{ext}$
$\mathbf{u}_i^{ext}{}_{\max}$	Upper saturation limit of input $\mathbf{u}_i^{ext}$
$u_{sat\min}$	Minimum allowable value of $\mathbf{u}_i^{ext}{}_{\min}$ or $\mathbf{u}_i^{ext}{}_{\max}$
U_{sat}	Feasible operating region of the swarm
$u_{sat\max}$	Physical saturation limit of the swarm inputs
a, b, c	Positive parameters
δ	Distance determines attraction or repulsion in swarm aggregation
$B_{\bar{r}}(\cdot)$	Hyper ball
Ω_e	Set describes swarm aggregation at steady state
$\bar{t}$	Convergence time in swarm aggregation
V_i	Lyapunov function
c_1	Radius of private area of swarm member.
$\mathbf{M}_i$	Mass of inertia matrix

$\mathbf{f}_i(\cdot,\cdot)$	Matrix contains centripetal, Corriolis, gravitational effects
$\mathbf{f}_i^k(\cdot,\cdot)$	The known part of $\mathbf{f}_i(\cdot,\cdot)$
$\mathbf{f}_i^u(\cdot,\cdot)$	The unknown part of $\mathbf{f}_i(\cdot,\cdot)$
$\underline{M}_i$	Lower bound on $\mathbf{M}_i$
$\overline{M}_i$	Upper bound on $\mathbf{M}_i$
$\mathbf{s}_i$	Sliding manifold for swarm aggregation
sgn(·)	Signum function
$d_{i.j}$	Desired inter agent distance in swarm formation
$\overline{\sigma}$	Attraction or repellent profile
$\mathbf{a}_\sigma, b_\sigma, A_\sigma$	Coefficient of attraction/repulsion profiles
$\mathbf{c}_\sigma$	Coefficient of attraction/repulsion profiles
λ	A positive constant
$B_{r1}(\cdot)$	Hyper ball
$\mathbf{u}_{des}$	Required control input in control allocation
H	Hamiltonian
$\bar{J}$	Performance index
$\boldsymbol{\lambda}_0$	Lagrangian multiplier
$\mathbf{q}$	Generalized coordinates of WMR
$\mathbf{G(q)}$	Matrix of column vector contains the allowable motion of the WMR
$\mathbf{f}$	Smooth vector field
h	Smooth scalar function

$L_f h$	Lie derivative
$\mathbf{g}_0$	Smooth vector field
v	Heading velocity of the WMR
ω	Angular velocity of the WMR
$\mathbf{g}_1$	First column vector of **G(q)**
$\mathbf{g}_2$	Second column vector of **G(q)**
$\mathbf{z}$	Vector with n generalized coordinates
$\mathbf{x}$	State vector
$\mathbf{y}$	Output vector
$\mathbf{h}(\cdot)$	Smooth vector field
$\tilde{\mathbf{g}}(\cdot)$	$n \times m$ Matrix with smooth column vector fields
$\mathbf{E(x)}$	Decoupling matrix
$\mathbf{y}_r$	Reference trajectory
$\mathbf{K}_i$	Positive constant matrix
D	Distance between centre of axle and tip of the robot
$\mathbf{w}$	Control input of WMR
ξ	State vector
$\tilde{\mathbf{z}}$	State transformation vector
$\mathbf{a}(\cdot), \mathbf{c}(\cdot)$	Vector fields
$\mathbf{b}(\cdot), \mathbf{d}(\cdot)$	Matrix contains column vector fields
$\boldsymbol{\eta}$	Output vector in dynamic feedback linearization
ω_R	Angular velocity of the right wheel of WMR

ω_L	Angular velocity of the left wheel of WMR
θ	Angle between the heading velocity of WMR and the fixed frame
l	Axle distance between the wheels
R_R	Radius of the right wheel of WMR
R_L	Radius of the left wheel of WMR
J_{wm}	Moment of inertia of the motor
$\dot{\omega}_{wm}$	Angular acceleration of the motor
K_{1wm}	Constant parameters associated with the motor
η_{wm}	Constant parameters associated with the motor
U_{wm}	Voltage applied to the motor via MultiQ
ω_{wm}	Angular velocity of the motor
μ_{wm}	Coulomb friction coefficient
K_{bwm}	Linear friction coefficient of the motor
$\mathbf{X}_{out}$	Output of the high level dynamics
k_{pi}	Positive constant
k_{di}	Positive constant
g_a	Magnitude of the attraction term
g_r	Magnitude of the repulsion term
a_1, a_2, a_3	Identified parameters of the RC servo motors
x, y	Coordinates of the body attached frame of the WMR

1. Introduction

In recent years many results have been published on co-ordination and cooperative control of multi agent systems. Earlier, researchers focused their attention on single mobile robot control for example, trajectory tracking of Wheel Mobile Robots (WMR) or analyzing the nonholonomic properties of WMRs. Coordination and control of the multi agent system have recently become possible due to the advancement of technology, computational power, less cost per unit. One important area, such as formation control, has evoked the interest of researchers in swarm applications [1]. Formation control helps to increase robustness and redundancy of the system, reduce the system cost and increase flexibility and efficiency [2]. Many applications need a formation control such as military missions, rescue in hazardous environments, sweeping an area, increase throughput of highway systems, and satellite clustering [2].

Inspired by the results of formation control, the control community has been working on importing biological principals to build the biologically inspired system very recently. Biological systems have successfully evolved and adapted to the highly complex and competitive nature tuned by evolutionary process over a million of years [3]. Their operational principles can be useful in complex engineering applications. It is found in nature that many living beings behave in groups such as flocks of birds, schools of fish and herds of animals [1].

Swarm like behavior gives many advantages to the group rather than individual behavior. For example, swarm behavior helps to find food easily and avoid predators, thus enabling the chance of survival [4]. Swarm members perform complex tasks that can not be achieved by a single member individually [5]. Further the swarm gets more

environmental information which can not be obtained by a single individual since it has limited sensing abilities [6]. Also, in military applications swarm members resist the outer aggression of an enemy more easily and improve their defiance ability [6].

Though the swarm behavior has advantages over an individual behavior, it has to deal with the computational burden since, the more the members the higher the numerical calculations. However, advanced powerful computers help to overcome this problem to a certain extent. Further, since there are many members, they should not collide with each other at any given time. Also, any of the members should not disperse from the swarm. Other than these issues, proper communication between members should be maintained. They have to update their states, which are position and velocity, to other members in order to maintain their cohesion. There will be time delays in transferring these data over the communication line.

1.1. Literature Review

This section presents the literature review on swarm control. Firstly, the swarm control on aggregation, formation, foraging, and target tracking along with various other applications will be discussed. Finally research done so far on energetic swarm control will be discussed.

1.1.1. Swarm Control

Swarming is found among single bacteria to large mammals in nature. Generally, there is no group leader and each individual behaves according to the interaction among themselves and certain environmental conditions. Their operation principle can be applied to coordinating unmanned air vehicles, formation control of mobile vehicles,

sweeping an area, control of unmanned under water sea vehicles, formation control of satellites, encircling a moving target or capturing it and military applications [4] ,[1].

The main issue of swarm control is how to coordinate and model large groups of mobile robots. The general idea to model the swarm behavior is to have a long range attraction and short range repulsion between individuals [1]. Artificial potential functions have been widely used for modeling the attraction and repulsion between members. In recent years artificial potential functions have been used for many applications such as mobile robot coordination towards the goal, robot navigation, obstacle avoidance, formation control and swarm control of autonomous vehicles. For example, they have been used for trajectory tracking of WMRs [7], [8], tracking multi agent systems [9], robot navigation [10], collision or obstacle avoidance [11]-[12], [13], [14], formation control of multi agent systems [12], [15] or space craft swarm navigation [16]. In [17] the authors considered the flocking of mobile agents where artificial potential functions are used for cohesion and collision avoidance. It is shown that all the agents travel at the same heading velocity and direction keeping the cohesion between them. Lyapunov and graph theories are used to analyze the stability of the mobile agents.

Artificial potential functions do suffer from many research related problems. One main issue is the local minima. When the artificial potential functions are used for formation control, the mobile robots may get trapped in local minima of the artificial potential functions if they are not close enough to the global minimum. Another example is, when artificial potential functions are used for obstacle avoidance, it is likely that if the goal is closer to the obstacle, then the mobile robots may not reach the goal.

In [18] the authors address the problem where artificial potential functions are used for robot formation, migration and obstacle avoidance. Authors address the problems for cases such as when a goal potential is overwhelmed by an obstacle potential, an obstacle potential is overwhelmed by a goal potential and an obstacle potential is overwhelmed in a swarm. The structure of the total potential is changed to multiplicative and additive for the above purpose. In [19] a virtual obstacle is used to avoid problems related to local minima.

Research done on swarm control so far can be basically categorized as swarm aggregation, swarm formation, foraging swarm and finally target tracking and enclosing swarm. In one of the early works [20], the authors studied the stability analysis of a one dimensional swarm. Swarm cohesion is analyzed in discrete time for one dimensional case with asynchronism to time delays.

A. Aggregation of Swarm

Aggregation is a fundamental swarming behavior seen in living beings. In order to form a swarm some kind of aggregation is expected. Recent research papers focus more on swarm aggregation. First order swarm aggregation is given in [1] . The authors used artificial attractive/repulsive functions for modeling the swarm. It was proved that the swarm agents move towards the swarm centre and form a hyper ball around it in a finite time. The swarm centre is stationary all the time. Also, a conservative explicit bound for the swarm size is derived. Lyapunov based proofs are provided for the stability of the swarm. When the swarm moves towards the centre, as the time progresses all the members become stationary and aggregate around the swarm centre.

Different classes of attraction and repulsion functions that can be used for swam modeling and aggregation is discussed in detail in [21]. Three different types of functions namely, linear attraction bounded repulsion, almost constant attraction and unbounded repulsion, and almost constant attraction and unbounded repulsion are discussed. Also for each type of attraction and repulsion functions swarm stability is analyzed and the bound for swarm size is calculated. Unbounded repulsion functions are very practical since they avoid the collision of agents. Also, these functions can be modified such that the agent dimensions can be taken into consideration.

Swarm aggregation in a pre defined shape in 2D space is given in [22]. The members from initial positions enter inside the shape, spread over the contour and become stabilized. Artificial force fields are used to force the members towards the shape and keep the swarm cohesive. Further, it is shown that when the shape is changed then the agents can re arrange them selves into the new shape and if some agents are removed or added, then they will again re arrange in side the shape. Also obstacle avoiding of agents towards the shape is also discussed.

In [4] the authors have considered a double integrator model for the swarm aggregation opposed to the model used in [1]. Swarm cohesion and the size are analyzed for various classes of attraction and repulsion functions given in [21]. For the double integrator model it is shown that the swarm aggregate around the swarm centre. The swarm centre is not stationary here and it travels with a constant velocity. Also, when the time moves on each individual converges to the velocity of the swarm center.

In [23] the authors considered swarm aggregation in a 2D space. Three artificial forces are considered for attraction, repulsion and friction forces. Friction force makes the

agent come to a complete stop when they are stabilized around the point considered. The whole swarm can be modeled as a second order ordinary dynamic equation and its stability and cohesion is analyzed.

Swarm aggregation and formation based on the school fish model is considered using motor schema method in [6]. Each member has three reaction regions: attraction, parallel area and reaction area. Further, according to the relative angle between two agents, each agent has five regions of division for the smooth turning of swarm. Five motor schemas basically move to goal, avoid obstacles, swirl obstacles, school vector and noise vector are used here. These motor schemas are used to aggregate, avoid obstacle and reach the goal.

B. Formation of Swarm

Formation control is considered as making mobile robots to form in a specific geometric shape by a suitable control algorithm [6], [24]. A good review on formation control is given in [2] where formation control strategies such as a behavior based approach, a leader follower approach and virtual structure methods are discussed.

In the leader follower approach, the leader is assigned the task and the followers have to stay with a corresponding position to the leader. Generally, in these approaches, the controller is centralized and any failure by the leader makes the whole system a failure. In [25] and [26], leader follower based formation control for nonholonomic mobile robots is considered with obstacle avoidance where robots can change their formation in order to avoid an obstacle. The behavior based approach [27], [28] is normally decentralized but stability proofs are generally difficult. Basic behaviors such as

moving to a goal, obstacle avoidance and formation keeping will be specified and the control action is weighted with these behaviors regarding to the situation [12].

In [29], the authors worked on controlling large number of robots to make formations on 2D shapes specified by implicit functions that are weighted sum of radial basis functions generated by interpolating from a set of constraint points. Gradient decent technique is used so that robots converge and spread along the 2D curve of the implicit functions. Repulsive terms are added to the controller to avoid collision between members. Also, when the shapes are dynamically split and changed the robots converge to the desired locations.

In [24] the authors used bivariate normal functions to control vector fields that swarm travel on to create formations. Limiting functions are used for tight control over vector fields from the center. Swarm geometry, individual member spacing and obstacle avoiding are addressed and simulation results are given to validate the results. Swarm can track line trajectories or sinusoidal trajectories while keeping the desired formation such as an ellipse.

The authors in [5] considered the vehicle dynamics for the swarm modeling in contrast to [1], where a first order model was used. A sliding mode control method is used to find a controller which makes the swarm agents follow the dynamics of [1] when they reach the sliding manifold in finite time. Further, when the swarm aggregates, making a formation by choosing different pairs of artificial potential is also discussed.

C. Target Tracking and Enclosing Swarm

Tracking a target or encircling the target is considered with the swarm control since recent years military applications require autonomous vehicle protection or capturing an enemy. In [30] the authors control the swarm in a formation around an object such as military convoy protection. The swarm will enclose the convoy in a circular or ellipse formation. Artificial potential fields are generated to create vector surfaces around the objects using normal and sigmoid functions. Swarm formation band is chosen from the centre of convoy such that the vector field outside the band from both sides pulls the swarm into the band to encircle the convoy. Limiting functions are used to control the vector fields inside and out side the band where the swarm needs formation.

The authors in [3] developed algorithm based on artificial potential functions to capture or intercept dynamically moving targets. Firstly, they worked with a kinematic model for both the target and pursuer, and derived controller to capture the target based on negative gradient of the potential function. Later, vehicle dynamics was used for the pursuer and the sliding mode method was used to enforce the system dynamics such that when it reaches the sliding surface the pursuer recovers the kinematic model developed earlier.

The authors in [31] extended their results of [3] with multi agents tracking a target and making a formation. Two objectives were achieved. One was tracking and enclosing a target and the other one was when the agents were enclosing the target they were possibly making a certain formation. The potential function contains two terms. One is for the formation control and the other part is for the agent-target tracking. A carefully chosen potential function which has global minimum when agents reach the necessary

inter individual distance between target and themselves, makes the formation control and tracking control. Further, vehicle dynamics is used for the agents and sliding mode control is used to achieve the objectives. In [32] the authors consider agents with nonholonomic dynamics for target tracking.

D. Foraging Swarm

The authors in [33] modeled foraging swarm that searches for food or rich nutrients in an environment avoiding obstacles. In [1], [21], [5] the swarm centre is stationary but the individuals try to aggregate around the swarm centre. However, in [33] the swarm centre is moving towards the favorable regions as well as keeping the cohesion. The authors consider quadratic, Gaussian and multimodal Gaussian attractant/repellant profiles to model the foraging swarms. Further, bounds on swarm size and cohesion analysis are given in detail.

Same authors in [34] further extend their results in [33] for the quadratic, Gaussian and multi modal Gaussian profiles and they consider a plane profile as well. Also for each profile numerous simulation results are provided to validate the theory and understand the foraging swarm behavior.

E. Other Applications of Swarm

In [35] , the authors show how the swarm and a human move together and the swarm follows the human. Here each robot has a local sensing ability. In [1], [5], [21], [33]-[34] and [36]-[38], each member has attraction and repulsion from all of the members. In [35] and [39] attraction and repulsion from other members will be due to the neighbor of the swarm. This will be highly helpful in making the swarm decentralized

and limit their sensing abilities. Simulation results show that the swarm can follow a human through a narrow corridor while avoiding obstacles.

Controlling a swarm in three dimensions based on an abstraction that reduces the planning problem from a higher dimensional space to a lower dimensional abstract space is considered in [40]. The abstraction is a product structure of the group and shape which is nine dimensional consisting of six dimensional group for the position and orientation of the swarm and three dimensional shape for the general shape of the swarm. Simulation results show a swarm move through a three dimensional corridor and changing their shape when the corridor changes its shape and the size.

The authors in [41] extended their results in [1], [5], [33], [34] be applicable for non-holonomic vehicle dynamics. Basically two sliding mode surfaces were defined for the translational speed and one corresponding to the orientation. Actual inputs are made to track the velocity reference and angle reference. Swarm aggregation, formation and foraging are considered with nonholonomic dynamics and simulations are given to validate the results. The sliding mode control is the widely used control method here. In mobile robot applications, due to its handling of robustness, the sliding mode control is one of the mostly used control methods.

1.1.2. Energetic Swarm Control

The energetic swarm control basically studies the internal energy associated within the system similar to that of molecular dynamics. For example, a glass of water kept on a stationary table doesn't have any kinetic energy on a macroscopic level, but if we look at it on a microscopic level, the water molecules travel at a very high speed and it has internal kinetic and potential energy associated with it [42].

In [37], the authors have defined different types of energy terms that are similar to the molecular dynamics theory. The total energy of the system is considered to be the combination of total kinetic energy and total potential energy. The total kinetic energy consists of two terms. One is the internal kinetic energy and the other one is the bulk kinetic energy. Total kinetic energy is the sum of the kinetic energy of the individual members during the translational motion. Bulk kinetic energy is the kinetic energy of the swarm center where the swarm centre is the average position of the individual members, similar to that of the centre of gravity in a rigid body.

Similarly, the total potential energy is the sum of the internal potential energy and the bulk potential energy. For the time being, the bulk potential energy is considered to be zero but when we consider a swarm moving in a 3D space under a gravitational force, we can consider the effects of the bulk potential energy. Internal potential energy is due to the attraction and repulsive forces acting on members by the other members.

Swarm internal energy is defined as the sum of the internal kinetic energy and the internal potential energy which is similar to the internal energy of the molecules in molecular physics theory. As discussed above, the internal kinetic energy is the difference between total kinetic energy and bulk kinetic energy. Since we consider bulk potential energy to be zero, the swarm internal energy is the difference between the total energy and bulk kinetic energy.

The swarm temperature is the most important term which manipulates the internal energy associated within the system. In [37] , the temperature is defined as the average of swarm internal energy. When the temperature is increased the agents are more aggressive and energetic. That means they travel faster and try to cover more area. If we plot the

velocity distribution, we would find that higher numbers of vehicles attain a higher velocity when we increase the temperature. This is similar to the Maxwell-Boltzmann velocity distribution where, when the temperature is increased, the ideal gas molecules get more energy and the density of molecules with higher velocity increases [43].

In [37] , two control objectives are achieved. Temperature is regulated at various desired temperatures and the swarm centre trajectory is tracked simultaneously. A PD controller is used for swarm centre trajectory tracking and feedback linearization is used for temperature regulation. In [34] the swarm centre is stationary all the time. But in an energetic swarm this is not necessarily the case. The swarm centre may be stationary if desired. Also in [34] when the agents aggregate the individual agents become stationary. The energetic swarm aggregation is the opposite of this aggregation. In an energetic swarm, the swarm centre can be stationary but the individual agents will be in motion all the time.

The temperature definition was changed in [38] from [37]. Here the swarm temperature is defined as the average of swarm internal kinetic energy. This is closer to the statistical mechanics since the temperature only relates to the velocity distribution. For the first time, to an energetic swarm, the swarm cohesion is analyzed. Simulation results are given to understand energetic swarm and velocity distribution.

Energetic swarm theory is applied for a group of WMRs in [44]. The lower level controller makes the tip of the robot follow the desired trajectory which is generated from a high level controller of the swarm. Repulsion function is modified such that each agent's private area is considered with dimension. In [36] , a potential energy controller is developed further. The high level controller has three objectives. It has to track the swarm

centre trajectory and regulate temperature and potential energies. The potential energy controller basically controls the swarm size by which the swarm is made cohesive all the time.

In [36]-[38] and [44], feedback linearization method is used to achieve the objectives such as tracking the desired swarm centre, desired temperature and desired potential. However, the stability of the system depends primarily on the initial conditions of the swarm members since the feedback linearization method is used. Also, the controller can not handle any disturbance applied to the system. In [48], energetic swarm control theory is developed with the sliding mode control method. The initial condition problem is eliminated and since the slide mode control method is a robust one, it handles any disturbance applied to the system. Further, the control allocation is introduced and it better solves the over actuated problem. The control allocation process distributes the control inputs among the actuators.

1.2. Thesis Objectives and Contributions

In this thesis, the energetic swarm control approach from [36]-[38] is explained and the proposed controllers in [48] are verified through numerous simulations of the high level swarm control system. It is found that the pseudo inverse method is not adequate enough to handle the control allocation process. SNOPT [49], an optimization solver, is used for the control allocation process. SNOPT efficiently solves the control allocation approach and handles saturation constraints on inputs. However, the saturation constraints cannot be lowered than a certain threshold value and the factors determines this minimum allowable value is studied. Allowable limits of the saturation constraints are found for a particular operating region of the potential and temperature values for the steady state case.

The main contribution of this thesis is the application of energetic swarm control to WMRs using dynamic feedback linearization as a low level controller. A lower level controller is necessary in order to apply energetic swarm on WMRs. This low level controller improves the trajectory tracking of WMRs. Further, the high-level and low level layers are combined together for the experimental implementation. Finally, the parameter identification of servo motors is done which improves experimental implementation of the energetic swarm.

The remaining chapters are organized as follows. Chapter 2 gives the background material on swarm control, tracking control of vehicles and the control allocation approach. Chapter 3 discusses the energetic swarm control and control allocation with and without saturation. Chapter 4 studies in detail the parametric identification of WMRs. Chapter 5 explains the procedure of low level control and practical implementation of

energetic swarm control with WMRs. Finally, in chapter 6 conclusions and future works are given.

2. Background Material

This section presents the necessary background material to understand the swarm control on swarm aggregation, swarm formation and foraging swarm. Further, the theory of control allocation which finds the actual control inputs for the energetic swarm will be discussed. Finally, tracking control of vehicles will be presented along with the tools to analyze nonholonomic properties of vehicles.

2.1. Swarm Control

The mathematical modeling and results of swarm aggregation will be presented as in [1]. Further, different class of attraction and repulsion functions will be discussed as in [21]. Swarm formation with vehicle dynamics is given as in [5] and finally, foraging swarm in an environment will be discussed as in [33] and [34]. These essentially help the reader to understand the swarm control before proceeding into energetic swarm control.

A. Swarm Aggregation

Consider a swarm system moving in an n-dimensional space and having M members with the following assumptions. Each member is considered as a point mass and its dimension is ignored. The motion is synchronous. The swarm motion that models the aggregation is described by the following first order equation

$$\dot{\mathbf{x}}_i = \sum_{j=1, j\neq i}^{M} \mathbf{g}(\mathbf{x}_i - \mathbf{x}_j) \qquad (1)$$

where for each member i, $i = 1,2,\ldots,M$, the position is expressed as $\mathbf{x}_i \in R^n$, $\mathbf{g}(\mathbf{x}_i - \mathbf{x}_j)$ is a function to create the attraction and repulsion between each members. $\mathbf{g}(\mathbf{x}_i - \mathbf{x}_j)$ is given by

$$\mathbf{g}(\mathbf{x}_i - \mathbf{x}_j) = -(\mathbf{x}_i - \mathbf{x}_j)(a - b\exp\left(\frac{\left\|\mathbf{x}_i - \mathbf{x}_j\right\|^2}{c}\right)) \tag{2}$$

where the norm is the Euclidean norm and $a,b,c \in R^+$. $\mathbf{g}(\mathbf{x}_i - \mathbf{x}_j)$ consists of attraction and repulsion terms. When the distance between two agents is larger than a certain distance δ, the agents try to attract each other since the attraction function is more dominant than the repulsion. But when they become lesser than the δ, the repulsion function will be more dominant and the agents will try to repulse each other. Between any two members, the resulting effort of attractive and repulsive forces will act along the line that connects them. The δ will be given by

$$\delta = \sqrt{c \ln\left(\frac{b}{a}\right)} \tag{3}$$

The resulting motion of each member is then the vector summation of attraction and repulsion effects by the other members. The swarm centre $\bar{\mathbf{x}} \in R^n$ is given by

$$\bar{\mathbf{x}} = \frac{\sum_{i=1}^{M} \mathbf{x}_i}{M} \tag{4}$$

The swarm centre in (4) with attraction repulsion functions given by (2) is stationary for all the time due to symmetry of $g(\cdot)$ in (2).

A free agent in a swarm is said to be if $\left\|\mathbf{x}_i - \mathbf{x}_j\right\| > \delta, \forall j \in \{1,...,M\}, j \neq i$. The forces acting on the free agent are due to the attraction forces by other members since its distance is greater than the δ.

A free agent in a swarm given by (1) with attraction/repulsion function $g(\cdot)$ given by (2) moves towards its swarm centre at time t. A Lyapunov function based proof shows that the free agent, which has only attraction from all its members, starts to move

towards the centre of the swarm. Therefore the members of the swarm start to form a cluster around the swarm center and aggregate around it.

It can be shown that the swarm members in aggregation will converge to a hyper ball given by

$$B_{\bar{r}}(\bar{\mathbf{x}}) = \{\mathbf{x}_i : \|\mathbf{x}_i - \bar{\mathbf{x}}\| \leq \bar{r}\} \tag{5}$$

where $\bar{r}$, the radius, which depends on parameters of (2) is given by

$$\bar{r} = \frac{b}{a}\sqrt{\frac{c}{2}}\exp(-\frac{1}{2}) \tag{6}$$

The convergence of swarm towards the swarm centre will occur in a finite time given by

$$\bar{t} = \max_{i \in S}\left\{-\frac{1}{2a}\ln\left(\frac{\bar{r}^2}{\|\mathbf{x}_i(0) - \bar{\mathbf{x}}\|^2}\right)\right\} \tag{7}$$

where $S \in \{1,...,M\}$.

These results show that the agents from any initial condition will be in motion towards the centre of the swarm, aggregate and form a cluster in a finite time. The bound $\bar{r}$ is a conservative one and the real swarm size will be much smaller than the $\bar{r}$.

Further, once the swarm aggregate around the swarm centre and when the time $t \to \infty$, motion of each member is given by $\mathbf{x}(t) \to \Omega_e$

where $\mathbf{x} = [\mathbf{x}_1^T \; . \; . \; \mathbf{x}_M^T]^T$ is the state vector and the set Ω_e is given by

$$\Omega_e = \{\mathbf{x} : \dot{\mathbf{x}} = 0\} \tag{8}$$

This result shows that once the swarm agents are in cohesion around the swarm centre, the agents become stationary as the time progresses.

B. A Class of Attraction and Repulsion Functions

Attraction and repulsion function plays a vital role in swarm modeling. It keeps the swarm cohesive and repulses the members when they are too close. Two different classes of attraction and repulsion functions will be discussed with their bound on swarm size. An interested reader can find one more class of attraction and repulsion function in [21].

A general case of attraction and repulsion function can be written as

$$\mathbf{g}(\|\mathbf{y}\|) = -\mathbf{y}[g_a(\|\mathbf{y}\|) - g_r(\|\mathbf{y}\|)] \tag{9}$$

where $g_a : R^+ \to R^+$ is the magnitude of the attraction for the swarm cohesion and the term $g_r : R^+ \to R^+$ is the magnitude of the repulsion for the collision avoidance between the agents. The g_a is more effective in longer range and the g_r is more dominant in shorter range. The norm is the Euclidean norm.

The following two assumptions are made for the $\mathbf{g}(\cdot)$. It is assumed that at a certain distance δ, the attraction and repulsion balance each other such that $g_a(\delta) = g_r(\delta)$. When $\|\mathbf{y}\| > \delta$, the attraction is higher than the repulsion such as $g_a(\|\mathbf{y}\|) > g_r(\|\mathbf{y}\|)$ and when $\|\mathbf{y}\| < \delta$, $g_a(\|\mathbf{y}\|) < g_r(\|\mathbf{y}\|)$. Another assumption is that we choose $g_a(\cdot)$ and $g_r(\cdot)$ such that we find functions $J_a : R^+ \to R^+$ and $J_r : R^+ \to R^+$, corresponding terms in the artificial potential function, to satisfy $\nabla_{\mathbf{y}} J_a(\|\mathbf{y}\|) = \mathbf{y} g_a(\|\mathbf{y}\|)$ and $\nabla_{\mathbf{y}} J_r(\|\mathbf{y}\|) = \mathbf{y} g_r(\|\mathbf{y}\|)$

The artificial potential function $J : R^{nM} \to R$ is given by

$$J(\mathbf{x}) = \sum_{i=1}^{M-1}\sum_{j=i+1}^{M}[J_a(\|\mathbf{y}\|) - J_r(\|\mathbf{y}\|)] = \sum_{i=1}^{M-1}\sum_{j=i+1}^{M} J_{ar}(\|\mathbf{y}\|) \tag{10}$$

where $\mathbf{x} = [\mathbf{x}_1^T \; . \; . \; \mathbf{x}_M^T]^T$ is the state vector. Then the equation (1) can be rewritten in terms of $J(\cdot)$ as

$$\dot{\mathbf{x}}_i = -\nabla_{\mathbf{x}_i} J(\mathbf{x}) \tag{11}$$

This can be interpreted as each agent is moving towards the negative gradient of the total potential $J(\mathbf{x})$ of the swarm. Each agent is trying to minimize its energy and so does the swarm when they aggregate around the swarm centre.

Now consider the first case of attractive/repulsive functions. The first case is the linear attraction and bounded repulsion function. Then the $g_a(\cdot)$ will be given for this case is

$$g_a(\|\mathbf{y}\|) = a \tag{12}$$

where $a > 0$ is a positive constant . Then the error is defined as

$$\mathbf{e}_i = \mathbf{x}_i - \bar{\mathbf{x}} \tag{13}$$

It can be shown that when $t \to \infty$ the error is bounded by

$$\|\mathbf{e}_i\| \le \frac{1}{aM} \sum_{j=1, j\neq i}^{M} g_r\left(\|\mathbf{x}_i - \mathbf{x}_j\|\right)\|\mathbf{x}_i - \mathbf{x}_j\| \tag{14}$$

If the $g_r(\cdot)$ is bounded by some positive constant $b > 0$, that is $g_r\left(\|\mathbf{x}_i - \mathbf{x}_j\|\right)\|\mathbf{x}_i - \mathbf{x}_j\| \le b$ then the bound on error is given by

$$\|\mathbf{e}_i\| \le \frac{b(M-1)}{aM} < \frac{b}{a} = \varepsilon \tag{15}$$

This gives the bound on the swarm size. Further this condition will be achieved in a finite time given by

$$\bar{t} = \max_{i \in S} \left\{ -\frac{1}{2a} \ln\left(\frac{\varepsilon^2}{2V_i(0)} \right) \right\} \tag{16}$$

where $S \in \{1,...,M\}$ and V_i is the Lyapunov function given by

$$V_i = \frac{1}{2} \mathbf{e}_i^T \mathbf{e}_i \tag{17}$$

The second case considered is the linearly bounded from below attraction and unbounded repulsion function. This function is very useful in practical applications since we have unbounded repulsion and the agents won't collide with each other. The $g_a(\cdot)$ will be given for this case is

$$g_a(\|\mathbf{y}\|) \geq a \tag{18}$$

where $a > 0$ is a positive constant and unbounded repulsion function $g_r(\cdot)$ is given by

$$g_r(\|\mathbf{y}\|) \leq \frac{b}{\|\mathbf{x}_i - \mathbf{x}_j\|^2} \tag{19}$$

where $b > 0$ is a positive constant. It can be shown for this case that the error is bounded as

$$2aM \sum_{i=1}^{M} \|\mathbf{e}_i\|^2 \leq bM(M-1) \tag{20}$$

This implies

$$\frac{1}{M-1} \sum_{i=1}^{M} \|\mathbf{e}_i\|^2 \leq \frac{b}{2a} \tag{21}$$

Then, taking the root mean square value of the error and defining $e_{rms} = \sqrt{\frac{1}{M}\sum_{i=1}^{M}\|\mathbf{e}_i\|^2}$, we can have

$$e_{ems} \le \sqrt{\frac{b}{2a}} \tag{22}$$

This gives the bound on the swarm size. Further, the unbounded repulsion can be modified to cope with the dimension of the vehicle if we modify the repulsion function such as $\lim_{\|\mathbf{x}_i-\mathbf{x}_j\|\to c_1^+} g_r\left(\|\mathbf{x}_i-\mathbf{x}_j\|\right)\|\mathbf{x}_i-\mathbf{x}_j\| \to \infty$ where c_1 is the radius of the private area concerned.

It is obvious that one has to select carefully attraction/repulsion functions for the swarm modeling. Attraction/repulsion functions are key factors for the swarm cohesion and bound on the swarm size.

C. Formation and Aggregation

In previous sections the dynamics considered is the first order point mass dynamics. In this subsection the swarm formation and aggregation will be discussed for swarm members with vehicle dynamics and the sliding mode control method is used to find the controller.

Consider a swarm system with M members where each member is moving in an n- dimensional space. The dynamics of the motion of each member is given by

$$\mathbf{M}_i(\mathbf{x}_i)\ddot{\mathbf{x}}_i + \mathbf{f}_i(\mathbf{x}_i, \dot{\mathbf{x}}_i) = \mathbf{u}_i \tag{23}$$

where $\mathbf{M}_i(\cdot) \in R^{n\times n}$ is the mass or inertia matrix, for each member i, $i = 1,2,\ldots,M$, the position is expressed as $\mathbf{x}_i \in R^n$, $\mathbf{f}_i(\cdot,\cdot) \in R^n$ contains the centripetal, Corriolis,

gravitational and disturbances effects and finally, $\mathbf{u}_i \in R^n$ is the control input for the each member.

The term $\mathbf{f}_i(\cdot,\cdot)$ can be given in two parts as in (24) with $\mathbf{f}_i^k(\cdot,\cdot)$ represents the known part and $\mathbf{f}_i^u(\cdot,\cdot)$ contains the unknown part. That is

$$\mathbf{f}_i(\mathbf{x}_i,\dot{\mathbf{x}}_i) = \mathbf{f}_i^k(\mathbf{x}_i,\dot{\mathbf{x}}_i) + \mathbf{f}_i^u(\mathbf{x}_i,\dot{\mathbf{x}}_i) \tag{24}$$

Further, let us assume the following bound on unknown part $\mathbf{f}_i^u(\cdot,\cdot)$ given as

$$\left\|\mathbf{f}_i^u(\mathbf{x}_i,\dot{\mathbf{x}}_i)\right\| \le \bar{f}_i, 1 \le i \le M \tag{25}$$

Similarly, the upper and lower bounds for $\mathbf{M}_i(\cdot)$ is given by (26) and it is assumed that it is non-singular.

$$\underline{M_i}\|\mathbf{y}\|^2 \le \mathbf{y}^T\mathbf{M}_i(\mathbf{x}_i)\mathbf{y} \le \overline{M_i}\|\mathbf{y}\|^2 \tag{26}$$

where $\mathbf{y} \in R^n$ is an arbitrary vector and $\underline{M_i} > 0$ and $\overline{M_i}$ are known.

Sliding mode control method is used to calculate the controller which forces the velocity of members along the negative gradient of potential function when the system reaches the sliding manifold.

Let us define the sliding manifold $\mathbf{s}_i = [s_1 \quad . \quad . \quad s_n]^T$ as

$$\mathbf{s}_i = \dot{\mathbf{x}}_i + \nabla_{\mathbf{x}_i} J(\mathbf{x}) \tag{27}$$

where $\mathbf{x} = [\mathbf{x}_1^T \; . \quad . \quad \mathbf{x}_M^T]^T$ is the state vector and, when $\mathbf{s}_i = 0$, we have

$$\dot{\mathbf{x}}_i = -\nabla_{\mathbf{x}_i} J(\mathbf{x}) \tag{28}$$

which is the original equation used for the swarm aggregation in (11)

The time derivative of $\mathbf{s}_i$ is given as

$$\dot{\mathbf{s}}_i = \ddot{\mathbf{x}}_i + \frac{\partial}{\partial t}\left(\nabla_{\mathbf{x}_i} J(\mathbf{x})\right) \tag{29}$$

In order to satisfy the sliding condition $\frac{1}{2}\frac{d}{dt}\mathbf{s}_i{}^T\mathbf{s}_i \le -\sum_{i=1}^{n}\eta_i|s_i|$, where $\eta_i > 0$, the controller is developed as

$$\mathbf{u}_i = -diag(\mathbf{k}_i)\,\mathrm{sgn}(\mathbf{s}_i) + \mathbf{f}_i^k \tag{30}$$

where $\mathbf{k}_i = [k_1 \quad . \quad . \quad k_n]^T$ and sgn(·) is the signum function. $k_j\ \forall j = 1,2,...,n$ is chosen as

$$k_j > \frac{1}{\underline{M}_i}\left(\overline{M}_i\bar{f}_i + \bar{J} + \eta_i\right) \tag{31}$$

The potential function has to be chosen such that $\left\|\frac{\partial}{\partial t}\left(\nabla_{\mathbf{x}_i} J(\mathbf{x})\right)\right\| \le \bar{J}$ where $\bar{J}$ is known.

All the agents reach the sliding manifold in a finite time given by

$$\bar{t} = \max_{i=1,\ldots,M}\left\{\frac{2V_i(0)}{\eta_i}\right\} \tag{32}$$

where V_i is given by

$$V_i = \frac{1}{2}\mathbf{s}_i^T\mathbf{s}_i \tag{33}$$

Formation is achieved by introducing formation constraints such as

$$\left\|\mathbf{x}_i - \mathbf{x}_j\right\| = d_{ij}, 1 \le i, j \le M \tag{34}$$

where $d_{i.j}$ is the desired inter agent distance. When the agents are in formation their relative distance is pair dependent. Let δ_{ij} denotes the distance between the two agents. Then, for each pair of agents i, j different artificial potential functions are considered such that $\delta_{ij} = d_{i.j}$. One can choose pair dependent artificial potential functions $J^{ij}(\mathbf{x})$ such that unique minimum occurs at $d_{i.j}$. If the artificial potential functions are chosen

such that $J(\mathbf{x}) = \sum_{i=1}^{M-1} \sum_{j=i+1}^{M} J^{ij}(\mathbf{x})$ has unique minimum at the desired formation, then the result is global, otherwise only local stability is found.

D. Foraging Swarm

In the previous three sections, the swarm centre is stationary all the time but the individuals are on the move towards the swarm centre to aggregate around it or make a formation. But here the swarm centre is moving and foraging in an environment such as to search for food, to find the target or to avoid unwanted obstacles. Swarm members, seeking swarm centre, move towards the food or target location since the swarm centre is moving towards a favorable region and the swarm members aggregate around the swarm centre. Foraging swarms can be modeled with plane, quadratic or Gaussian type profiles.

The equation that models the foraging swarm is given by

$$\dot{\mathbf{x}}_i = -\nabla_{\mathbf{x}_i} \bar{\sigma}(\mathbf{x}_i) + \sum_{j=1, j\neq i}^{M} \mathbf{g}(\mathbf{x}_i - \mathbf{x}_j) \tag{35}$$

where $\bar{\sigma} : R^n \to R$ is the attraction or repellent profile. For example, it can represent a profile of nutrients. It is assumed that if $\bar{\sigma} < 0$ the nutrient is rich, $\bar{\sigma} > 0$ means a noxious environment and $\bar{\sigma} = 0$ represents a neutral one. The $\mathbf{g}(\cdot)$ considered here is as in (2).

The swarm centre velocity is given by

$$\dot{\bar{\mathbf{x}}} = -\frac{1}{M} \sum_{i=1}^{M} \nabla_{\mathbf{x}_i} \bar{\sigma}(\mathbf{x}_i) \tag{36}$$

This shows that the swarm centre is now moving along the average of negative gradient of individual profiles.

Now, let us consider the motion along the plane attraction/repellent profile given as

$$\bar{\sigma}(\mathbf{y}) = \mathbf{a}_\sigma^T \mathbf{y} + b_\sigma \tag{37}$$

where $\mathbf{a}_\sigma \in R^n$, $b_\sigma \in R$ and from (36), the swarm centre velocity is given by $\dot{\bar{\mathbf{x}}} = -\mathbf{a}_\sigma$. That is the swarm centre moves towards the rich nutrients where the minimum occurs with constant velocity. Also, it can be proved for this profile that the swarm stays in cohesion.

The next type of profile is the quadratic attraction/repellent profile given as

$$\bar{\sigma}(\mathbf{y}) = \frac{A_\sigma}{2}\left\|\mathbf{y} - \mathbf{c}_\sigma\right\|^2 + b_\sigma \tag{38}$$

where $A_\sigma \in R$, $\mathbf{c}_\sigma \in R^n$ and $b_\sigma \in R$.This profile has either a maximum or minimum globally on $\mathbf{c}_\sigma$ depending on the sign of A_σ. The error between swarm centre and $\mathbf{c}_\sigma$ is defined as

$$\mathbf{e}_\sigma = \bar{\mathbf{x}} - \mathbf{c}_\sigma \tag{39}$$

It can be proven that when $t \to \infty$, if $A_\sigma > 0$, $\bar{\mathbf{x}} \to \mathbf{c}_\sigma$ and if $A_\sigma < 0$ and $\bar{\mathbf{x}}(0) \neq \mathbf{c}_\sigma$, then $\bar{\mathbf{x}} \to \infty$. The results show that the swarm centre is in search of rich nutrients along this profile. Further, for a finite time and for any small $\lambda > 0$, the swarm aggregate around $\bar{\mathbf{x}}$ given by $\mathbf{x}_i \to B_{r_1}(\bar{\mathbf{x}})$ where the hyper ball $B_{r_1}(\bar{\mathbf{x}}) = \{\mathbf{x}_i : \|\mathbf{x}_i - \bar{\mathbf{x}}\| \leq r_1\}$ and r_1 is given by

$$r_1 = \frac{b(M-1)}{aM + A_\sigma - \lambda}\sqrt{\frac{c}{2}}\exp\left(-\frac{1}{2}\right) \tag{40}$$

Finally, let us consider a multimodal Gaussian attraction/repellent profile given as

$$\bar{\sigma}(\mathbf{y}) = -\sum_{i=1}^{M} \frac{A_\sigma^i}{2}\exp\left(-\frac{\left\|\mathbf{y} - \mathbf{c}_\sigma^i\right\|^2}{l_\sigma^i}\right) + b_\sigma \tag{41}$$

where $A_\sigma^i \in R$, $b_\sigma \in R$, $\mathbf{c}_\sigma^i \in R^n$ and $l_\sigma^i \in R$. When A_σ^i takes positive or negative values then the profile consists of hills or valleys. Here, there are chances that if the attraction

force is not large enough depending on the initial conditions of swarm agents, some agents can be trapped inside the local minima. This can cause small groups of individuals at various locations in the profile. Similar proofs for swarm size and cohesion analysis is given in [34] and an interested reader can refer [34] for more detail.

2.2. Control Allocation

The control allocation is used to find control inputs when the system is over actuated. In an under actuated system, the numbers of control inputs or actuators are less than the degree of freedom. On the other hand, in an over actuated system we have more numbers of actuators than the degree of freedom in order to achieve a desired solution. An over actuated system has two main advantages. One is that it can be utilized for fault tolerant since it can have many solutions for a desired control when the actuators are not saturated. Another advantage is that it has the ability to deal with the saturation. Since every actuator has a physical limit, if one actuator saturates then the other actuator can provide the required control input to achieve the desired solution [47]. For more details of different kinds of control allocation approaches please refer to [53]. A linear control allocation problem will be discussed as in [53].

A linear control allocation problem is defined as

$$\mathbf{Bu} = \mathbf{u}_{des} \tag{42}$$

where $\mathbf{B} \in R^{m \times n}$ is the matrix of effectiveness of actuator, $\mathbf{u}_{des} \in R^{m}$ is the required control input and $\mathbf{u} \in R^{n}$ is the control effort provided by each actuators. When $m < n$ the system is over actuated and $\mathbf{u}$ will be found by the control allocation approach.

For example, given that $\mathbf{B}=[1\ \ 2]$, $\mathbf{u}_{des}=5$ the $\mathbf{u}=[u_1\ u_2]^T$ can be $[0\ \ 2.5]^T$, $[1.0\ \ 2.0]^T$ or $[5.0\ \ 0.0]^T$ to satisfy the desired control input needed. Further, if there are saturation limits for the actuators for example, if $-6\le u_1\le +6, -2\le u_2\le +2$, then the $\mathbf{u}=[u_1\ u_2]^T$ can have many answers. But if the saturation limits are $-2\le u_1\le +2$ and $-1\le u_2\le +1.5$, then one solution exists for $\mathbf{u}=[u_1\ u_2]^T$. Further, if the saturation limits are $-1\le u_1\le +1$ and $-1\le u_2\le +1$, then no solution exists.

When there are multiple solutions we need to figure out a way to select control inputs. One way is to find the controllers such that they minimize a performance index which relates to the control energy. A pseudo inverse method can be used to solve the control allocation problem.

Let us define the performance index $\bar{J}\in R$ as

$$\min_{\mathbf{u}}\bar{J}=\frac{1}{2}\mathbf{u}^T\mathbf{W}\mathbf{u} \tag{43}$$

where $\mathbf{W}\in R^{n\times n}$ is the weighting matrix.

The Hamiltonian $H\in R$ is defined as

$$H=\frac{1}{2}\left(\mathbf{u}^T\mathbf{W}\mathbf{u}\right)+\boldsymbol{\lambda}_o\left(\mathbf{B}\mathbf{u}-\mathbf{u}_{des}\right) \tag{44}$$

where $\boldsymbol{\lambda}_0\in R^{1\times m}$ being the Lagrangian multiplier.

The partial derivative of H w.r.t $\mathbf{u}$ is given by

$$\frac{\partial H}{\partial \mathbf{u}}=\left(\mathbf{W}\mathbf{u}\right)+\left(\boldsymbol{\lambda}_o\mathbf{B}\right)^T \tag{45}$$

Similarly, the partial derivative of H w.r.t $\boldsymbol{\lambda}_0$ is given by

$$\frac{\partial H}{\partial \boldsymbol{\lambda}_o} = (\mathbf{Bu} - \mathbf{u}_{des}) \tag{46}$$

Setting (45), (46) to zero gives us

$$(\mathbf{Wu}) = -\mathbf{B}^T \boldsymbol{\lambda}_o{}^T \tag{47}$$

and

$$\mathbf{Bu} = \mathbf{u}_{des} \Rightarrow \mathbf{BW}^{-1}\mathbf{Wu} = \mathbf{u}_{des} \tag{48}$$

Substituting (47) into (48) gives us

$$\mathbf{BW}^{-1}\left(-\mathbf{B}^T \boldsymbol{\lambda}_o{}^T\right) = \mathbf{u}_{des} \tag{49}$$

Then $\boldsymbol{\lambda}_0{}^T$ is given by

$$\boldsymbol{\lambda}_o{}^T = -\left(\mathbf{BW}^{-1}\mathbf{B}^T\right)^{-1}\mathbf{u}_{des} \tag{50}$$

From (47) and (50) the $\mathbf{u}$ is given by

$$\mathbf{u} = \mathbf{W}^{-1}\mathbf{B}^T\left(\mathbf{BW}^{-1}\mathbf{B}^T\right)^{-1}\mathbf{u}_{des} \tag{51}$$

The answer for the $\mathbf{u}$ enables to distribute the control effort among the actuators to match the $\mathbf{u}_{des}$.

2.3. Tracking Control of Vehicles

For the energetic swarm application, WMRs are considered to form the swarm members. One reason is that many WMRs can be built quickly in a short period of time to be considered as a swarm in an academic environment. This section discusses the control properties of a WMR and how the trajectory controllers can be developed. The WMR trajectory tracking is a popular research topic over the last decade since it is nonholonomic.

Let $\mathbf{q} = [x \quad y \quad \theta]^T$ be the generalized coordinates of WMR. The nonholonomic constraint of the WMR is given by

$$\begin{bmatrix} \sin\theta & -\cos\theta & 0 \end{bmatrix} \begin{bmatrix} \dot{x} \\ \dot{y} \\ \dot{\theta} \end{bmatrix} = \begin{bmatrix} 0 \\ 0 \\ 0 \end{bmatrix} \tag{52}$$
$$\mathbf{A}\dot{\mathbf{q}} = 0$$

That is the lateral motion of the WMR is zero. Then the allowable motion can be expressed by the following driftless form

$$\dot{\mathbf{q}} = \mathbf{G}(\mathbf{q})\mathbf{w} \tag{53}$$

where $\mathbf{w} \in R^m$ is the control input. $\mathbf{G}(\mathbf{q}) \in R^{n \times m}$ is the matrix of column vectors contains the allowable motion of the WMR. Firstly, important mathematical tools such as Lie derivative, Lie bracket and Frobenius theorem which are greatly used to analyze nonholonomic systems will be introduced as in [52].

A. Lie Derivative

Let $\mathbf{f} : R^n \to R^n$ be a smooth vector field on R^n and $h : R^n \to R$ be a smooth scalar function. The Lie derivative of h with respect to $\mathbf{f}$, defined as $L_{\mathbf{f}} h = \nabla h \mathbf{f}$, is the directional derivative of the function h along the direction of the vector $\mathbf{f}$ and it is a scalar function.

The Lie derivative can be taken recursively and defined as

$$\begin{aligned} L_{\mathbf{f}}{}^0 h &= h \\ L_{\mathbf{f}}{}^i h &= L_{\mathbf{f}}(L_{\mathbf{f}}{}^{i-1} h) = \nabla(L_{\mathbf{f}}{}^{i-1} h)\mathbf{f} \quad for\ i = 1,2,..... \end{aligned} \tag{54}$$

Also, the following holds for a vector field $\mathbf{g}_0$

$$L_{\mathbf{g}_0} L_{\mathbf{f}} h = \nabla(L_{\mathbf{f}} h)\mathbf{g}_0 \tag{55}$$

B. Lie Bracket

The Lie bracket of vector fields $\mathbf{f}$ and $\mathbf{g}_0$ is defined as

$$[\mathbf{f},\mathbf{g}_0] = \nabla\mathbf{g}_0\mathbf{f} - \nabla\mathbf{f}\mathbf{g}_0 \tag{56}$$

The Lie bracket $[\mathbf{f},\mathbf{g}_0]$ is generally written as $ad_{\mathbf{f}}\mathbf{g}_0$

Similarly, as Lie derivative, repeated Lie brackets are defined as

$$\begin{aligned} ad_{\mathbf{f}}^0\mathbf{g}_0 &= \mathbf{g}_0 \\ ad_{\mathbf{f}}^i\mathbf{g}_0 &= [\mathbf{f}, ad_{\mathbf{f}}^{i-1}\mathbf{g}_0] \ \ for\, i = 1,2,..... \end{aligned} \tag{57}$$

C. Frobenius Theorem

A set of linearly independent vector fields $\mathbf{f}_1,\mathbf{f}_2,.....,\mathbf{f}_m$ is completely integrable if and only if it is involutive. The linearly independent vector fields $\mathbf{f}_1,\mathbf{f}_2,.....,\mathbf{f}_m$ is said to be involutive if the Lie bracket of any pair of vector fields belongs to the distribution $\Delta = span\{\mathbf{f}_1,\mathbf{f}_2,.....,\mathbf{f}_m\}$.

Now, the kinematic equation of WMR, that is the allowable motion (53), can be expressed by

$$\begin{bmatrix} \dot{x} \\ \dot{y} \\ \dot{\theta} \end{bmatrix} = \begin{bmatrix} \cos\theta & 0 \\ \sin\theta & 0 \\ 0 & 1 \end{bmatrix} \begin{bmatrix} v \\ \omega \end{bmatrix} \tag{58}$$

where v is the heading velocity of the WMR and ω is the angular velocity. It can be rewritten as

$$\begin{aligned} \begin{bmatrix} \dot{x} \\ \dot{y} \\ \dot{\theta} \end{bmatrix} &= \begin{bmatrix} \cos\theta \\ \sin\theta \\ 0 \end{bmatrix} v + \begin{bmatrix} 0 \\ 0 \\ 1 \end{bmatrix} \omega \\ &= \mathbf{g}_1(\mathbf{q})v + \mathbf{g}_2(\mathbf{q})\omega \end{aligned} \tag{59}$$

The distribution of $\mathbf{g}_1$ and $\mathbf{g}_2$ is given by $\Delta = span\{\mathbf{g}_1, \mathbf{g}_2\}$. The Lie bracket of $\mathbf{g}_1$ and $\mathbf{g}_2$ along with $\mathbf{g}_1$, $\mathbf{g}_2$ is given by

$$[\mathbf{g}_1 \quad \mathbf{g}_2 \quad [\mathbf{g}_1, \mathbf{g}_2]] = \begin{bmatrix} \cos\theta & 0 & \sin\theta \\ \sin\theta & 0 & -\cos\theta \\ 0 & 1 & 0 \end{bmatrix} \tag{60}$$

The rank of the Lie bracket of $\mathbf{g}_1$ and $\mathbf{g}_2$ is three and the Lie bracket of $\mathbf{g}_1$ and $\mathbf{g}_2$ cannot be written as linear dependant of $\mathbf{g}_1$ and $\mathbf{g}_2$ hence, the system is not integrable and it is nonholonomic.

It is proved that the feedback stabilization at a given posture is not possible by a smooth time invariant control for the above kinematic equation. Three mainly used different kinds of controllers are discussed namely converting the kinematics into a chained form, the input out linearization and the dynamic feedback linearization.

2.3.1. Chained Form

The kinematic equation (58) can be converted into a very popular chained form by static state feedback as in [50]. A system with two inputs $\mathbf{u} = [u_1 \quad u_2]^T$ and n generalized coordinates can be converted into the following (61) chained form by a suitable coordinate transformation $\mathbf{z} = [z_1 \quad \cdot \quad \cdot \quad z_n]^T = \mathbf{T(q)}$ and a static state feedback.

$$\begin{aligned} \dot{z}_1 &= u_1 \\ \dot{z}_2 &= u_2 \\ \dot{z}_3 &= z_2 u_1 \\ \cdot &= \cdot \\ \cdot &= \cdot \\ \dot{z}_n &= z_{n-1} u_1 \end{aligned} \tag{61}$$

In order to change the kinematic equation (58) into the chained form (61), apply the following change of coordinates

$$\begin{aligned} z_1 &= \theta \\ z_2 &= x\cos\theta + y\sin\theta \\ z_3 &= x\sin\theta - y\cos\theta \end{aligned} \tag{62}$$

and the static state feedback

$$\begin{aligned} v &= u_2 + z_3 u_1 \\ \omega &= u_1 \end{aligned} \tag{63}$$

Then the kinematic equation (58) is converted into the following chained form

$$\begin{aligned} \dot{z}_1 &= u_1 \\ \dot{z}_2 &= u_2 \\ \dot{z}_3 &= z_2 u_1 \end{aligned} \tag{64}$$

One can search for controllers for the above system.

2.3.2. Input-Output Linearization

The kinematic equation (58) can be input-output linearized as in [51]. Consider the system of the following form

$$\begin{aligned} \dot{\mathbf{x}} &= \mathbf{f}(\mathbf{x}) + \tilde{\mathbf{g}}(\mathbf{x})\mathbf{u} \\ \mathbf{y} &= \mathbf{h}(\mathbf{x}) \end{aligned} \tag{65}$$

where the state vector is given by $\mathbf{x} \in R^n, \mathbf{f}(\cdot)$ and $\mathbf{h}(\cdot)$ are smooth vector fields, $\tilde{\mathbf{g}}(\cdot)$ is the $n \times m$ matrix contains smooth column vector fields $\tilde{\mathbf{g}}(\cdot) = [\tilde{\mathbf{g}}_1 \ \cdot \ \cdot \ \tilde{\mathbf{g}}_m]$, control input vector is given by $\mathbf{u} = [u_1 \ \cdot \ \cdot \ u_m]^T$ and finally, the output vector is represented by $\mathbf{y} \in R^p$ with $p > m$. This is a multi input multi output system (MIMO).

The system is input-output linearized when the output function in (65) is repeatedly differentiated until the input appears. The first differentiation of the output function is given by (66) for $i = 1,....., p$

$$\begin{aligned} \dot{y}_i &= \frac{\partial h_i(\mathbf{x})}{\partial \mathbf{x}} \dot{\mathbf{x}} = \frac{\partial h_i(\mathbf{x})}{\partial \mathbf{x}} \{\mathbf{f}(\mathbf{x}) + \tilde{\mathbf{g}}(\mathbf{x})\mathbf{u}\} \\ &= \frac{\partial h_i(\mathbf{x})}{\partial \mathbf{x}} \mathbf{f}(\mathbf{x}) + \frac{\partial h_i(\mathbf{x})}{\partial \mathbf{x}} \tilde{\mathbf{g}}(\mathbf{x})\mathbf{u} \\ &= L_{\mathbf{f}} h_i(\mathbf{x}) + \sum_{j=1}^{m} L_{\tilde{\mathbf{g}}_j} h_i(\mathbf{x}) u_j \end{aligned} \tag{66}$$

If $L_{\tilde{\mathbf{g}}_j} h_i(\mathbf{x}) = 0 \forall j = 1,....,m$, then the control inputs don't appear in the output equation hence, it needs repeated differentiation until one of the inputs appears in the output equation. If it takes r differentiations, then the general form of differential equation for i^{th} output is given by

$$y_i^{r_i} = L_{\mathbf{f}}^{r_i} h_i(\mathbf{x}) + \sum_{j=1}^{m} L_{\tilde{\mathbf{g}}_j} L_{\mathbf{f}}^{r_i - 1} h_i(\mathbf{x}) u_j \tag{67}$$

Then the whole output vector is given by

$$\begin{bmatrix} y_1^{r_1} \\ \cdot \\ \cdot \\ y_p^{r_p} \end{bmatrix} = \begin{bmatrix} L_{\mathbf{f}}^{r_1} h_1(\mathbf{x}) \\ \cdot \\ \cdot \\ L_{\mathbf{f}}^{r_p} h_p(\mathbf{x}) \end{bmatrix} + \begin{bmatrix} \sum_{j=1}^{m} L_{\tilde{\mathbf{g}}_j} L_{\mathbf{f}}^{r_1 - 1} h_1(\mathbf{x}) \\ \cdot \\ \cdot \\ \sum_{j=1}^{m} L_{\tilde{\mathbf{g}}_j} L_{\mathbf{f}}^{r_p - 1} h_p(\mathbf{x}) \end{bmatrix}_{p \times m} \begin{bmatrix} u_1 \\ \cdot \\ u_m \end{bmatrix}_{m \times 1} \tag{68}$$

$$\mathbf{y}^{(r)} = \mathbf{P}(\mathbf{x}) + \mathbf{E}(\mathbf{x})\mathbf{u}$$

where $\mathbf{E}(\mathbf{x})$, the $p \times m$ matrix, is the decoupling matrix which is nonsquare. Then apply the input transformation as follows

$$\mathbf{u} = \left\{(\mathbf{E}^{\mathrm{T}}\mathbf{E})^{-1}\mathbf{E}^{\mathrm{T}}\right\}(\tilde{\mathbf{v}} - \mathbf{P}(\mathbf{x})) \tag{69}$$

where $\tilde{\mathbf{v}}$ is the new input. Then the equation (68) becomes

$$\mathbf{y}^{(r)} = \tilde{\mathbf{v}} \tag{70}$$

Let the tracking error be defined as

$$\mathbf{e} = \mathbf{y}_r - \mathbf{y} \tag{71}$$

where $\mathbf{y}_r$ is the reference trajectory. If the new input $\tilde{\mathbf{v}}$ is chosen as

$$\tilde{\mathbf{v}} = \mathbf{y}_r^{(r)} + \mathbf{K}_1\mathbf{e}^{(r-1)} + ... + \mathbf{K}_{r-1}\dot{\mathbf{e}} + \mathbf{K}_r\mathbf{e} \tag{72}$$

where $\mathbf{K}_i \; \forall i = 1,....,r$ is a positive constant matrix and the closed loop system becomes

$$\mathbf{e}^{(r)} + \mathbf{K}_1\mathbf{e}^{(r-1)} + ... + \mathbf{K}_{r-1}\dot{\mathbf{e}} + \mathbf{K}_r\mathbf{e} = 0 \tag{73}$$

In order to apply the above input-output linearization to the equation (58), select the output vector as $\mathbf{y} = [x + D\cos\theta \;\; y + D\sin\theta \;\; \theta]^T$ where D is the distance between the centre of axle and tip of the robot. The output is differentiated once to get

$$\begin{aligned} \dot{\mathbf{y}} &= \begin{bmatrix} \cos\theta & -D\sin\theta \\ \sin\theta & D\cos\theta \\ 0 & 1 \end{bmatrix} \begin{bmatrix} v \\ \omega \end{bmatrix} \\ &= \mathbf{E}\mathbf{u} \end{aligned} \tag{74}$$

Applying the control law as

$$\mathbf{u} = \left\{(\mathbf{E}^{\mathbf{T}}\mathbf{E})^{-1}\mathbf{E}^{\mathbf{T}}\right\}(\tilde{\mathbf{v}}) \tag{75}$$

with the new input $\tilde{\mathbf{v}}$ chosen as

$$\tilde{\mathbf{v}} = \dot{\mathbf{y}}_r + \mathbf{K}_1\mathbf{e} \tag{76}$$

Then the kinematic equation (58) is input-output linearized to track the desired trajectory.

2.3.3. Dynamic Feedback Linearization

In this section, the dynamic feedback linearization will be discussed as in [45]. Dynamic feedback linearization problem is to find a controller of the following form for a driftless nonlinear system given in (53)

$$\begin{aligned}\dot{\boldsymbol{\xi}} &= \mathbf{a}(\mathbf{q},\boldsymbol{\xi}) + \mathbf{b}(\mathbf{q},\boldsymbol{\xi})\mathbf{u} \\ \mathbf{w} &= \mathbf{c}(\mathbf{q},\boldsymbol{\xi}) + \mathbf{d}(\mathbf{q},\boldsymbol{\xi})\mathbf{u}\end{aligned} \tag{77}$$

where $\boldsymbol{\xi} \in R^v$ is a state vector, $\mathbf{u} \in R^m$ is the new input, $\mathbf{a}(\cdot) \in R^v$ and $\mathbf{c}(\cdot) \in R^m$ are vector fields and matrices $\mathbf{b}(\cdot) \in R^{v \times m}$ and $\mathbf{d}(\cdot) \in R^{m \times m}$ contain column vector fields. The closed loop system of (53) and (77) will be linear under a state transformation $\tilde{\mathbf{z}} = \mathbf{T}(\mathbf{q},\boldsymbol{\xi})$. Define the output vector of (58) as

$$\boldsymbol{\eta} = \begin{bmatrix} x \\ y \end{bmatrix} \tag{78}$$

First differentiation of the output gives

$$\dot{\boldsymbol{\eta}} = \begin{bmatrix} \cos\theta & 0 \\ \sin\theta & 0 \end{bmatrix} \begin{bmatrix} v \\ \omega \end{bmatrix} \tag{79}$$

Since the $\dot{\boldsymbol{\eta}}$ is not affected by the ω, it is necessary to differentiate until both the inputs appear in a non-singular way. In order to avoid differentiation of the original inputs, since $\xi \in R^1$, a new state ξ is necessary such that it becomes the integrator for the original input. Define ξ as

$$\begin{aligned} v &= \xi \\ \dot{\xi} &= \tilde{a} \\ \Rightarrow \dot{\boldsymbol{\eta}} &= \begin{bmatrix} \xi\cos\theta \\ \xi\sin\theta \end{bmatrix} \end{aligned} \tag{80}$$

Differentiating (80) gives

$$\ddot{\boldsymbol{\eta}} = \begin{bmatrix} \cos\theta & -\xi\sin\theta \\ \sin\theta & \xi\cos\theta \end{bmatrix} \begin{bmatrix} \tilde{a} \\ \omega \end{bmatrix} \tag{81}$$

Define $[\tilde{a} \quad \omega]^T$ assuming that it is non-singular when $\xi \neq 0$, as follows:

$$\begin{bmatrix} \tilde{a} \\ \omega \end{bmatrix} = \begin{bmatrix} \cos\theta & -\xi\sin\theta \\ \sin\theta & \xi\cos\theta \end{bmatrix}^{-1} \begin{bmatrix} u_1 \\ u_2 \end{bmatrix} \tag{82}$$

where $\mathbf{u} = [u_1 \quad u_2]^T$ is the new control input. Then the system (81) becomes

$$\ddot{\boldsymbol{\eta}} = \begin{bmatrix} u_1 \\ u_2 \end{bmatrix} \tag{83}$$

The dynamic compensator is given by

$$\begin{aligned} \dot{\xi} &= u_1 \cos\theta + u_2 \sin\theta \\ v &= \xi \\ \omega &= \frac{u_2 \cos\theta - u_1 \sin\theta}{\xi} \end{aligned} \tag{84}$$

Now, define the state transformation $\tilde{\mathbf{z}} = \mathbf{T}(\mathbf{q}, \xi)$ as follows:

$$\begin{bmatrix} \tilde{z}_1 \\ \tilde{z}_2 \\ \tilde{z}_3 \\ \tilde{z}_4 \end{bmatrix} = \begin{bmatrix} x \\ y \\ \xi\cos\theta \\ \xi\sin\theta \end{bmatrix} \tag{85}$$

Then the system in the new coordinates becomes

$$\begin{bmatrix} \dot{\tilde{z}}_1 \\ \dot{\tilde{z}}_2 \\ \dot{\tilde{z}}_3 \\ \dot{\tilde{z}}_4 \end{bmatrix} = \begin{bmatrix} 0 & 0 & 1 & 0 \\ 0 & 0 & 0 & 1 \\ 0 & 0 & 0 & 0 \\ 0 & 0 & 0 & 0 \end{bmatrix} \begin{bmatrix} \tilde{z}_1 \\ \tilde{z}_2 \\ \tilde{z}_3 \\ \tilde{z}_4 \end{bmatrix} + \begin{bmatrix} 0 \\ 0 \\ 1 \\ 1 \end{bmatrix} \begin{bmatrix} u_1 \\ u_2 \end{bmatrix} \tag{86}$$

This is a fully linearized system. In other words (86) can be rewritten as

$$\begin{bmatrix} \ddot{\tilde{z}}_1 \\ \ddot{\tilde{z}}_2 \end{bmatrix} = \begin{bmatrix} u_1 \\ u_2 \end{bmatrix} \tag{87}$$

The controller (84) is singular if the velocity of the WMR is zero. This situation should be avoided.

3. Energetic Swarm Control

This section introduces the energetic swarm control. Sliding mode control is primarily used to calculate virtual controllers and the control allocation is used to find actual control inputs. Firstly, the control allocation approach will be discussed without saturation constraints but later, saturation constraints are brought with the control allocation. Simulation results are provided to study the energetic swarm behavior.

3.1. Problem Statement

This section presents the theory of energetic swarm control developed as in [48]. Consider a swarm system with M members. The following second order model represents the energetic swarm motion:

$$\begin{aligned} m_i \dot{\mathbf{v}}_i &= h_i \mathbf{u}_i - b_i \mathbf{v}_i + \mathbf{d}_i(t) \\ \dot{\mathbf{x}}_i &= \mathbf{v}_i \end{aligned} \tag{88}$$

where for each member i, $i = 1,2,\ldots,M$, mass is given by m_i, $\mathbf{x}_i \in R^n$ represents the position, $\mathbf{v}_i \in R^n$ represents the velocity, h_i is the control coefficient associated with the control input given by $\mathbf{u}_i \in R^n$, b_i is the coefficient of the viscous damping $b_i \mathbf{v}_i$ and finally, $\mathbf{d}_i(t) \in R^n$ is the disturbance. The following assumptions are considered.

Assumption 1

The following energetic swarm control theory will be developed for an n dimensional case. Later, in section 3.4, the simulations will be carried out to validate the theorem for a 2-dimensional case. Also, in chapter 5, the high level swarm layer (88)

considered is for a 2-D case since here the energetic swarm control theory will be applied for a WMRs system (165).

Assumption 2

In this chapter, we consider particle dynamics (88) to develop the energetic swarm control theory. However, later in chapter 5 it is shown that the energetic swarm can be applied for vehicles with nonholonomic dynamics with a combination of a low level layer (165)-(174). Future research will focus on rigid body dynamics.

Assumption 3

The mass m_i, the coefficient of the viscous damping b_i and the control coefficient h_i are known for each agent.

Assumption 4

There will be no communication delay among the members in updating their states and their motion is synchronous. That is no time delay is assumed in transferring the states of one member to the other members. This system is a centralized one when considering the experimental implementation. It means that, though there is no leader follower approach here, each agent has to transfer its state to every other member. Future research will focus on each member transferring its states to the neighbors only.

Assumption 5

The system is controllable. That is $h_i \neq 0 \forall i = 1,....,M$. Further, we assume full state measurement of the system.

Assumption 6

It is assumed that the disturbance is bounded by a positive coefficient β_i , $\forall t \geq 0$.

$$\|\mathbf{d}_i(t)\| \leq \beta_i \; \forall i = 1,.....,M \tag{89}$$

To validate the theory, for simulations, sinusoidal inputs will be considered as the disturbance wherever necessary.

The control input $\mathbf{u}_i$ is the sum of external and internal inputs given as:

$$\mathbf{u}_i = \mathbf{u}_i^{in} + \mathbf{u}_i^{ext} \tag{90}$$

where $\mathbf{u}_i^{ext} \in R^n$ is the external input which makes the swarm to achieve multiple control objectives such as following desired trajectory and tracking the temperature and potential while $\mathbf{u}_i^{in} \in R^n$, the internal input used for the cohesion and collision avoidance between the members of the swarm, is of the following form given as in [37]

$$\mathbf{u}_i^{in} = -\sum_{j=1, j\neq i}^{M} \mathbf{g}(\mathbf{x}_i - \mathbf{x}_j) \tag{91}$$

where $\mathbf{g}: R^n \to R^n$ is the artificial function to create attraction and repulsion forces between members given by

$$\mathbf{g}(\mathbf{x}_i - \mathbf{x}_j) = -(\mathbf{x}_i - \mathbf{x}_j)[g_a^{ij}(\|\mathbf{x}_i - \mathbf{x}_j\|) - g_r^{ij}(\|\mathbf{x}_i - \mathbf{x}_j\|)] \tag{92}$$

where $g_a : R^n \to R^+$ is the magnitude of attraction force for the cohesion between each members and $g_r : R^n \to R^+$ is the magnitude of the repulsion force for the collision avoidance between each members. Further, it is assumed that the g_a has a long range attraction and g_r has a short range repulsion. For example, one choice for the $\mathbf{g}(\cdot)$ is to have a constant attraction and unbounded repulsion between the members i and j given by the following terms

$$g_a(\|\mathbf{y}\|) = \frac{A}{\|\mathbf{y}\|} \tag{93}$$

$$g_r(\|\mathbf{y}\|) = \frac{B}{\|\mathbf{y}\|^2} \tag{94}$$

where $A, B \in R^+$. In this particular $\mathbf{g}(\cdot)$, the repulsion forces become dominant than the attraction forces if the agents are closer to each other and the attraction forces are dominant if the members are too far with respect to each other. This $\mathbf{g}(\cdot)$ is of conservative type; that is no energy is added or removed to or from the system since if we consider the whole system the net effect of $\mathbf{g}(\cdot)$ is zero.

Next, the macroscopic quantities such as swarm centre, swarm temperature and swarm potential are defined as following in order to control the overall behavior of the swarm members. It is important to note that the collective behavior of the swarm members is considered rather than an individual member behavior. The swarm centre $\bar{\mathbf{x}} \in R^n$ defined in (95) is the weighted position of each swarm member and the swarm centre velocity $\bar{\mathbf{v}} \in \Re^n$ is given by (96).

$$\bar{\mathbf{x}} = \sum_{i=1}^{M} \bar{\omega}_i \mathbf{x}_i \Big/ \sum_{i=1}^{M} \bar{\omega}_i \tag{95}$$

$$\bar{\mathbf{v}} = \sum_{i=1}^{M} \bar{\omega}_i \mathbf{v}_i \Big/ \sum_{i=1}^{M} \bar{\omega}_i \tag{96}$$

where $\bar{\omega}_i$ is a positive coefficient. Here, one of the objectives of $\mathbf{u}_i^{ext}$ is to make the swarm centre to track a given desired trajectory.

Swarm temperature, another control objective of $\mathbf{u}_i^{ext}$, is what makes the swarm an energetic system. The swarm temperature, defined as the average of swarm internal kinetic energy in [38], is given by the following expression

$$T(\mathbf{v}) = \frac{1}{M}\left(E_k(\mathbf{v}) - E_b(\bar{\mathbf{v}})\right) \tag{97}$$

where E_k in (98) is the weighted kinetic energy of the swarm and E_b in (99) is the weighted bulk kinetic energy of the swarm. $\tilde{\omega}_i$ is a positive coefficient.

$$E_k(\mathbf{v}) = \frac{1}{2}\sum_{i=1}^{M} \tilde{\omega}_i \|\mathbf{v}_i\|^2 \tag{98}$$

$$E_b(\mathbf{v}) = \frac{1}{2}\left(\sum_{i=1}^{M} \tilde{\omega}_i\right) \|\bar{\mathbf{v}}\|^2 \tag{99}$$

If the swarm centre is on a translation, the swarm possesses bulk kinetic energy. However, even if the bulk kinetic energy is zero, swarm has kinetic energy since it is due to the individual swarm members' back and forth motion relative to the swarm centre. For a homogeneous case, the swarm temperature is directly proportional to the velocity difference between the members [38].

The final control objective of the $\mathbf{u}_i^{ext}$ is to track a potential like function $J \in R^+$ by which the swarm is kept in cohesion. That is it keeps the swarm size bounded. The swarm size $\rho \in \Re^+$ is defined as

$$\rho = \max_{i=1,2.....M} \left(\|\mathbf{x}_i - \bar{\mathbf{x}}\|\right) \tag{100}$$

A particular choice of the potential function J is given by

$$J = \frac{1}{2}\sum_{i=1}^{M} \alpha_i \|\mathbf{x}_i - \bar{\mathbf{x}}\|^2 \tag{101}$$

where α_i is the connection weight. This potential function can be considered as the swarm members are connected with the swarm centre by linear attraction or repulsion potential functions depending on the choice of α_i.

3.2. Sliding Control Design

The virtual control inputs for the swarm centre trajectory tracking, temperature and potential tracking will be calculated using the sliding mode control as proposed in [48]. The actual inputs will be calculated using the control allocation approach which be discussed in the next section.

A. Tracking Control

Let us define the tracking error $\tilde{\mathbf{x}}$ and the sliding surface $\bar{\mathbf{s}}$ as

$$\tilde{\mathbf{x}} = \bar{\mathbf{x}} - \bar{\mathbf{x}}_{des} \tag{102}$$

$$\bar{\mathbf{s}} = \begin{bmatrix} \bar{s}_1 \\ \cdot \\ \cdot \\ \bar{s}_n \end{bmatrix} = \dot{\tilde{\mathbf{x}}} + diag(\bar{\boldsymbol{\lambda}})\tilde{\mathbf{x}} \tag{103}$$

where $\bar{\mathbf{x}}_{des}$ is the desired swarm centre and $\bar{\boldsymbol{\lambda}} = [\lambda_1 \quad . \quad . \quad \lambda_n]^T$ is a vector with strictly positive constant gain terms. The first differentiation of $\bar{\mathbf{s}}$ is given by

$$\dot{\bar{\mathbf{s}}} = \varsigma + diag(\bar{\boldsymbol{\lambda}})\dot{\tilde{\mathbf{x}}} - \ddot{\bar{\mathbf{x}}}_{des} + \frac{\sum_{i=1}^{M} \frac{\bar{\omega}_i}{m_i} \mathbf{d}_i(t)}{\sum_{i=1}^{M} \bar{\omega}_i} + \frac{\sum_{i=1}^{M} \frac{\bar{\omega}_i}{m_i} h_i \mathbf{u}_i^{ext}}{\sum_{i=1}^{M} \bar{\omega}_i} \tag{104}$$

where ς is given by

$$\varsigma = \frac{\sum_{i=1}^{M} \frac{\bar{\omega}_i}{m_i} h_i \mathbf{u}_{in}^i - \sum_{i=1}^{M} \frac{\bar{\omega}_i}{m_i} b_i \mathbf{v}^i}{\sum_{i=1}^{M} \bar{\omega}_i} \tag{105}$$

The virtual input $\upsilon_c \in R^n$ for the swarm centre tracking is chosen as

$$\mathbf{v}_c = \sum_{i=1}^{M} \frac{\bar{\omega}_i}{m_i} h_i \mathbf{u}_i^{ext} \Big/ \sum_{i=1}^{M} \bar{\omega}_i \tag{106}$$

The virtual controller $\mathbf{v}_c$ is then selected as

$$\mathbf{v}_c = -\left(\boldsymbol{\varsigma} + diag(\bar{\boldsymbol{\lambda}})\dot{\tilde{\mathbf{x}}} - \ddot{\bar{\mathbf{x}}}_{des}\right) - diag(\mathbf{k}_c)\,\mathrm{sgn}(\bar{\mathbf{s}}) \tag{107}$$

where $\mathbf{k}_c$ is a vector of positive constant gain terms given by

$$\mathbf{k}_c = \begin{bmatrix} k_{1c} & k_{2c} & \cdots & k_{nc} \end{bmatrix}^T \tag{108}$$

The time derivative of $\bar{\mathbf{s}}$ then becomes by using (104) , (107) as follows

$$\dot{\bar{\mathbf{s}}} = \frac{\sum_{i=1}^{M} \frac{\bar{\omega}_i}{m_i} \mathbf{d}_i(t)}{\sum_{i=1}^{M} \bar{\omega}_i} - diag(\mathbf{k}_c)\,\mathrm{sgn}(\bar{\mathbf{s}}) \tag{109}$$

In order to satisfy the following (110) sliding condition

$$\frac{1}{2}\frac{d}{dt}\bar{\mathbf{s}}^T\bar{\mathbf{s}} \le -\sum_{j=1}^{n} \eta_c \left|\bar{s}_j\right| \tag{110}$$

$\mathbf{k}_c$ will be chosen as following with η_c strictly a positive constant.

$$k_{jc} \ge \sum_{i=1}^{M} \frac{\bar{\omega}_i}{m_i} \beta_i \Big/ \sum_{i=1}^{M} \bar{\omega}_i + \eta_c \quad for\ j = 1,2,\ldots\ldots,n \tag{111}$$

Finally, in order to avoid the chattering the virtual controller is modified with the boundary layer as follows

$$\mathbf{v}_c = -\left(\boldsymbol{\varsigma} + diag(\bar{\boldsymbol{\lambda}})\dot{\tilde{\mathbf{x}}} - \ddot{\bar{\mathbf{x}}}_{des}\right) - diag(\mathbf{k}_c)\,sat(diag(\boldsymbol{\varepsilon}_c)\bar{\mathbf{s}}) \tag{112}$$

where $sat(\cdot)$ is the saturation function and $\boldsymbol{\varepsilon}_c = \begin{bmatrix} \frac{1}{\varepsilon_1} & . & . & \frac{1}{\varepsilon_n} \end{bmatrix}^T$, the thickness of the boundary layer, is a vector with positive constant gain terms.

B. Swarm Temperature Tracking

Next, the virtual controller for the swarm temperature will be discussed. The sliding surface s_T for the swarm temperature tracking is defined as

$$s_T = T(\mathbf{v}) - T_{des} \tag{113}$$

where T_{des} is the desired swarm temperature. The first derivative of s_T is given by

$$\dot{s}_T = \frac{\sigma + \gamma + \psi}{M} + \frac{1}{M}\left\{\sum_{i=1}^{M} \frac{h_i}{m_i}\left(\tilde{\omega}_i \mathbf{v}_i - \varpi \bar{\omega}_i \bar{\mathbf{v}}\right)^T \mathbf{u}_{ext}^i\right\} - \dot{T}_{des} \tag{114}$$

where ϖ is a coefficient given by

$$\varpi = \sum_{i=1}^{M} \tilde{\omega}_i \Big/ \sum_{i=1}^{M} \bar{\omega}_i \tag{115}$$

and the terms σ, γ, ψ are given by

$$\begin{aligned}
\sigma &= \left(\sum_{i=1}^{M} h_i \frac{\tilde{\omega}_i}{m_i} (\mathbf{u}_i^{in})^T \mathbf{v}_i\right) - \varpi \bar{\mathbf{v}}^T \left(\sum_{i=1}^{M} h_i \frac{\bar{\omega}_i}{m_i} \mathbf{u}_i^{in}\right) \\
\gamma &= \sum_{i=1}^{M}\left((\mathbf{v}_i)^T \frac{\tilde{\omega}_i}{m_i} \mathbf{d}_i(t)\right) - \varpi \bar{\mathbf{v}}^T \left(\sum_{i=1}^{M} \frac{\bar{\omega}_i}{m_i} \mathbf{d}_i(t)\right) \\
\psi &= \bar{\mathbf{v}}^T \varpi \left(\sum_{i=1}^{M} \frac{\bar{\omega}_i}{m_i} b_i \mathbf{v}_i\right) - \sum_{i=1}^{M}\left((\mathbf{v}_i)^T \frac{\tilde{\omega}_i}{m_i} b_i \mathbf{v}_i\right)
\end{aligned} \tag{116}$$

The virtual input $\upsilon_T \in R$ for the swarm temperature tracking is then chosen as

$$\upsilon_T = \frac{1}{M}\left\{\sum_{i=1}^{M} \frac{h_i}{m_i}\left(\tilde{\omega}_i \mathbf{v}_i - \varpi \bar{\omega}_i \bar{\mathbf{v}}\right)^T \mathbf{u}_{ext}^i\right\} \tag{117}$$

The virtual controller υ_T for the swarm temperature tracking is selected as

$$\upsilon_T = -\frac{\sigma + \psi}{M} - k_T \operatorname{sgn}(s_T) + \dot{T}_{des} \tag{118}$$

where k_T is a positive constant gain term.

Time derivative of $\dot{s}_T$ then becomes by using (114), (118) as follows

$$\dot{s}_T = \frac{\gamma}{M} - k_T \operatorname{sgn}(s_T) \tag{119}$$

The upper bound of γ is calculated using (89) as

$$\gamma \le \left(\sum_{i=1}^{M} \frac{\beta_i \tilde{\omega}_i}{m_i} \|\mathbf{v}_i\| + \varpi \|\bar{\mathbf{v}}\| \sum_{i=1}^{M} \frac{\beta_i \bar{\omega}_i}{m_i} \right) \tag{120}$$

Then using (120), k_T is chosen as (121) with η_T a positive constant in order to satisfy sliding condition $s_T \dot{s}_T \le -\eta_T |s_T|$.

$$k_T(\mathbf{v}) = \frac{1}{M} \left(\sum_{i=1}^{M} \frac{\beta_i \tilde{\omega}_i}{m_i} \|\mathbf{v}_i\| + \varpi \|\bar{\mathbf{v}}\| \sum_{i=1}^{M} \frac{\beta_i \bar{\omega}_i}{m_i} \right) + \eta_T \tag{121}$$

Finally, in order to avoid the chattering the virtual controller is modified with the boundary layer as follows (122) and ε_T is the thickness of the boundary layer.

$$\upsilon_T = -\frac{\sigma + \psi}{M} - k_T \, sat\left(\frac{s_T}{\varepsilon_T} \right) + \dot{T}_{des} \tag{122}$$

C. Swarm Potential tracking

Finally, the virtual controller design for the swarm potential tracking will be discussed. The sliding surface s_J for the swarm potential tracking is defined as

$$s_J = \dot{J} + \lambda_J (J - J_{des}) \tag{123}$$

where J_{des} is the desired swarm potential and λ_J is a positive constant. The first derivative of s_J is given by

$$\dot{s}_J = \tilde{\xi} + \sum_{i=1}^{M} \left(\alpha_i \frac{h_i}{m_i} (\mathbf{x}_i - \bar{\mathbf{x}}) - \frac{\bar{\omega}_i}{m_i} h_i \chi \right)^T \mathbf{u}_i^{ext} + \sum_{i=1}^{M} \left(\alpha_i \frac{1}{m_i} (\mathbf{x}_i - \bar{\mathbf{x}}) - \frac{\bar{\omega}_i}{m_i} \chi \right)^T \mathbf{d}_i(t) + \lambda_J \dot{J} \tag{124}$$

where $\tilde{\xi}$ is given by (125)

$$\tilde{\xi} = \sum_{i=1}^{M} \alpha_i (\mathbf{v}_i - \bar{\mathbf{v}})^T (\mathbf{v}_i - \bar{\mathbf{v}}) + \sum_{i=1}^{M} \left(\alpha_i \frac{h_i}{m_i} (\mathbf{x}_i - \bar{\mathbf{x}}) - \frac{\bar{\omega}_i}{m_i} h_i \chi \right)^T \mathbf{u}_i^{in} - \sum_{i=1}^{M} \left(\alpha_i \frac{b_i}{m_i} (\mathbf{x}_i - \bar{\mathbf{x}}) - \frac{\bar{\omega}_i}{m_i} b_i \chi \right)^T \mathbf{v}_i \tag{125}$$

and the term χ is defined as

$$\chi = \sum_{j=1}^{M} \alpha_j (\mathbf{x}_j - \bar{\mathbf{x}}) \Big/ \sum_{j=1}^{M} \bar{\omega}_j \tag{126}$$

The virtual input υ_J for the swarm potential tracking is then chosen as

$$\upsilon_J = \sum_{i=1}^{M} \left(\alpha_i \frac{h_i}{m_i} (\mathbf{x}_i - \bar{\mathbf{x}}) - \frac{\bar{\omega}_i}{m_i} h_i \chi \right)^T \mathbf{u}_i^{ext} \tag{127}$$

The virtual controller for the swarm potential tracking is selected as

$$\upsilon_J = -\left(\tilde{\xi} + \lambda_J \dot{J} \right) - k_J \operatorname{sgn}(s_J) \tag{128}$$

where k_J is a positive constant gain term.

The time derivative of $\dot{s}_J$ then becomes by using (124), (128) as follows

$$\dot{s}_J = \sum_{i=1}^{M} \left(\alpha_i \frac{1}{m_i} (\mathbf{x}_i - \bar{\mathbf{x}}) - \frac{\bar{\omega}_i}{m_i} \chi \right)^T \mathbf{d}_i(t) - k_J \operatorname{sgn}(s_J) \tag{129}$$

In order to satisfy the sliding condition $s_J \dot{s}_J \le -\eta_J |s_J|$ choose k_J as (130) where η_J is a positive constant

$$k_J = \sum_{i=1}^{M} \beta_i \left(\alpha_i \frac{1}{m_i} \|\mathbf{x}_i - \bar{\mathbf{x}}\| + \frac{\bar{\omega}_i}{m_i} \sum_{j=1}^{M} \alpha_j \|\mathbf{x}_j - \bar{\mathbf{x}}\| \Big/ \sum_{j=1}^{M} \bar{\omega}_j \right) + \eta_J \tag{130}$$

Finally, in order to avoid the chattering the virtual controller is modified with the boundary layer as follows (131) and ε_J is the thickness of the boundary layer.

$$\upsilon_J = -\left(\tilde{\xi} + \lambda_J \dot{J} \right) - k_J \, sat\left(\frac{s_J}{\varepsilon_J} \right) \tag{131}$$

3.3. Control Allocation without Saturation

Actual inputs that match the virtual input requirements will be found using the control allocation as in [48]. The energetic swarm system is an over actuated system. Since the system (88) is an n-dimensional case the number of output n_o is $n_o = n+2$. That is tracking the desired swarm centre, and the desired swarm temperature and potential values. If the number of swarm members are given by M, then the number of inputs n_i will be $n_i = M \times n$. The swarm is over actuated when the number of inputs exceeds the number of outputs. That means the solution is not unique. There exists more than one solution for an over actuated system.

In order to find the actual inputs we need to use the control allocation as discussed in section 2.2 . The actual control input vector $\mathbf{u} \in R^{nM}$ is given by

$$\mathbf{u} = \left[\left(\mathbf{u}_1^{ext}\right)^T \quad \left(\mathbf{u}_2^{ext}\right)^T \quad \cdots \quad \left(\mathbf{u}_M^{ext}\right)^T \right]^T \tag{132}$$

Now, the virtual input vector υ_c (106) can be re-written as

$$\mathbf{B}_c \mathbf{u} = \upsilon_c \tag{133}$$

where $\mathbf{B}_c$ is given by (134) with $\mathbf{I} \in R^{n \times n}$ is an identity matrix

$$\mathbf{B}_c = \frac{1}{\sum_{i=1}^{M} \overline{\omega}_i} \left[h_1 \frac{\overline{\omega}_1}{m_1} \mathbf{I}_{n \times n} \quad h_2 \frac{\overline{\omega}_2}{m_2} \mathbf{I}_{n \times n} \quad \cdots \quad h_M \frac{\overline{\omega}_M}{m_M} \mathbf{I}_{n \times n} \right]_{n \times m} \tag{134}$$

Similarly, the virtual input for the swarm temperature (117) can be re-written as

$$\mathbf{B}_T \mathbf{u} = \upsilon_T \tag{135}$$

where $\mathbf{B}_T$ is given by

$$\mathbf{B}_T =$$

$$\frac{1}{M}\left[\frac{h_1}{m_1}(\tilde{\omega}_1\mathbf{v}_1 - \varpi\bar{\omega}_1\bar{\mathbf{v}})^T \quad \frac{h_2}{m_2}(\tilde{\omega}_2\mathbf{v}_2 - \varpi\bar{\omega}_2\bar{\mathbf{v}})^T \quad \ldots \quad \frac{h_M}{m_M}(\tilde{\omega}_M\mathbf{v}_M - \varpi\bar{\omega}_M\bar{\mathbf{v}})^T\right] \tag{136}$$

Finally, the virtual input for the swarm potential (127) can be re-written as

$$\mathbf{B}_J\mathbf{u} = \upsilon_J \tag{137}$$

where $\mathbf{B}_J$ is given by

$$\mathbf{B}_J = \begin{bmatrix} \alpha_1\frac{h_1}{m_1}(\mathbf{x}_1 - \bar{\mathbf{x}}) - \frac{\bar{\omega}_1}{m_1}h_1\chi \\ \alpha_2\frac{h_2}{m_2}(\mathbf{x}_2 - \bar{\mathbf{x}}) - \frac{\bar{\omega}_2}{m_2}h_2\chi \\ \vdots \\ \alpha_M\frac{h_M}{m_M}(\mathbf{x}_M - \bar{\mathbf{x}}) - \frac{\bar{\omega}_M}{m_M}h_M\chi \end{bmatrix}^T \tag{138}$$

The equations (133), (135), (137) can be combined together as the following relation

$$\begin{bmatrix} \mathbf{B}_c \\ \mathbf{B}_T \\ \mathbf{B}_J \end{bmatrix}\mathbf{u} = \begin{bmatrix} \boldsymbol{\upsilon}_c \\ \upsilon_T \\ \upsilon_J \end{bmatrix} \tag{139}$$

That is the virtual inputs of the swarm centre, swarm temperature and swarm potential are related to the actual control input $\mathbf{u}$ by the following equation

$$\mathbf{B}\mathbf{u} = \boldsymbol{\upsilon} \tag{140}$$

where $\mathbf{B} \in R^{(n+2)\times nM}$ is the control effectiveness matrix given by

$$\mathbf{B} = \begin{bmatrix} \mathbf{B}_c \\ \mathbf{B}_T \\ \mathbf{B}_J \end{bmatrix} \tag{141}$$

and $\boldsymbol{\upsilon} \in R^{n+2}$ is the virtual input vector consists of virtual inputs of the swarm centre, swarm temperature and swarm potential given by

$$\boldsymbol{\upsilon} = [\boldsymbol{\upsilon}_c^T \quad \upsilon_T \quad \upsilon_J]^T \tag{142}$$

The actual control input will be calculated by formulating the following objective function:

$$\min_{\mathbf{u}} \frac{1}{2}\mathbf{u}^T\mathbf{W}\mathbf{u}, \text{ subject to } \mathbf{B}\mathbf{u} = \mathbf{v} \tag{143}$$

where $\mathbf{W} \in \Re^{nM \times nM}$ is a weighting matrix given by

$$\mathbf{W} = \begin{bmatrix} w_{11}\mathbf{I}_{n\times n} & w_{12}\mathbf{I}_{n\times n} & \cdots & w_{1M}\mathbf{I}_{n\times n} \\ w_{21}\mathbf{I}_{n\times n} & w_{22}\mathbf{I}_{n\times n} & \cdots & w_{2M}\mathbf{I}_{n\times n} \\ \vdots & \vdots & \vdots & \vdots \\ w_{M1}\mathbf{I}_{n\times n} & w_{M2}\mathbf{I}_{n\times n} & \cdots & w_{MM}\mathbf{I}_{n\times n} \end{bmatrix}_{nM\times nM} \tag{144}$$

and each w_{ij} is a weighting coefficient. The pseudo inverse which minimizes the objective function given in (143) is used to solve this control allocation problem. The feasible solution for the $\mathbf{u}$ is given by

$$\mathbf{u} = \left(\mathbf{W}^{-1}\mathbf{B}^T(\mathbf{B}\mathbf{W}^{-1}\mathbf{B}^T)^{-1}\right)\mathbf{v} \tag{145}$$

The above solution solves the over actuated problem and finds the actual control input.

3.4. Simulation Results of Energetic Swarm

In this section, simulation is done to study the behavior of the energetic swarm and to show the validity of the proposed [48] sliding controller design and the control allocation approach given in the above section. The desired swarm centre trajectory, for all the simulations, is selected as $\bar{\mathbf{x}}_{des} = [5.0\cos(t)\ \ 5.0\sin(t)]^T$. The disturbance in equation (88) is chosen as $\mathbf{d}_i(t) = [2.0\sin(t)\ \ 2.0\sin(t)]^T$. The attraction term in (93) is given by $\frac{0.2}{\|\mathbf{y}\|}$ and the repulsion tem in (94) is given by $\frac{0.2}{\|\mathbf{y}\|^2}$.

The desired temperature is set at $T_{des} = 5.0$ and the desired potential is selected as $J_{des} = 5.0$. The number of agents is six for all the experiments. Three sets of results are

shown here. The first set of experiment is to validate all three controllers given by the following figures. In Fig.1, trajectories followed by each individual are shown while Fig.2 shows the swarm size for the selected $T_{des} = 5.0$ and $J_{des} = 5.0$. From Fig.1 it is obvious that the trajectories followed by each individual are highly chaotic. Energetic swarm control focuses on controlling the collective behavior of the swarm rather than controlling the individual's behavior or its trajectory following. Fig.1 shows how the individuals behave for a particular temperature and potential values but, collectively they track the desired swarm centre. By changing the primary parameters temperature and potential, one can change the entire swarm behavior.

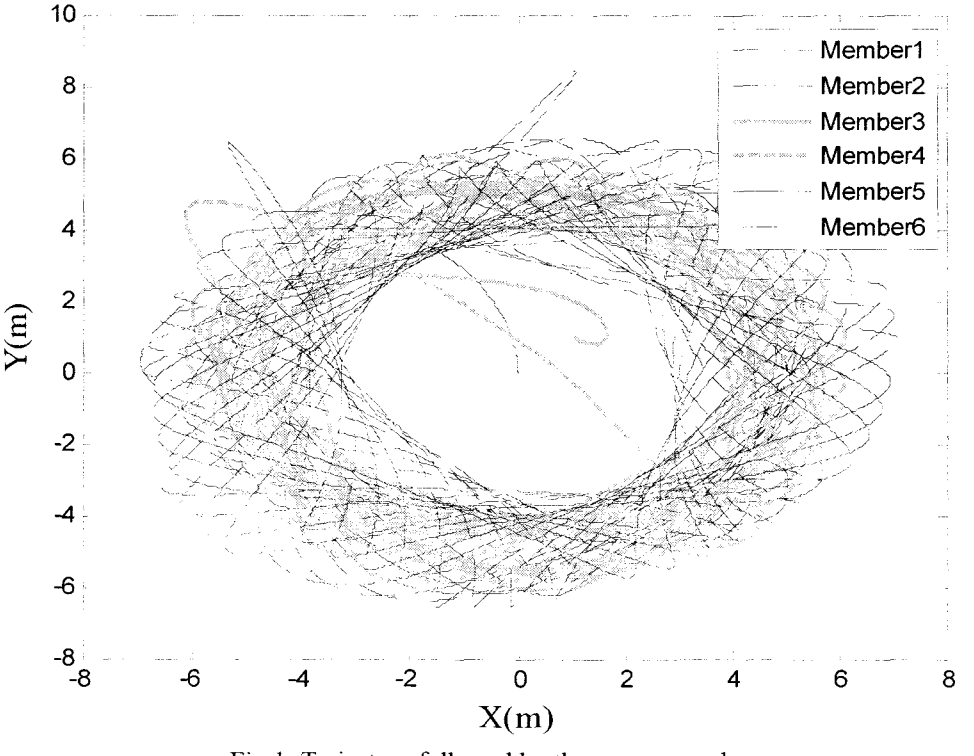

Fig.1. Trajectory followed by the swarm members

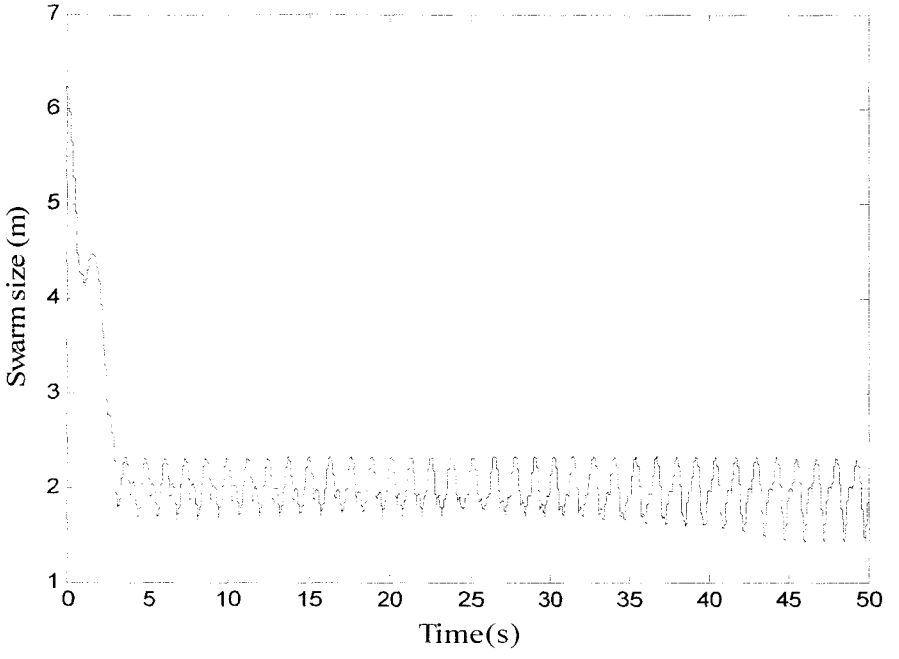

Fig.2. Swarm size

Fig.3 shows the trajectory tracking of the swarm centre while Fig.4 illustrates that the swarm temperature is regulated at $T_{des} = 5.0$

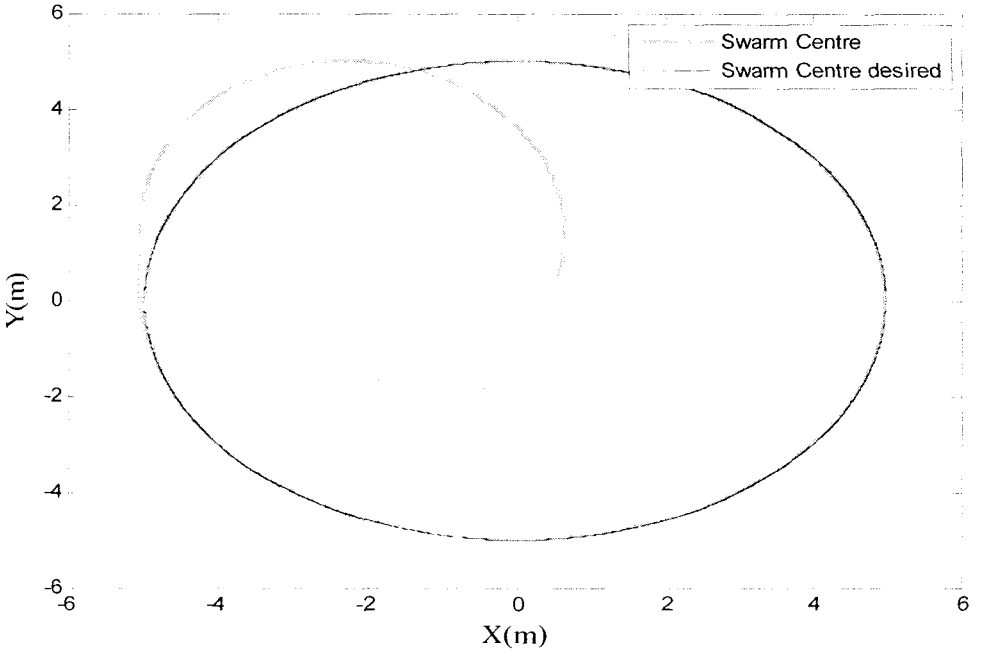

Fig.3. Trajectory tracking of the swarm centre

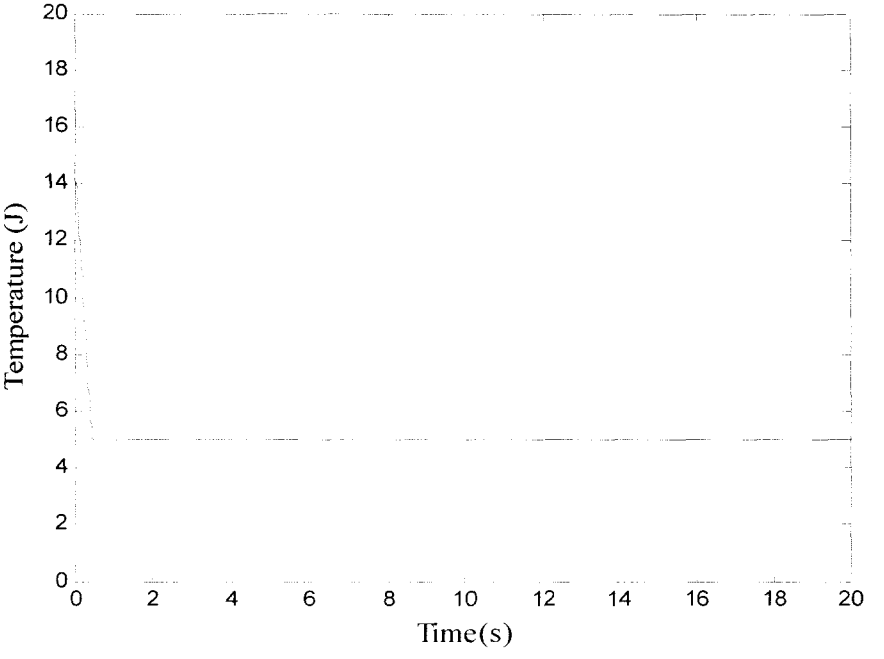

Fig.4. Swarm temperature regulation

Fig.5 shows the potential regulation at $J_{des} = 5.0$

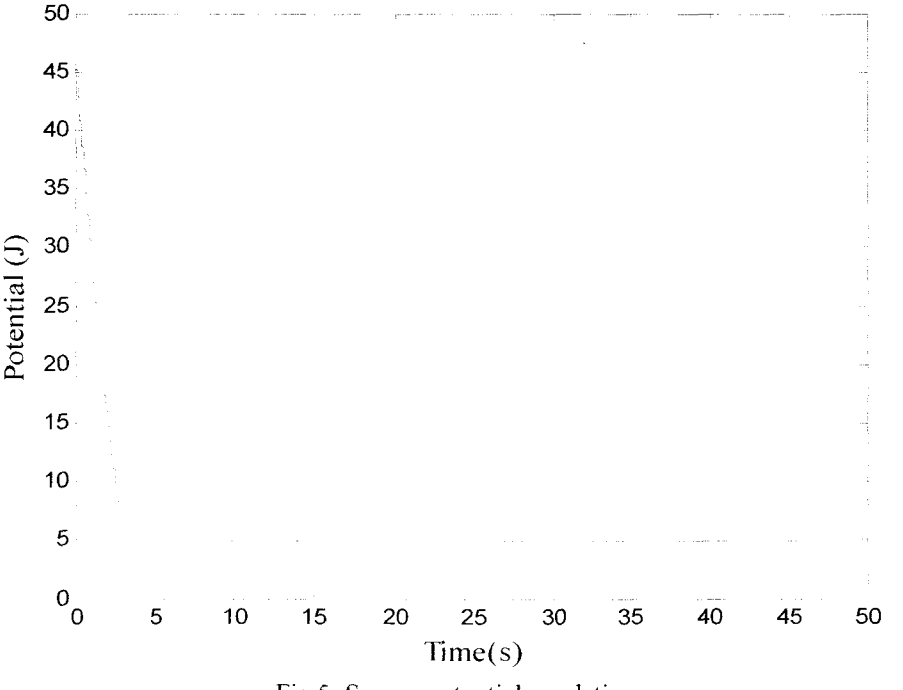

Fig.5. Swarm potential regulation

In the second set of experiment, the potential is kept at $J_{des} = 5.0$ but T_{des} is increased to $T_{des} = 10.0$, $T_{des} = 20.0$ and $T_{des} = 40.0$ respectively. The objective is to study the swarm's foraging behavior when the swarm temperature is increased. Fig.6, Fig.7, and Fig.8 show the individual swarm member's trajectories for the $T_{des} = 10.0$, $T_{des} = 20.0$ and $T_{des} = 40.0$ respectively. When the swarm temperature is increased, the swarm gets more internal kinetic energy and the swarm is more energetic. This is similar to water molecules kept on a stationary table, move faster and aggressively when we add some heat energy. Each individual travels at higher speed and they sweep more area keeping the maximum swarm size constant with respect to the fixed potential $J_{des} = 5.0$. These figures explain that more foraging behavior can be observed when the swarm temperature is increased.

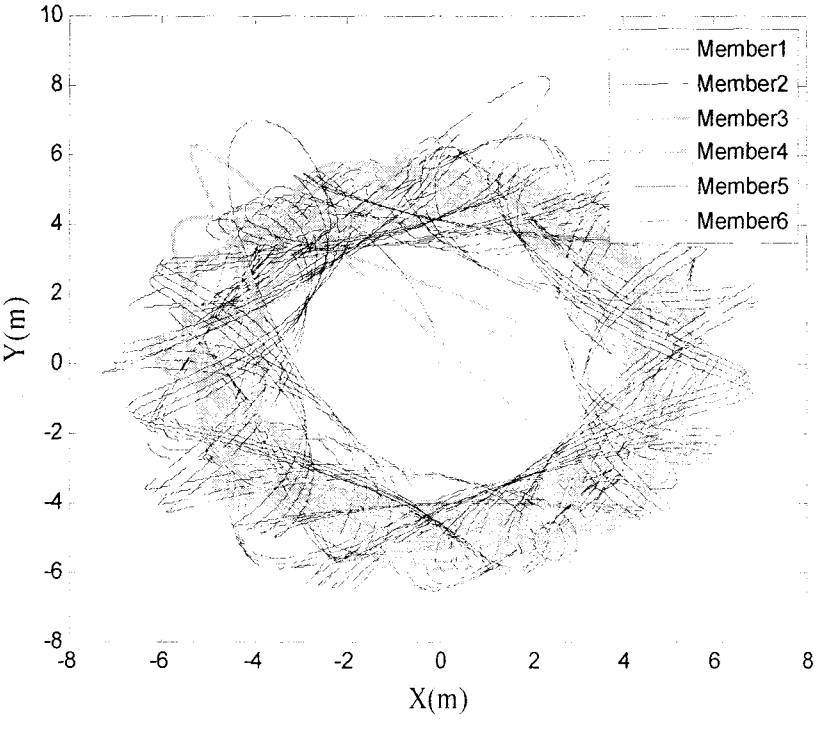

Fig.6. Swarm members trajectories at $T_{des} = 10.0$

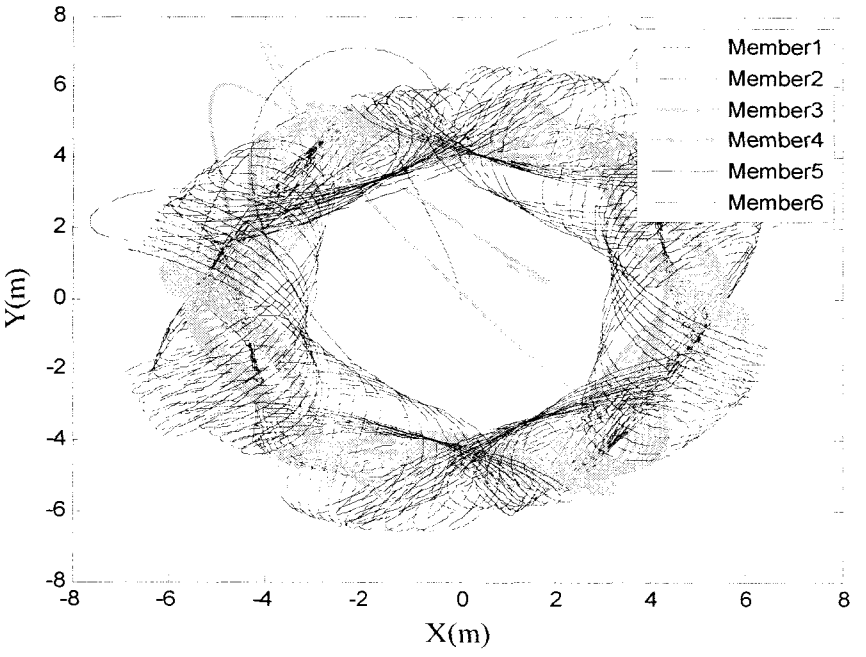

Fig.7. Swarm members trajectories at $T_{des} = 20.0$

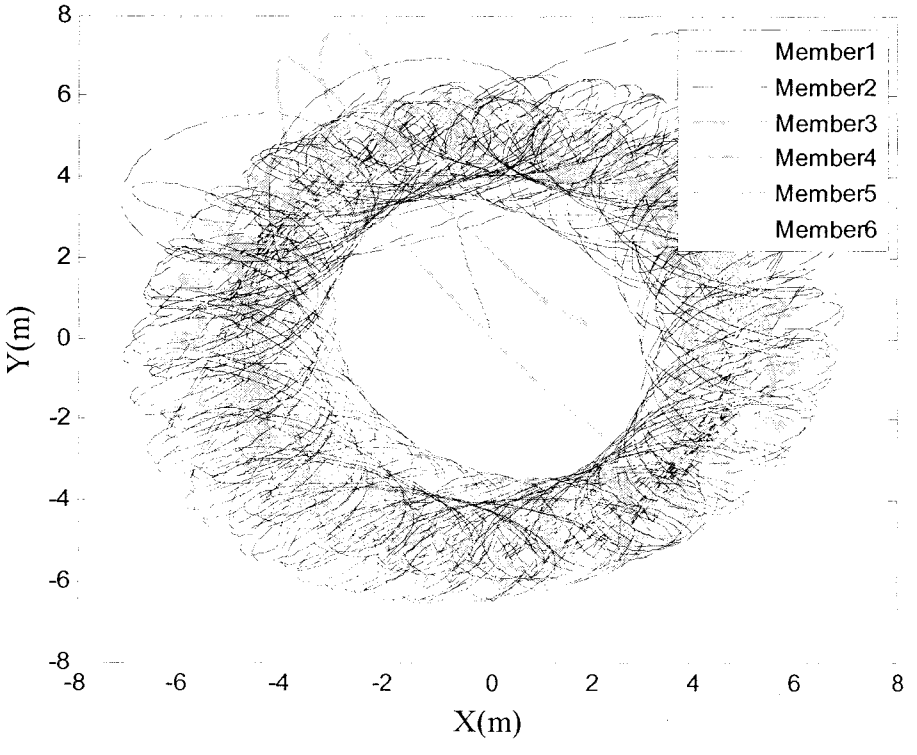

Fig.8. Swarm members trajectories at $T_{des} = 40.0$

In the third set of experiment the swarm temperature is kept at a constant value $T_{des} = 5.0$ but the swarm potential is increased from $J_{des} = 10.0, J_{des} = 20.0$ and $J_{des} = 40.0$ respectively. The objective is to understand the relationship between swarm size and the swarm potential. From Fig.9, Fig.10, and Fig.11, it can be seen that when the swarm potential is increased the swarm size increases. Increasing the swarm potential lessens the cohesiveness of the individual members. When the swarm size increases the attractive forces are more dominant than the repulsive forces since the swarm gets more room to travel in the area.

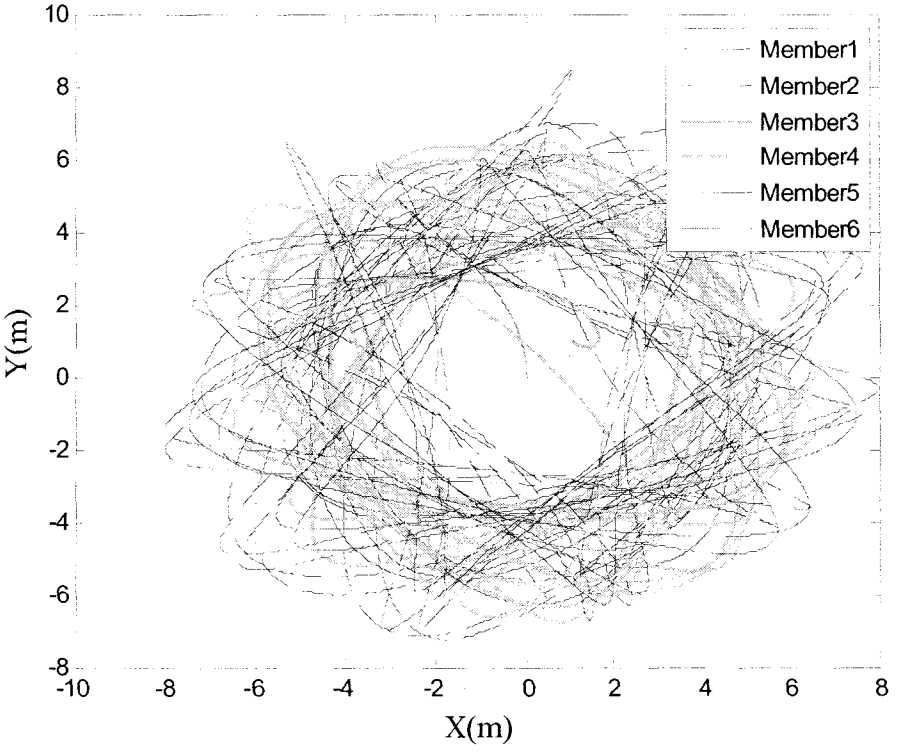

Fig.9. Swarm members trajectories at $J_{des} = 10.0$

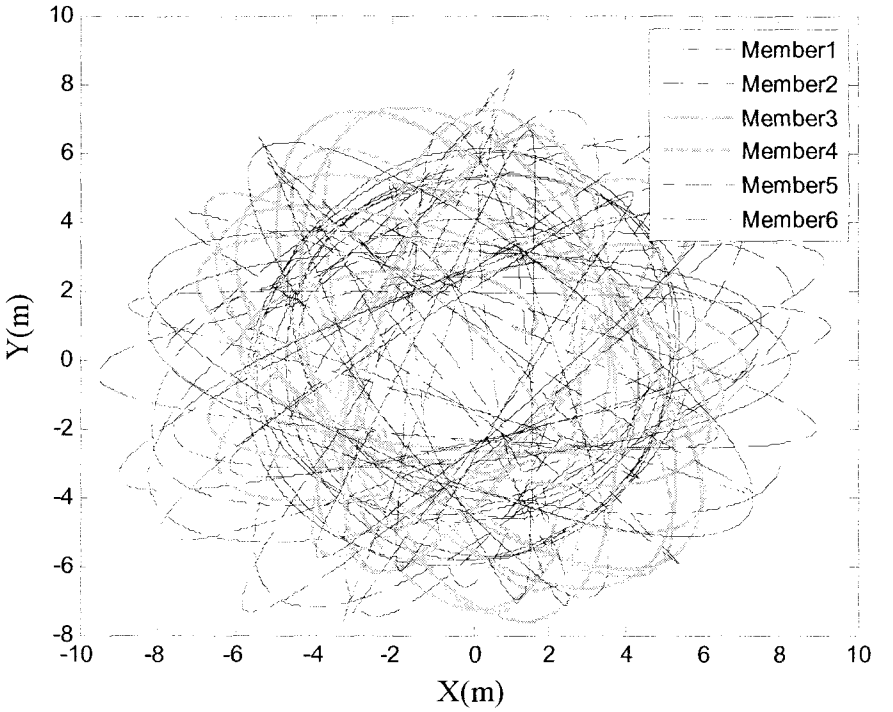

Fig.10. Swarm members trajectories at $J_{des} = 20.0$

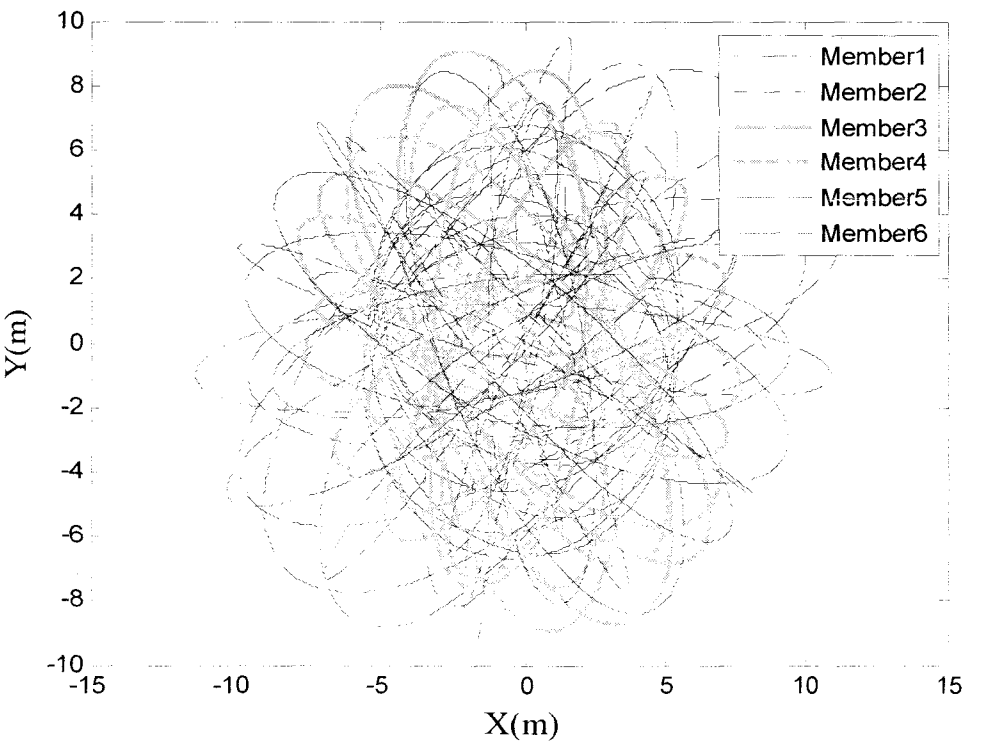

Fig.11. Swarm members trajectories at $J_{des} = 40.0$

The above experiments illustrate that by changing the control variables swarm temperature and potential, the swarm can be made to forage and sweep an area with different kinds of behaviors. Swarm temperature controls the aggressiveness of the members and the foraging behavior of them and the radius of coverage can be controlled by the swarm potential.

3.5. Control Allocation with Saturation

The pseudo inverse approach that was used to minimize the objective function in section 3.3 fails when the solution is not feasible. Further, there is no saturation bound on $\mathbf{u}$, which is not suitable for the practical implementation of the swarm. In real applications the actuators have physical limits. These two problems can be overcome by using the SNOPT [49] optimization solver, a general purpose program for large scale nonlinear programming, minimizes linear or nonlinear functions that have constraints or bounds on variables.

The constraints on the actual control input vector $\mathbf{u}$ are brought with the control allocation algorithm in order to account for the saturation on the inputs. The objective function (143) will be modified as follows [56]:

$$\begin{aligned} &\min_{\mathbf{u}} \frac{1}{2}\mathbf{u}^T\mathbf{W}\mathbf{u}, \\ &\text{subject to} \\ &\mathbf{B}\mathbf{u} = \boldsymbol{\upsilon} \\ &\mathbf{u}_i^{ext}{}_{\min} \le \mathbf{u}_i^{ext} \le \mathbf{u}_i^{ext}{}_{\max},\ i = 1,2,\ldots M \end{aligned} \tag{146}$$

where $\mathbf{u}_i^{ext}{}_{\min}$ and $\mathbf{u}_i^{ext}{}_{\max}$ correspond to the lower and upper saturation limits of the input $\mathbf{u}_i^{ext}$ respectively. For example, in a servo motor $\mathbf{u}_i^{ext}{}_{\max}$ can correspond to the maximum

positive voltage that can be applied to make the motor rotate in clockwise and $\mathbf{u}_{i\ \min}^{ext}$ can be that of in the opposite direction.

However, $\mathbf{u}_{i\ \min}^{ext}, \mathbf{u}_{i\ \max}^{ext}$ can not be lowered than a threshold value, otherwise the control allocation problem (146) is not feasible. That is the SNOPT cannot find feasible solution for the actual control input that satisfies the virtual input requirements. That mean we have to find and set the allowable $\mathbf{u}_{i\ \min}^{ext}, \mathbf{u}_{i\ \max}^{ext}$ values such that they are above the minimum allowable values so that allocation problem would be feasible and, also below the maximum allowable values which depend on the physical limits of the actuators.

Fig.12 shows that for one of the members in the swarm, $\mathbf{u}_{i\ \min}^{ext}, \mathbf{u}_{i\ \max}^{ext}$ are set to $+/-5$. These limits are well below the minimum allowable values.

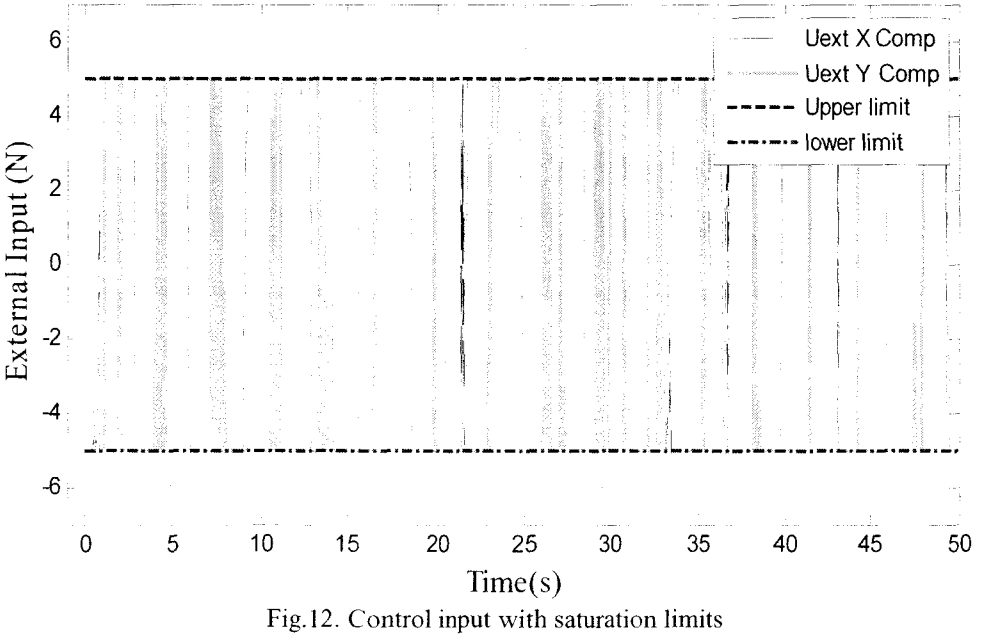

Fig.12. Control input with saturation limits

Fig.13 shows the corresponding error plot between the required virtual inputs and the SNOPT solutions for the desired virtual inputs. It is obvious that the SNOPT cannot satisfy the virtual input demand if we set the $\mathbf{u}_{i\,\min}^{ext}, \mathbf{u}_{i\,\max}^{ext}$ below the threshold value.

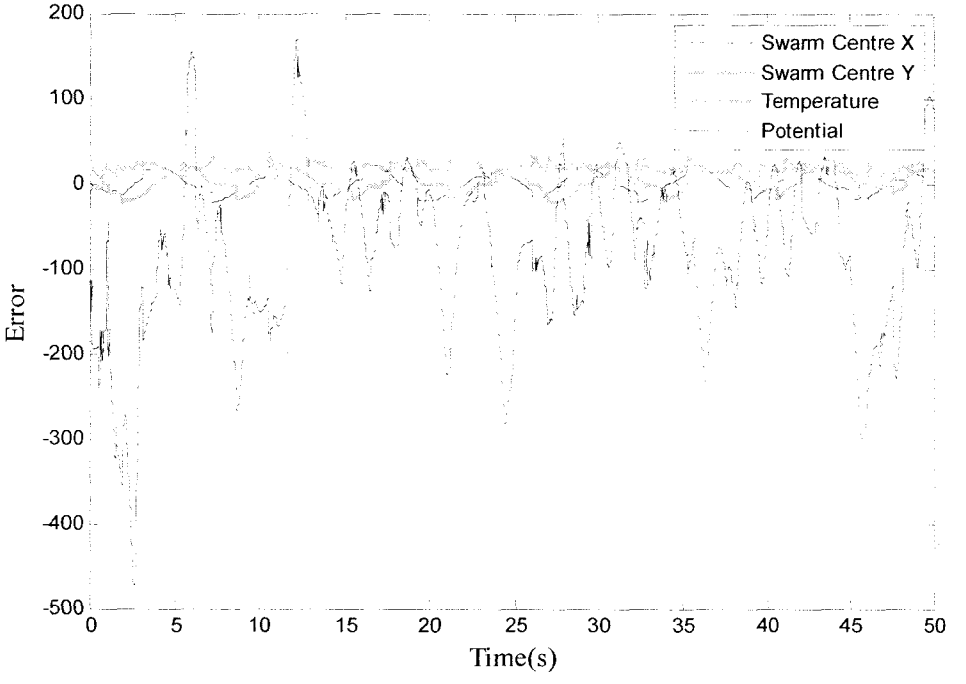

Fig.13. Difference between the desired virtual input and the SNOPT solution

The minimum allowable values of $\mathbf{u}_{i\,\min}^{ext}, \mathbf{u}_{i\,\max}^{ext}$ depends on various factors such as the desired temperature and potential values T_{des} and J_{des}, the desired swarm centre trajectory $\bar{\mathbf{x}}_{des}$ and the initial condition of the swarm members.

It is found that the minimum allowable values can be varied for transient and steady state cases. As such, the minimum allowable values of $\mathbf{u}_{i\,\min}^{ext}, \mathbf{u}_{i\,\max}^{ext}$ can further be set to two different values. In order to get a feasible solution for the allocation problem throughout the run time, one set of values may be used for the transient case and another set for the steady state case. For instance, during the transient phase if the minimum

allowable values are higher than the steady state case values, we can set the threshold to some higher values and then once the system stabilizes we can lower the minimum allowable $\mathbf{u}_i^{ext}{}_{\min}, \mathbf{u}_i^{ext}{}_{\max}$ values. By doing so, the SNOPT satisfies the virtual input constraints with feasible solution throughout the run time of the swarm.

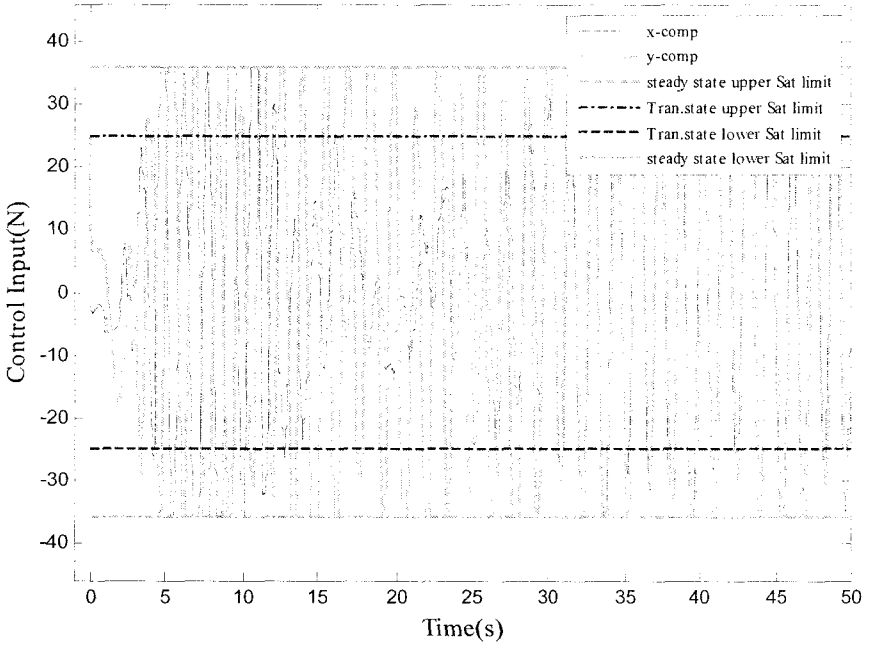

Fig.14. Control input with two sets of saturation limits

Fig.14 shows for one of the members of the swarm, two allowable limits are set for $\mathbf{u}_i^{ext}{}_{\min}, \mathbf{u}_i^{ext}{}_{\max}$; one for the transient case and the another one for the steady state case. During the transient phase the value is $+/-25$ but in the steady state case the value is $+/-36$. The SNOPT matches the virtual input requirement for both the cases.

In the steady state case, the primary factors that influence the minimum allowable values of $\mathbf{u}_i^{ext}{}_{\min}, \mathbf{u}_i^{ext}{}_{\max}$ are the desired temperature and potential values. The steady

state minimum allowable values for $\mathbf{u}_i^{ext}{}_{\min}, \mathbf{u}_i^{ext}{}_{\max}$ are found experimentally at different operating conditions over the domain

$$5.0 \le T \le 20 \tag{147}$$

$$5.0 \le J \le 20 \tag{148}$$

varying only the temperature and potential but keeping other conditions fixed. The surface plot in Fig.15 shows how the minimum allowable value varies with respect to the temperature and potential values given for the range (147), (148) .

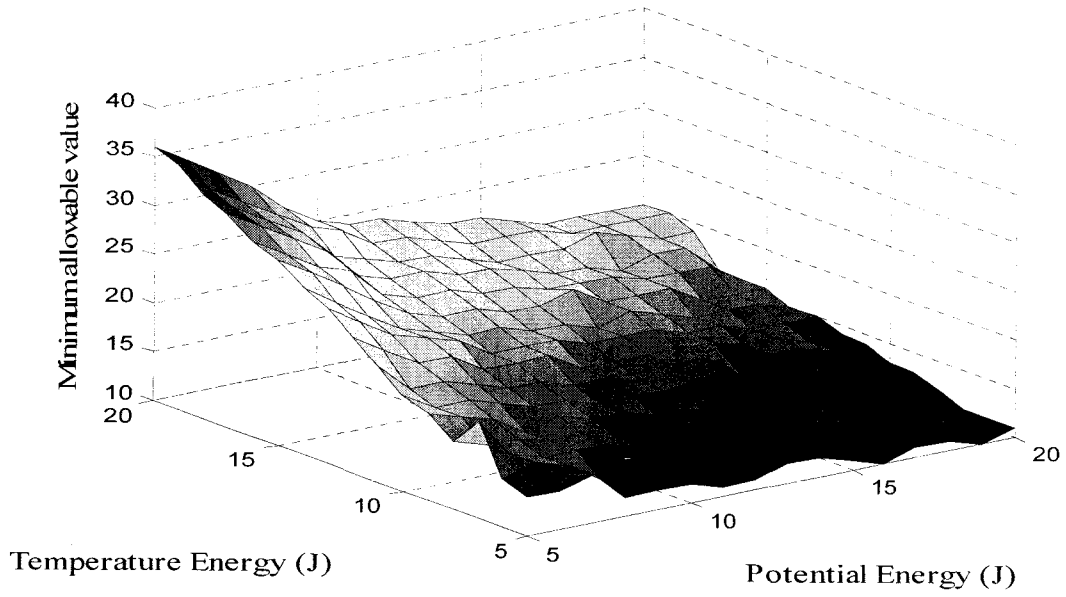

Fig.15. Minimum allowable values of the control input

The result shows that when we increase the temperature the minimum allowable value increases. This is expected since, when we increase the temperature swarm gets more energy and its velocity increases. The swarm is more energetic and it sweeps more area. When the temperature increases while the potential is kept unchanged, the swarm needs more control effort in order to restrict the swarm size. The virtual controller of the temperature (122) primarily depends on σ, ψ during the steady state. In a viscous

environment ψ is more dominant since when the velocity increases the viscous term gets a higher value and the virtual controller for the temperature increases [55]. The swarm needs more control effect to cope with that. If the swarm moves in a non viscous environment σ is more dominant since ψ is zero. Also when the temperature increases σ gets a higher value. This makes more control effort from the controller. The minimum allowable values increase when the desired temperature is increased.

On the other hand, if the potential increases while keeping the swarm temperature fixed, the minimum allowable value decreases for $\mathbf{u}_i^{ext}{}_{\min}, \mathbf{u}_i^{ext}{}_{\max}$. When the potential increases the swarm size increases and it gives the swarm members more room to travel. That is the attraction of the swarm members is more dominant than the repulsion between the members. When the swarm members are confined to a lesser swarm size, the repulsion term in (92) gets more dominant and the swarm controller needs more control effort to keep the members in side the swarm size [55]. As a consequence, the minimum allowable value is higher when potential is small and gets lower when the potential increases.

Let us consider the minimum allowable value of $\mathbf{u}_i^{ext}{}_{\max}$ and denote it by $u_{sat\min}$. Then the feasible operating region U_{sat} of the saturation limits is bounded by [55]

$$u_{sat\min}(T,J) \le U_{sat} \le u_{sat\max} \tag{149}$$

where $u_{sat\max}$ is the physical saturation limit of the actuator. That is the feasible operating region should be above the minimum allowable value in order for the SNOPT to satisfy the virtual input constraints and lesser than the physical saturation limit of the actuator.

When in steady state, the desired temperature T_{des} and potential J_{des} values dominates the upper bound of $u_{sat\min}$. That is if the T_{des} and J_{des} are not varying with time, which is the most common case in this thesis, then the following lower bound on the operating region will be considered [55]

$$u_{sat\min} \le c_0 + c_1 T + c_2 J \le U_{sat} \tag{150}$$

where c_0, c_1, c_2 are determined over the domain (147), (148). The coefficients will be $c_0 = 12.0$, $c_1 = 1.45$, $c_2 = -0.20$ and they satisfy the condition (150) inside the operating region (147), (148). Also, the values should satisfy the condition in (149). That is they should hold

$$c_0 + c_1 T + c_2 J \le U_{sat} \le u_{sat\max} \tag{151}$$

The upper bound of $u_{sat\min}$ in steady state case for a general case, where we need to track time varying T_{des} and J_{des}, will be a nonlinear function and will depend upon on the following parameters [56]

$$u_{sat\min}\left(T, \dot{T}, J, \dot{J}, \ddot{J}\right) \tag{152}$$

However, an approximate lower bound on the operating region can be proposed for a more general case of the swarm as following [56]

$$u_{sat\min} \le c_0 + c_1 T + c_2 J + c_3 \dot{T} + c_4 \dot{J} + c_5 \ddot{J} \tag{153}$$

The coefficients $c_0, c_1, c_2, c_3, c_4, c_5$ need to be determined depending on the desired temperature and potential values. One can expect the same discussion (149)-(153) for the minimum allowable value of $\mathbf{u}_i^{ext}{}_{\min}$. In general, these two limits are equal but their sign or direction is different.

4. Modeling and Identification of Wheeled Vehicles

In order to implement the swarm system experimentally, WMRs are chosen as the primary application since it is much easier to make a swarm with WMRs in an academic environment. As WMRs are actuated by Radio Controlled (RC) servo motors, it is important to model and identify the parameters of the RC servo motor and its dynamic behavior when it is attached with the WMRs. This chapter focuses on the modeling and parameter identification of the WMRs as in [54].

4.1. Kinematic Model of the Wheeled Vehicle

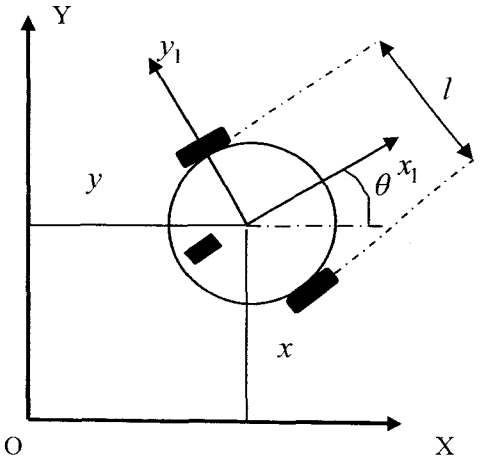

Fig.16. The WMR configuration w.r.t a fixed frame

Fig.16 shows the schematic top view of the WMR. Let us assume that the wheels do not slip. Then the kinematic equation (58) of the WMR is modified as following with v and ω are expressed in terms of angular velocities of the right and left wheels.

$$\dot{x} = \frac{1}{2}(\omega_R R_R + \omega_L R_L)\cos\theta$$
$$\dot{y} = \frac{1}{2}(\omega_R R_R + \omega_L R_L)\sin\theta \qquad (154)$$
$$\dot{\theta} = \frac{1}{l}(\omega_R R_R - \omega_L R_L)$$

where x, y are the coordinates of the body attached frame in the fixed frame OXY, θ is the angle between the heading velocity and the fixed frame, R_R and R_L are the radius of the right and left wheel respectively, ω_R and ω_L are the angular velocities of the right and left servo motors and finally, l is the axle distance between both the wheels. Fig.17 and Fig.18 show one of the WMRs built in the Control and Information System (CIS) lab for the model verification and experimental implementation of the swarm system.

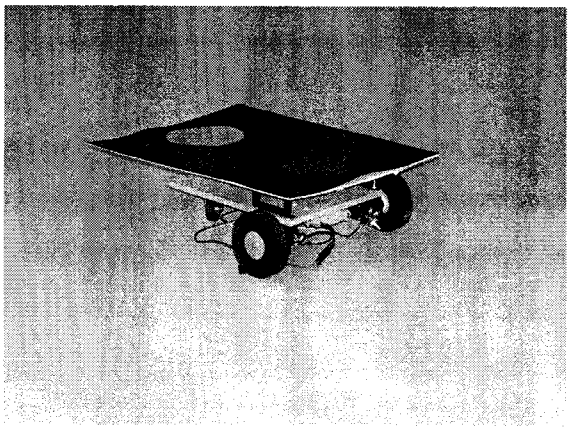

Fig.17. The perspective view of the WMR

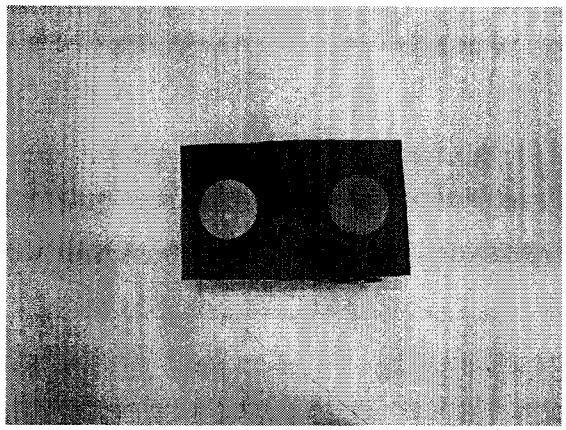

Fig.18. Top view of the WMR with color objects

4.2. Dynamic Model of the Vehicle Actuators

Each WMR is attached with two RC servo motors that are modified for the continuous rotation. Since it is modified, the pulse width is proportional to the angular velocity of the motor in the operating range. The input to the motor is the voltage across

data acquisition card (MultiQ) and it is transmitted wirelessly and converted into pulse width. The modeling equation, governing the dynamics of the motor, given in [54] is

$$J_{wm}\dot{\omega}_{wm} = K_{1wm}U_{wm} - \eta_{wm}\omega_{wm} - K_{bwm}\omega_{wm} - \mu_{wm}\text{sgn}(\omega_{wm}) \tag{155}$$

where J_{wm} denotes the moment of inertia, $\dot{\omega}_{wm}$ represents the angular acceleration, K_{1wm} and η_{wm} are constant parameters associated with the motor, the voltage applied to the motor via the MultiQ is given by U_{wm}, ω_{wm} is the angular velocity of the motor, the linear friction coefficient of the motor is given by K_{bwm} and finally, μ_{wm} is the Coulomb friction coefficient.

4.2.1. State Equations of the Wheeled Vehicles

The state equation of the wheel vehicle is the combination of kinematic equation of the WMR and the dynamic equation of the actuators given by (156) . The equation (155) is considered for both the left and right wheels of WMR with subscripts L and R denoting those respectively and the term wm is removed for the ease of representation.

$$\begin{aligned}
&\dot{x} - \frac{1}{2}(\omega_R R_R + \omega_L R_L)\cos\theta \\
&\dot{y} = \frac{1}{2}(\omega_R R_R + \omega_L R_L)\sin\theta \\
&\dot{\theta} = \frac{1}{l}(\omega_R R_R - \omega_L R_L) \\
&\dot{\omega}_L = \frac{1}{J_L}\left(K_{1,L}U_L - \eta_L\omega_L - K_{b,L}\omega_L - \mu_L\,\text{sgn}(\omega_L)\right) \\
&\dot{\omega}_R = \frac{1}{J_R}\left(K_{1,R}U_R - \eta_R\omega_R - K_{b,R}\omega_R - \mu_R\,\text{sgn}(\omega_R)\right)
\end{aligned} \tag{156}$$

4.3. Apparatus

The swarm experiment was done in the CIS lab. The WMRs were built with two front drive wheels and one rear castor wheel. The wheels were driven by the HS-422 servo motors which had been modified to allow continuous rotation. Since it is modified, then the pulse width is proportional to the angular velocity of the wheel in the linear operating region considered. The block diagram of the experimental setup is shown in Fig.20.

Vision feedback is used to get WMR's position and the orientation. Arrays of overhead webcams are setup as in Fig.19. There are nine webcams connected individually with nine vision processing computers in order to reduce the processing power and computational time of central host computer. These vision processing computers process the image captured and send the data of the WMR's position and orientation over a network interface to the central server host computer. The test bed roughly covers an area of $5 \times 5m$. The maximum reachable frequency of the webcams is 25Hz.

The host computer, based on data received from the vision processing computers, calculates the inputs to the WMRs. Then the corresponding input values are written on the MultiQ board to which a RC transmitter is attached. Typically 2.5V was taken as the neutral position for the MultiQ interface. The signal is changed into D/A by multiQ and send to the wireless transmitter. The RC wireless receiver, attached with the WMRs, receives the corresponding data and converts back into A/D. To the motors, the signal is sent in as the pulse width. C++ is used as the programming language for the vision processing task and all other control related tasks.

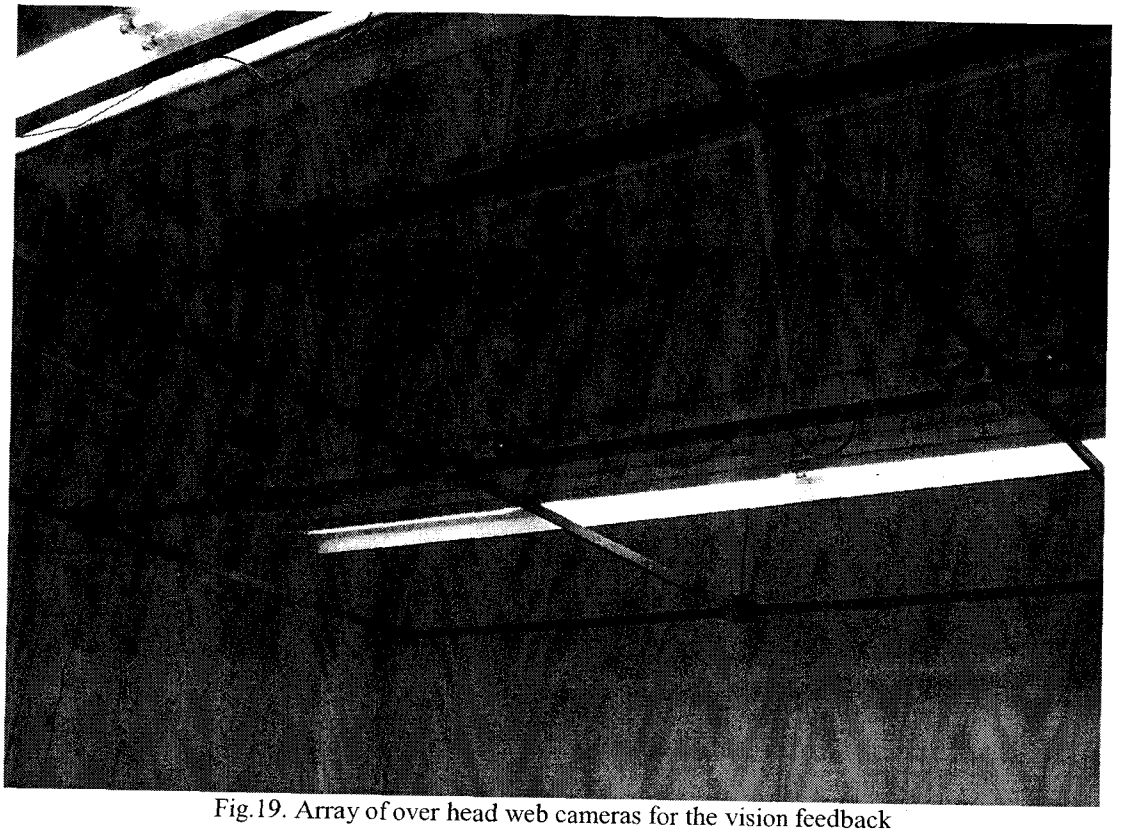

Fig.19. Array of over head web cameras for the vision feedback

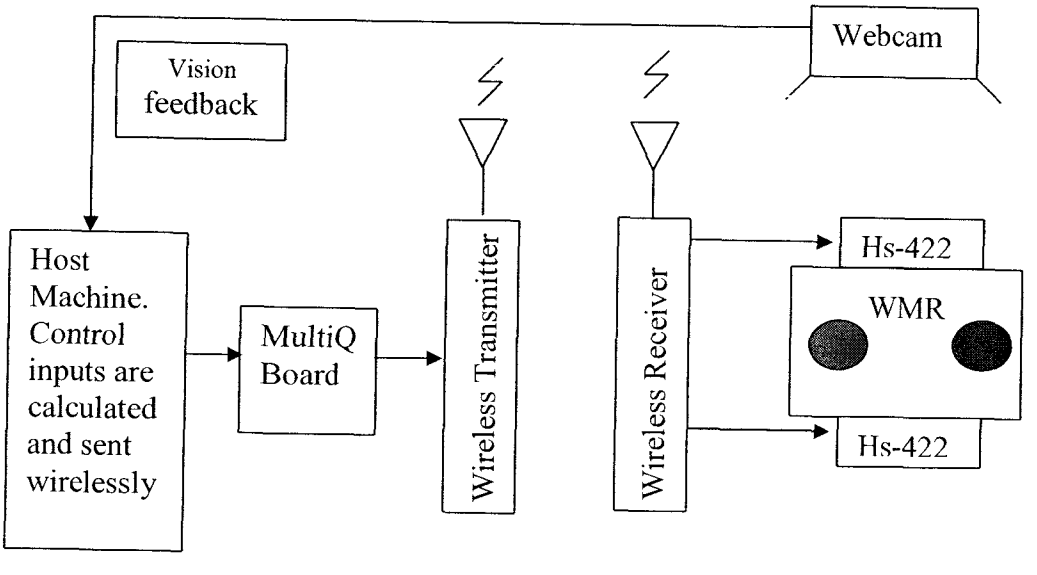

Fig.20. Block diagram of the experimental setup

4.4. Parameter Identification

Vision sensing is used for the position feedback and the central finite difference is used to find the first and second derivatives wherever necessary in the following subsections.

4.4.1. Parameter Identifications of the Actuators

Two different color objects, equally spaced from the axle of the motor, are attached in a cross bar as shown in Fig.21 . The vision library in the CIS lab captures the image and processes it in order to find the centroid of the color targets. The angle is found from the centroidal information. Angular velocity and angular acceleration of the motor are found using the central finite difference method.

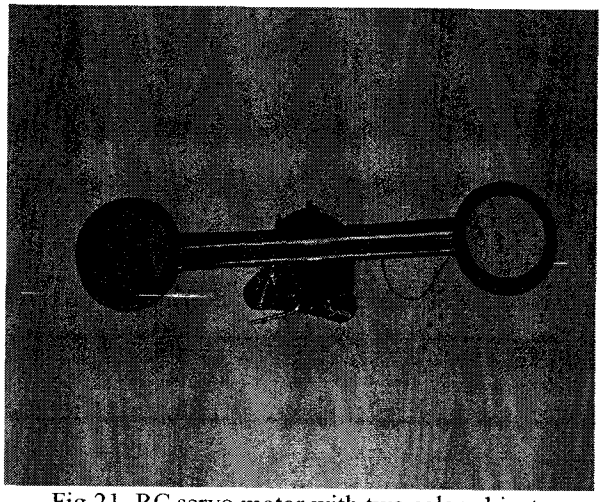

Fig.21. RC servo motor with two color objects

The equation (155) is re arranged since we can minimize the number of parameters to be identified as follows:

$$\dot{\omega} = a_1 U - a_2 \omega - a_3 \operatorname{sgn}(\omega) \tag{157}$$

where a_1, a_2, a_3 are given by

$$
\begin{aligned}
a_1 &= \frac{K_1}{J} \\
a_2 &= \frac{\eta + K_b}{J} \\
a_3 &= \frac{\mu}{J}
\end{aligned}
\tag{158}
$$

The subscript wm is removed for the ease. The least square curve fitting method is used to find out the parameters in (158) . Let $t \in [t_1, t_f]$ be the run time of the experiment. The equation in (157) is then re arranged for the $\forall t \in [t_1, t_f]$ as

$$
\begin{pmatrix}
U(t_1) & -\omega(t_1) & -\text{sgn}(\omega(t_1)) \\
. & . & . \\
. & . & . \\
. & . & . \\
U(t_f) & -\omega(t_f) & -\text{sgn}(\omega(t_f))
\end{pmatrix}
\begin{bmatrix} a_1 \\ a_2 \\ a_3 \end{bmatrix}
=
\begin{bmatrix} \dot{\omega}(t_1) \\ . \\ . \\ . \\ \dot{\omega}(t_f) \end{bmatrix}
\tag{159}
$$

The over determined system (159) can be solved for the parameters a_1, a_2, a_3 using the pseudo inverse method.

Let $\mathbf{A}, \mathbf{Y}, \mathbf{X}$ be given by

$$
\begin{aligned}
\mathbf{A} &= \begin{pmatrix}
U(t_1) & -\omega(t_1) & -\text{sgn}(\omega(t_1)) \\
. & . & . \\
. & . & . \\
. & . & . \\
U(t_f) & -\omega(t_f) & -\text{sgn}(\omega(t_f))
\end{pmatrix} \\
\mathbf{Y} &= \begin{bmatrix} \dot{\omega}(t_1) \\ . \\ . \\ . \\ \dot{\omega}(t_f) \end{bmatrix} \\
\mathbf{X} &= \begin{bmatrix} a_1 \\ a_2 \\ a_3 \end{bmatrix}
\end{aligned}
\tag{160}
$$

Then using the pseudo inverse approach the parameters of the RC motor are given by

$$\mathbf{X} = \left(\mathbf{A}^T\mathbf{A}\right)^{-1}\mathbf{A}^T\mathbf{Y} \tag{161}$$

Two sets of initial conditions (IC) are used to find the parameters of the right and left wheel motors as shown in Table 1.

Time(s)	IC#1	IC#2
$t \leq 5$	$U(t) = 0.0V$	$U(t) = 0.0V$
$t > 5$	$U(t) = 0.5V$	$U(t) = -0.5V$

Table 1. Initial conditions for the parameter identification

Table 2 summarizes the identified parameters a_1, a_2, a_3 for the right wheel motor. The values of a_1, a_2, a_3 are the average values of a number of data samples taken. Same initial conditions are considered for all the different sets of data samples. Also the deviation column gives the maximum and minimum variation of parameters a_1, a_2, a_3 from the average values.

Parameters of the right wheel motor	IC#1	Max/Min Deviation	IC#2	Max/Min Deviation
a_1	243.3405	±14.7115	415.223	±11.749
a_2	9.028315	±0.740805	15.1073	±0.299
a_3	-0.7417085	±1.2905115	-2.585695	±1.420975

Table 2. Parameters of the right wheel motor

Fig.22 and Fig.23 show the angular acceleration and angular velocity of the right wheel motor for the IC#1 respectively. Experimental data set versus the simulation data set, using the estimated parameters in the Table 2, is shown in those figures.

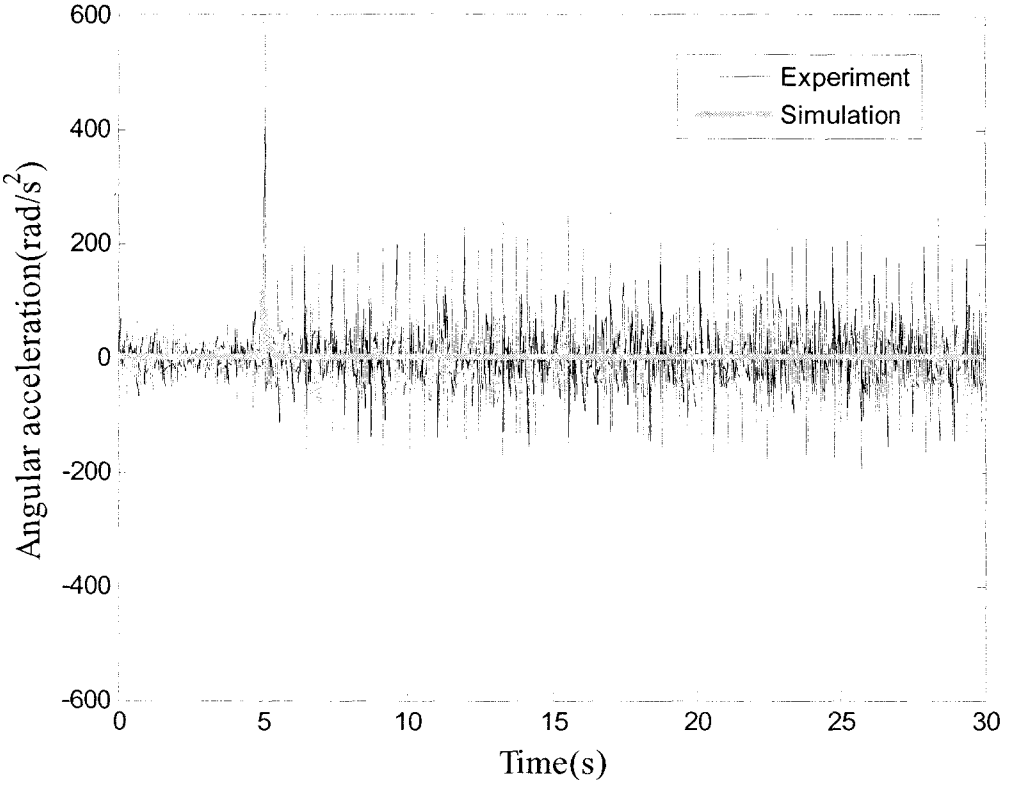

Fig.22. Angular acceleration of the right wheel motor for the IC#1

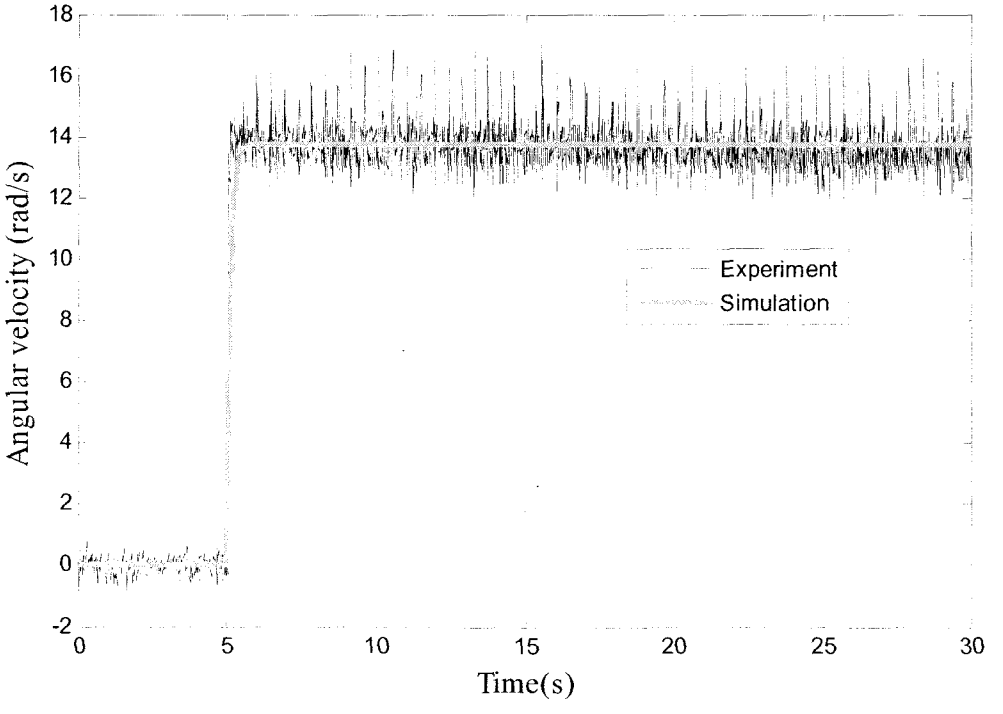

Fig.23. Angular velocity of the right wheel motor for the IC#1

Fig.24 and Fig.25 show the angular acceleration and angular velocity of the right wheel motor for the IC#2 respectively. Experimental data set versus the simulation data set, using the estimated parameter in the Table 2, is shown in those figures.

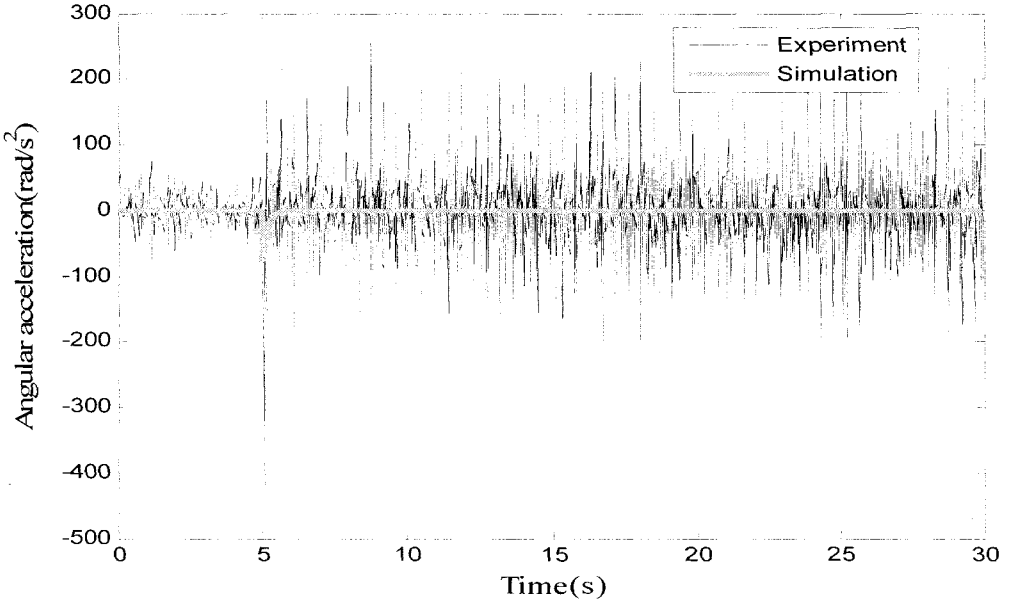

Fig.24. Angular acceleration of the right wheel motor for the IC#2

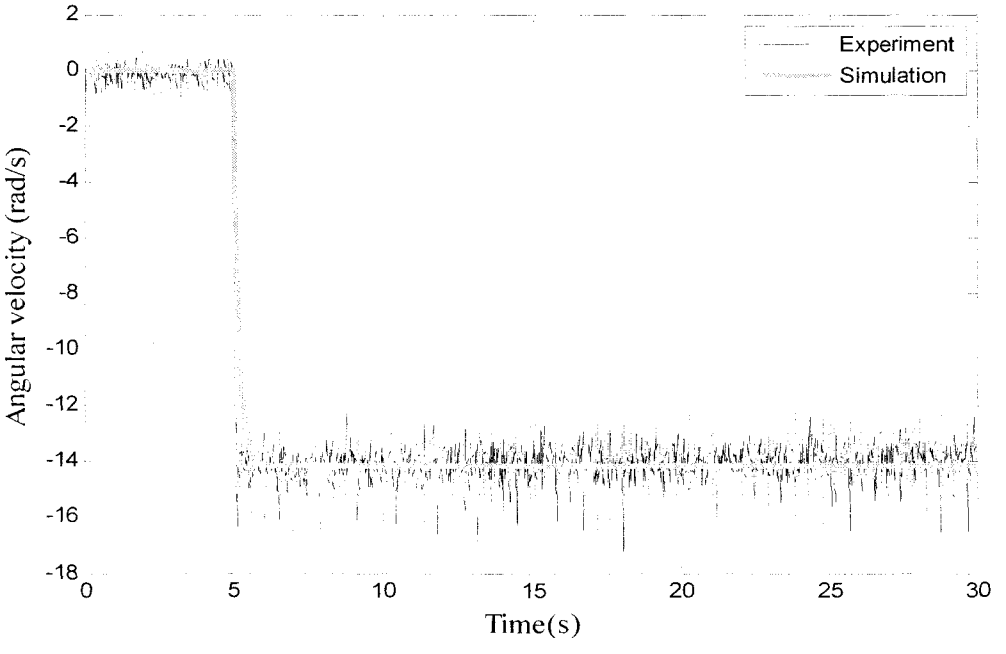

Fig.25. Angular velocity of the right wheel motor for the IC#2

Similarly, Table 3 summarizes the parameters a_1, a_2, a_3 for the left wheel motor. Similar plots for the left the wheel motor can be obtained for the verification but those are omitted here.

Parameters for the left wheel motor	IC#1	Max/Min Deviation	IC#2	Max/Min Deviation
a_1	124.65	±37.357	354.603	±15.25
a_2	4.51495	±4.41181	11.5469	±3.515975
a_3	-6.50073	±2.07883	-2.52157	±1.98958

Table 3. Parameters of the left wheel motor

4.4.2. Model Verification of the Actuators

Now, the average values of the parameters a_1, a_2, a_3 are taken for the right and left wheel motors from the IC#1 and IC#2. Table 4 summarizes the updated values of the parameters a_1, a_2, a_3 for the right and left wheel motors.

Parameters	Right wheel motor	Left wheel motor
a_1	329.2818	239.6265
a_2	12.0678	8.0310
a_3	-1.6637	-4.51115

Table 4. Parameters of right and left wheel motors

This time a sinusoidal input is applied for both the actuators as shown in Table 5. The sinusoidal input is shown such that it does not go beyond the saturation limit of the motors.

Time(s)	IC#3	
	Right wheel motor	Left wheel motor
$t \leq 5$	$U_R = 0.0V$	$U_L = 0.0V$
$t > 5$	$U_R = 0.5\sin(t)$	$U_L = 0.5\sin(t)$

Table 5. Initial conditions for the model verification of the motors

Fig.26 and Fig.27 show the validation of motor parameters for the right and left wheel motors respectively.

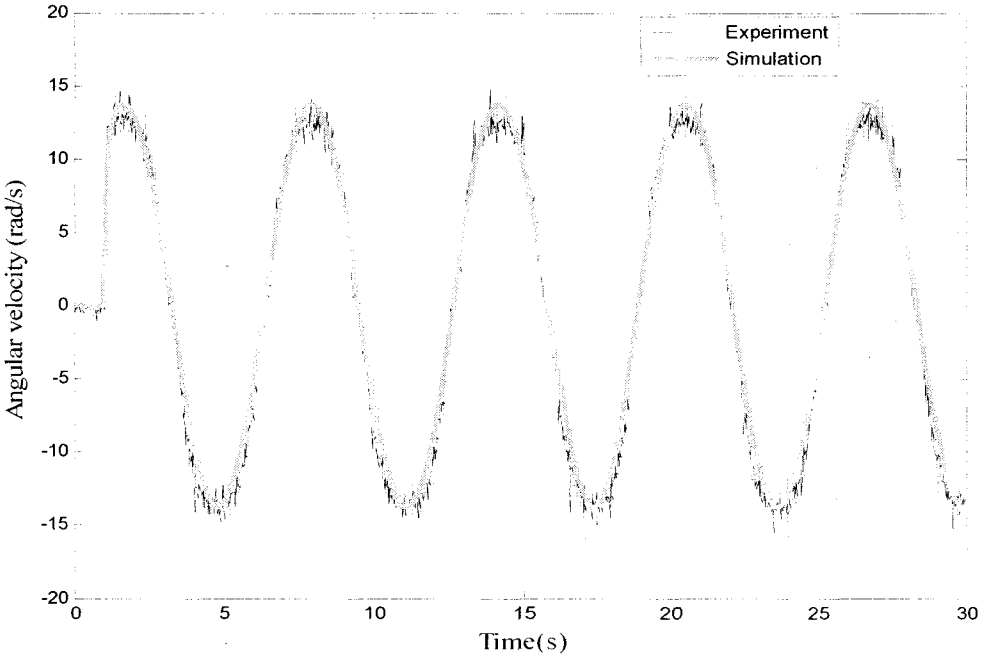

Fig.26. Angular velocity of the right wheel motor for the IC#3

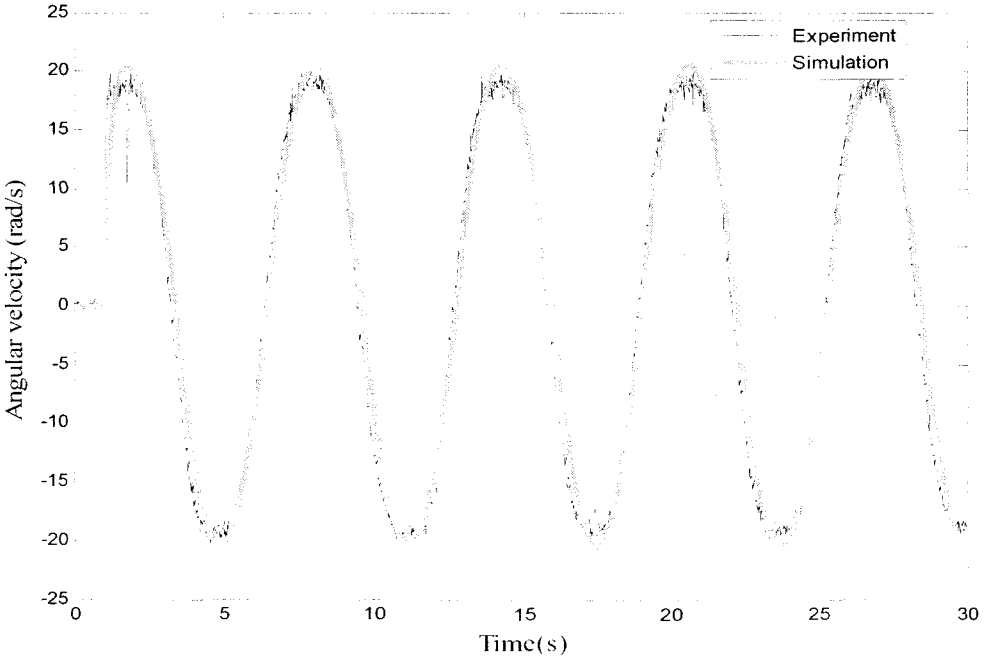

Fig.27. Angular velocity of the left wheel motor for the IC#3

4.4.3. Parameter Identification of the Wheeled Vehicles

The values for the parameters a_1, a_2, a_3 found in previous section need to be checked and fine tuned when they are attached with the WMRs since, when they are attached with WMRs, the rotational friction changes considerably due to the weight of the WMRs. That means when ever the motors are attached with a WMR with different mass and structural configuration, it is necessary to re evaluate the parameters a_1, a_2, a_3 for that particular configuration. For a swarm system, one can assume without loss of generality, that all the members will be homogeneous ones w.r.t mass and structure. It means that, if we could find the parameters for one WMR, we can assume same values for the parameters a_1, a_2, a_3 for all the members.

The equations (156) and (157) are rearranged as in (162) in order to find the angular velocities of the motors and parameters are again re identified for both the left and right wheel motors.

$$
\begin{aligned}
\omega_R &= \frac{1}{2}\left(\frac{2\dot{x}}{R_R\cos\theta} + \frac{l\dot{\theta}}{R_R}\right) iff\ \theta \neq \frac{n\pi}{2}\ \forall n = 1,3,... \\
\omega_R &= \frac{1}{2}\left(\frac{2\dot{y}}{R_R\sin\theta} + \frac{l\dot{\theta}}{R_R}\right) iff\ \theta \neq n\pi\ \forall n = 0,1,2... \\
\omega_L &= \frac{1}{2}\left(\frac{2\dot{x}}{R_L\cos\theta} - \frac{l\dot{\theta}}{R_L}\right) iff\ \theta \neq \frac{n\pi}{2}\ \forall n = 1,3,... \\
\omega_L &= \frac{1}{2}\left(\frac{2\dot{y}}{R_L\sin\theta} - \frac{l\dot{\theta}}{R_L}\right) iff\ \theta \neq n\pi\ \forall n = 0,1,2... \\
\dot{\omega}_R &= a_{1.R}U_R - a_{2.R}\omega_R - a_{3.R}\,\mathrm{sgn}(\omega_R) \\
\dot{\omega}_L &= a_{1.L}U_L - a_{2.L}\omega_L - a_{3.L}\,\mathrm{sgn}(\omega_L)
\end{aligned}
\qquad (162)
$$

This time the translational motion and the rotational motion of the WMR are considered for the parameter identification process. Table 6 summarizes the ICs for the translational motion of the WMR.

Time(s)	IC#4	
	$x=0.511\ \ y=\ 0.3747\ \ \theta=0.7184rad$	
	Right Wheel	Left Wheel
$t \le 5$	$U_R = 0.0V$	$U_L = 0.0V$
$t > 5$	$U_R = 0.5V$	$U_L = 0.5V$

Table 6. Initial conditions for the translational motion of the WMR

Two color objects are attached with the WMR this time for the vision feedback and x, y, θ are obtained. As mentioned earlier the central difference method is used to calculate the $\dot{x}, \dot{y}, \dot{\theta}$. ω_R, ω_L and the parameters a_1, a_2, a_3 for the left and right wheel motors are calculated as in (162).

Fig.28 and Fig.29 show the experimental vs. simulation data of the velocity components in the X and Y directions of the WMR for the IC#4 respectively.

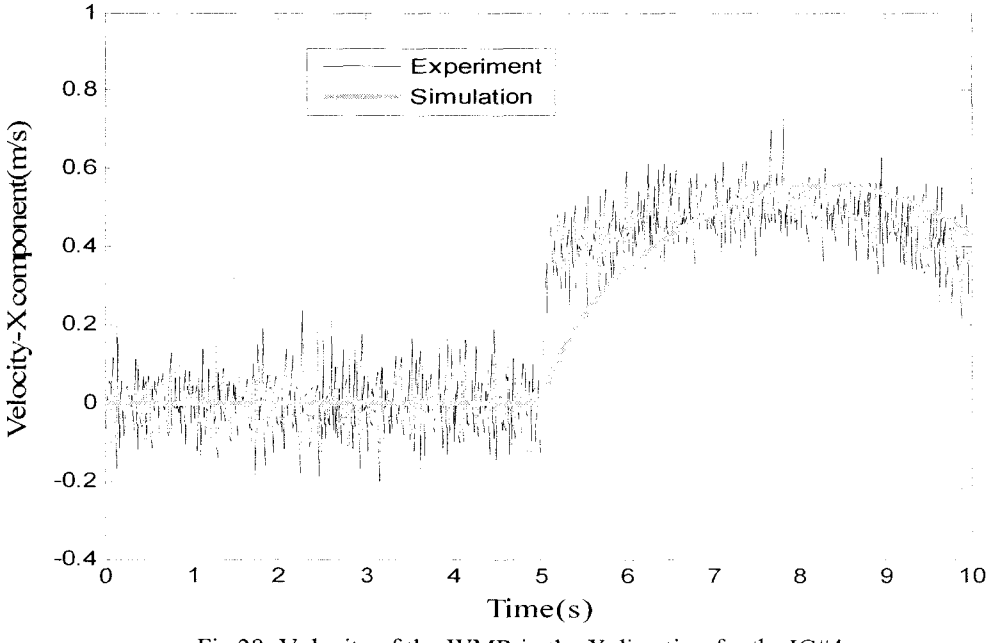

Fig.28. Velocity of the WMR in the X direction for the IC#4

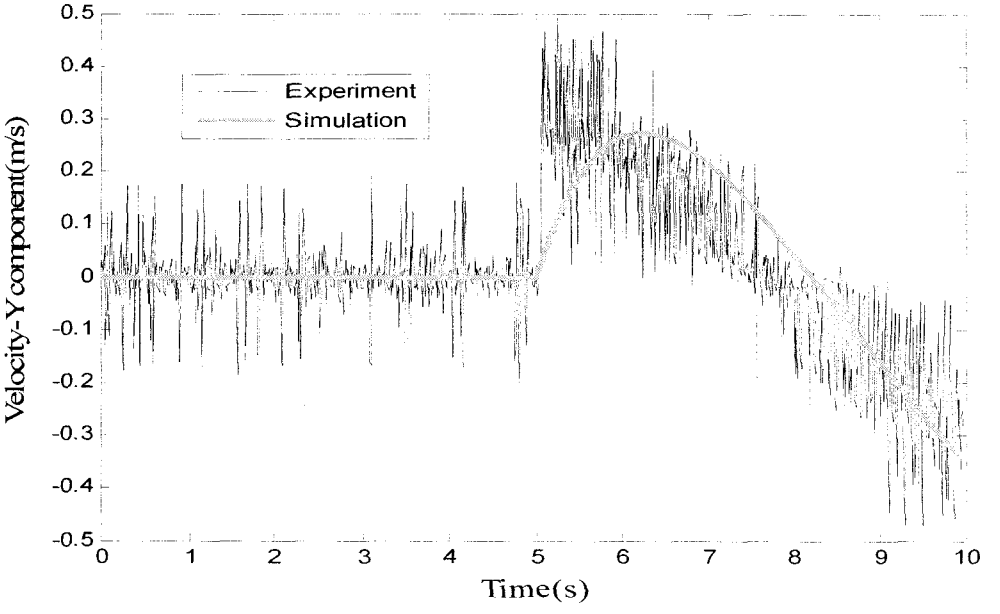

Fig.29. Velocity of the WMR in the Y direction for the IC#4

Fig.30 and Fig.31 show the angular velocity of the WMR and the angle turned for the IC#4 respectively.

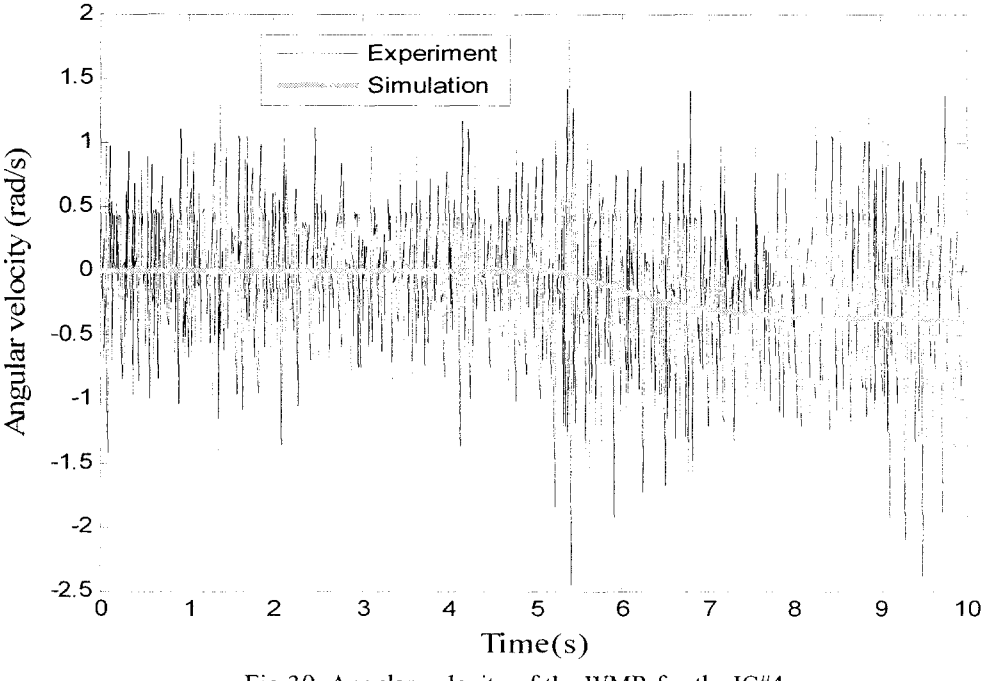

Fig.30. Angular velocity of the WMR for the IC#4

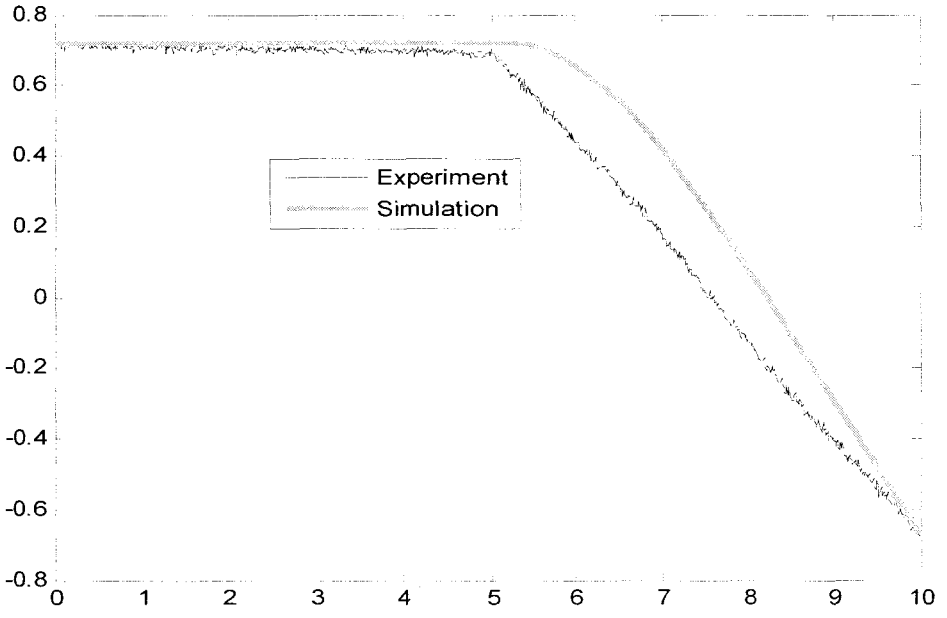

Fig.31. Angle of the WMR for the IC#4

Finally, Fig.32 and Fig.33 show the position of the WMR and path traveled during the run time for the IC#4 respectively.

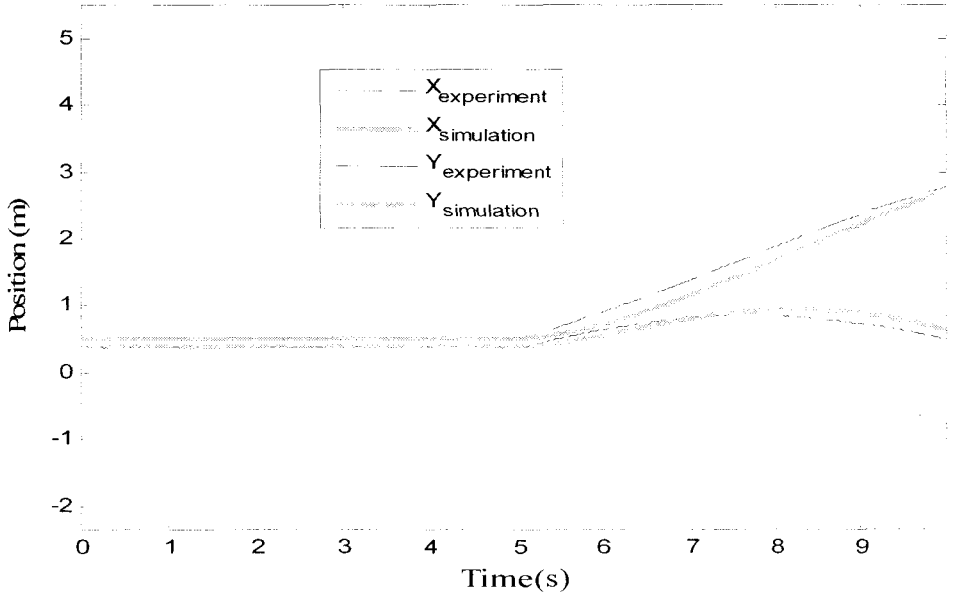

Fig.32. Position of the WMR for the IC#4

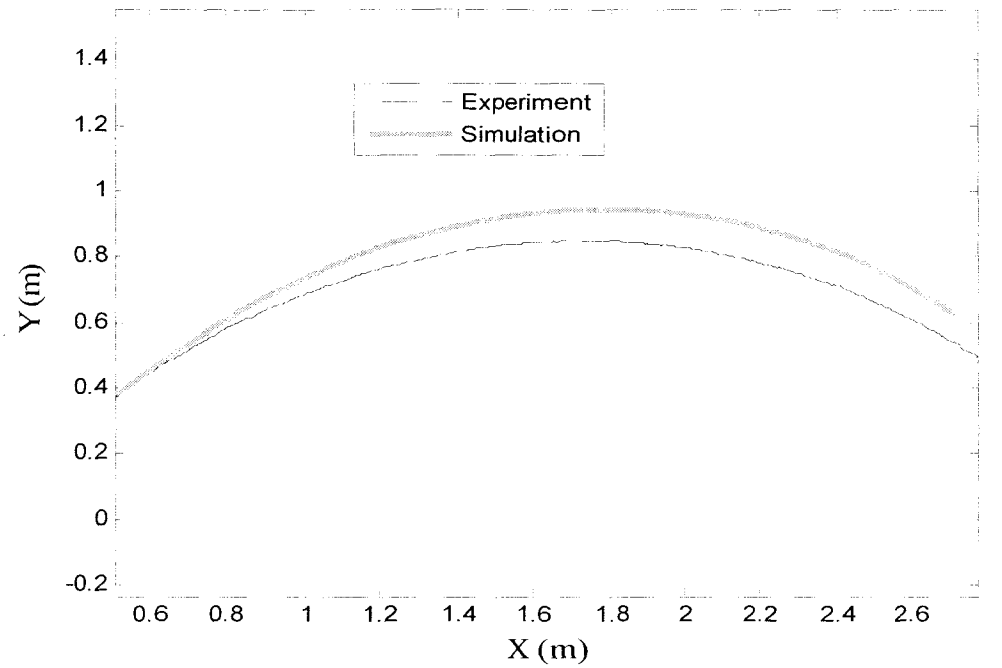

Fig.33. Path followed by the WMR for the IC#4

Similarly, Table 7 summarizes the ICs used for the rotational motion of the WMR.

Time(s)	IC#5	
	$x = 1.3545$ $y = 0.7871$ $\theta = -0.4444 rad$	
	Right Wheel	Left Wheel
$t \leq 5$	$U_R = 0.0V$	$U_L = 0.0V$
$t > 5$	$U_R = 0.5V$	$U_L = -0.5V$

Table 7. Initial conditions for the rotational motion of the WMR

Fig.34 and Fig.35 show the experimental vs. simulation data of the velocity components in the X and Y directions of the WMR for the IC#5 respectively. It is pure rotational motion.

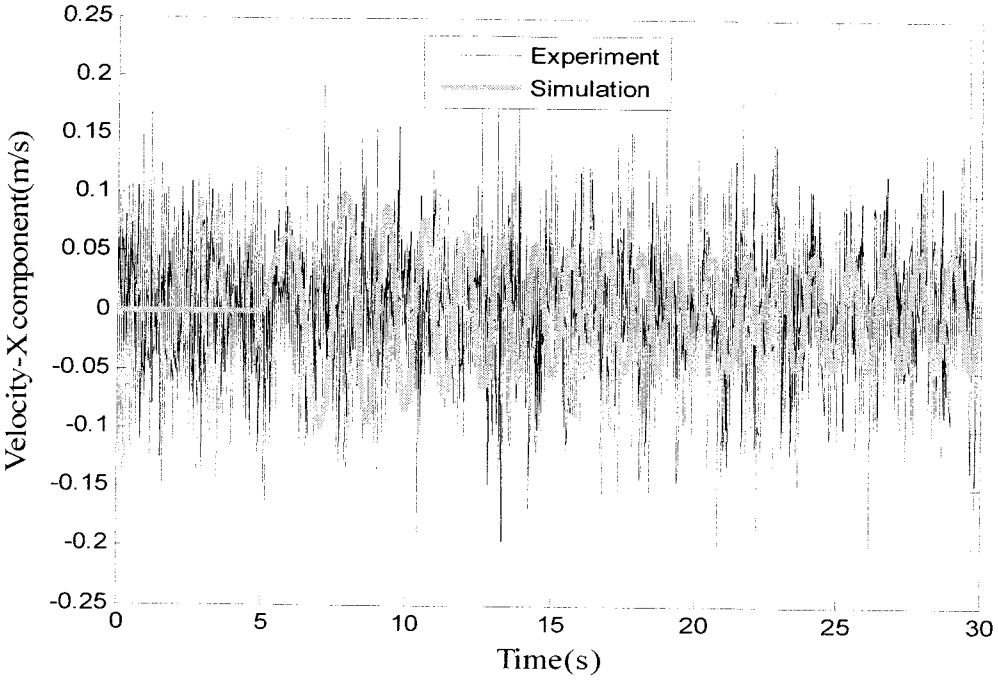

Fig.34. Velocity of the WMR in the X direction for the IC#5

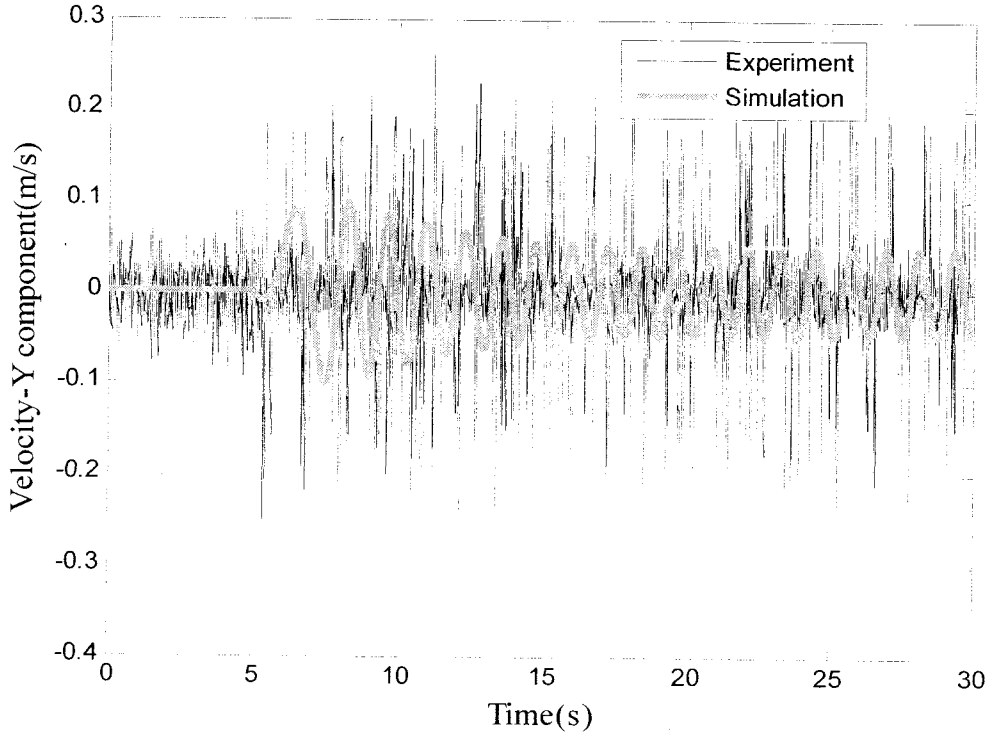

Fig.35. Velocity of the WMR in the Y direction for the IC#5

Fig.36 and Fig.37 show the angular velocity of the WMR and the angle turned for the IC#5 respectively.

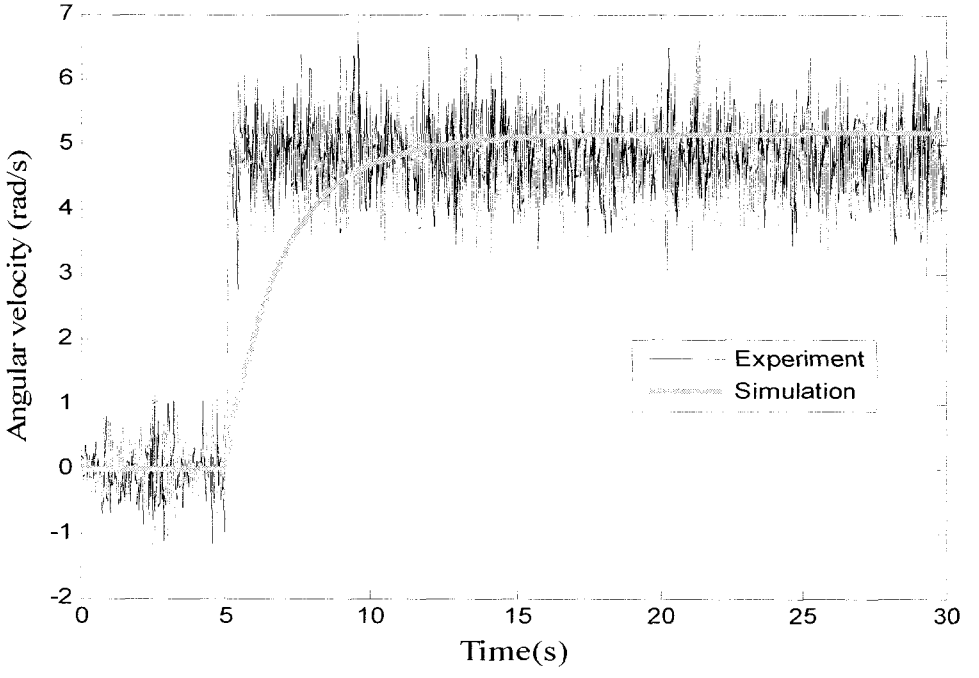

Fig.36. Angular velocity of the WMR for the IC#5

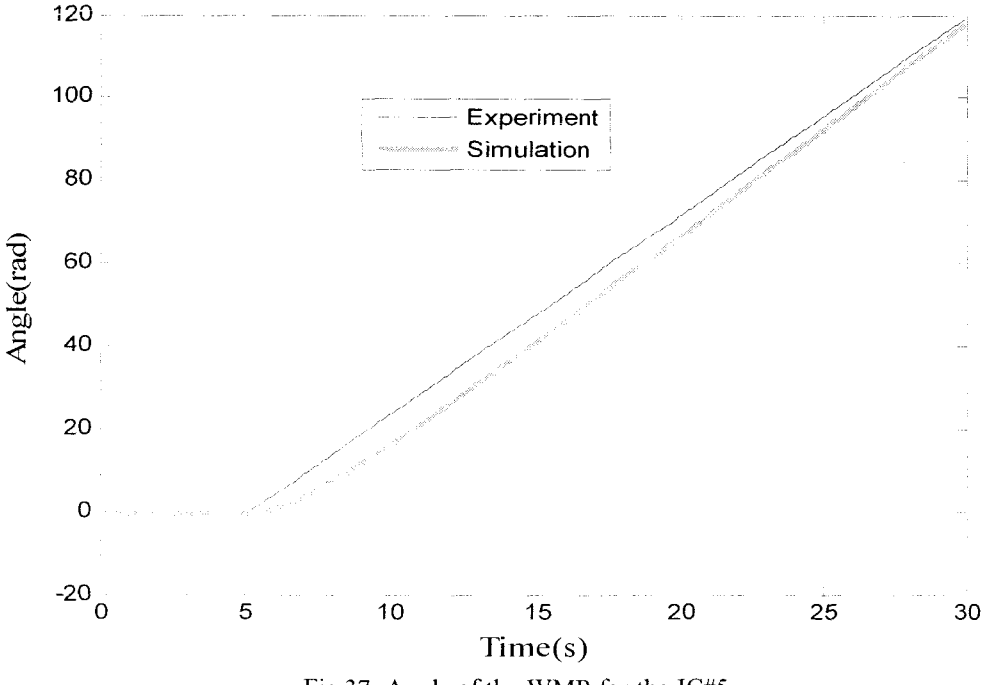

Fig.37. Angle of the WMR for the IC#5

Finally, Fig.38 shows the position of the WMR for the IC#5.

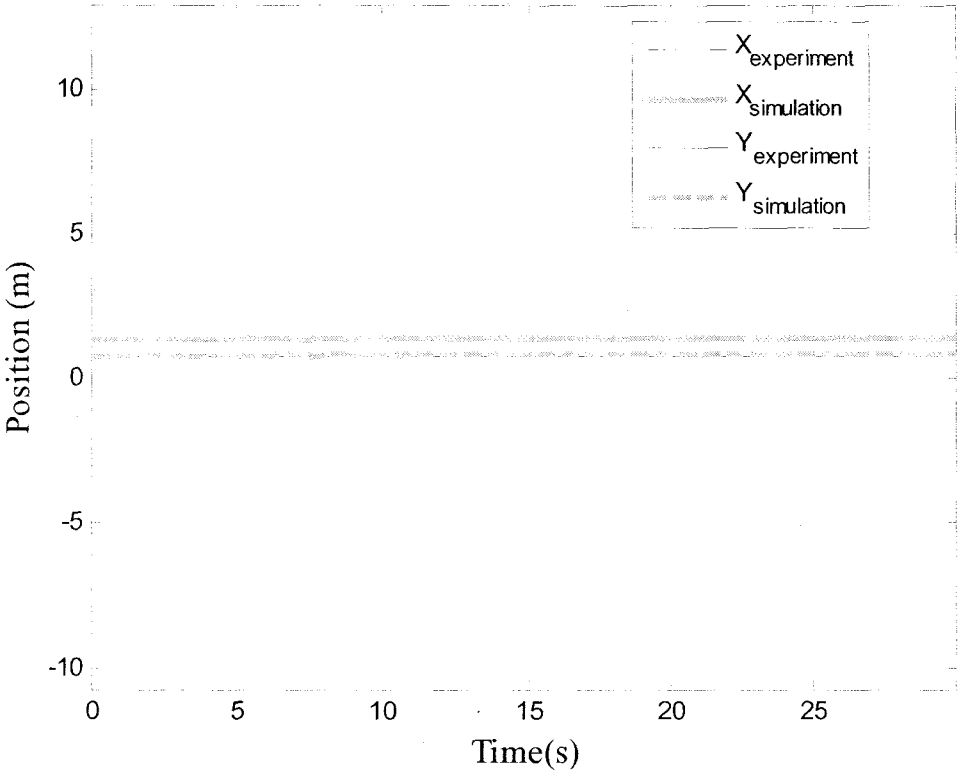

Fig.38. Position of the WMR for the IC#5

Table 8 summarizes the updated values for the parameters of a_1, a_2, a_3 with subscript L and R denoting the left and right wheel respectively.

Parameters	IC#4	Max/Min Deviation	IC#5	Max/Min Deviation
$a_{1,R}$	24.89375	±16.2381	20.5380	±2.1410
$a_{2,R}$	0.730149	±1.226	0.7231	±0.0311
$a_{3,R}$	0.9006	±9.28434	-1.7613	±0.5548
$a_{1,L}$	38.2014	±2.8059	18.7796	±1.9764
$a_{2,L}$	1.18651	±0.2794	0.50305	±0.1486
$a_{3,L}$	-0.4206	±3.7983	2.6065	±2.7233

Table 8. Parameters of the right and left wheel motors when attached with the WMR

4.5. Model Verification of the WMR

Now, similar to the model verification of the actuators earlier, the average values of the parameters a_1, a_2, a_3 is taken for the right and left wheel motors from IC#4 and IC#5. Table 9 summarizes the updated values of the parameters a_1, a_2, a_3 for the right and left wheel motors.

Parameters	Right wheel motor	Left wheel motor
a_1	23.15147	30.4327
a_2	0.72736	0.9131
a_3	-0.1642	-0.79022

Table 9. Parameters of the right and left wheel

A new set of inputs is applied this time for the WMR as shown in Table 10. The inputs are chosen such that they do not go beyond the saturation limits of the motors.

Time(s)	IC#6	
	Right motor	Left motor
$t \leq 5$	$U_R = 0.0V$	$U_L = 0.0V$
$t > 5$	$U_R = 0.3$	$U_L = 0.5$

Table 10. Initial conditions for the model verification of the motors

Fig.39 and Fig.40 show the experimental vs. simulation data of the velocity components in the X and Y directions of the WMR for the IC#6 respectively. It is noted that the simulation and experiment results match each other initially but there is a notable deviation after some time period. This is primarily due to the noise in the vision sensor feedback. Better results could be obtained had angular velocity and translational velocity values been measured by suitable sensors rather than using central finite difference method to calculate those values from position and orientation values.

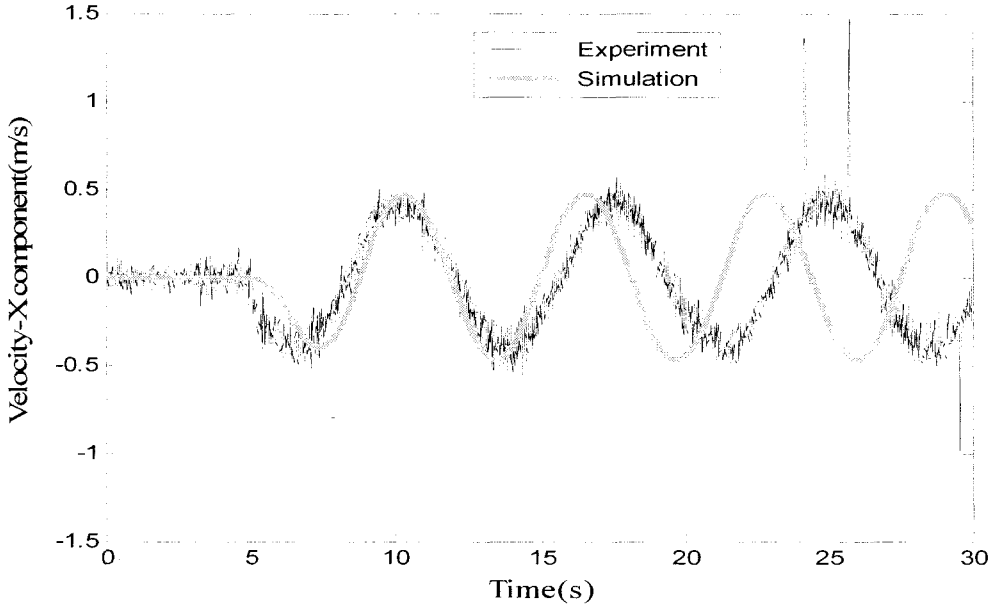

Fig.39. Velocity of the WMR in the X direction for the IC#6

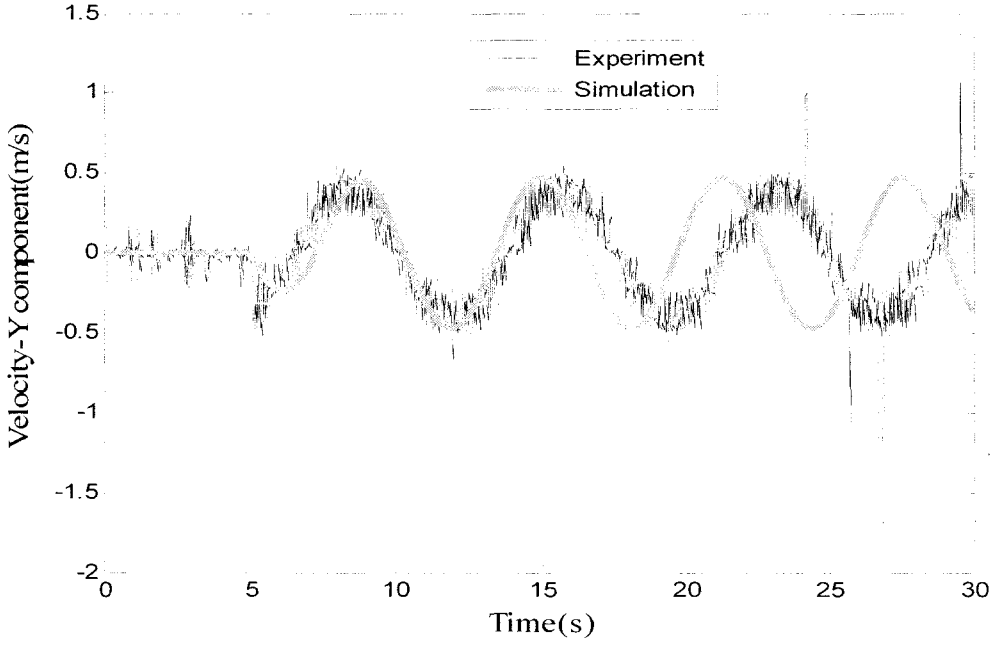

Fig.40. Velocity of the WMR in the Y direction for the IC#6

Fig.41 and Fig.42 show the angular velocity of the WMR and the angle turned for the IC#6 respectively.

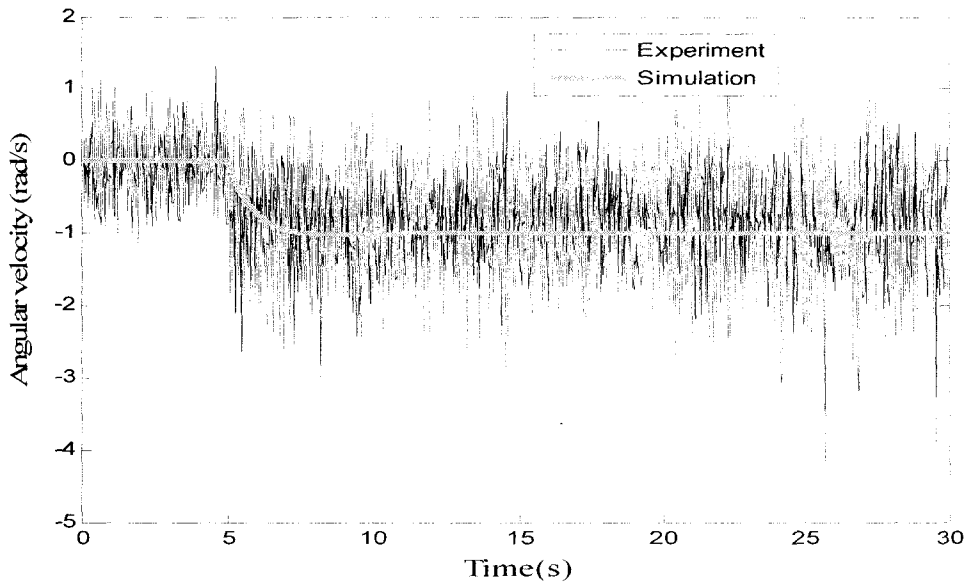

Fig.41. Angular velocity of the WMR for the IC#6

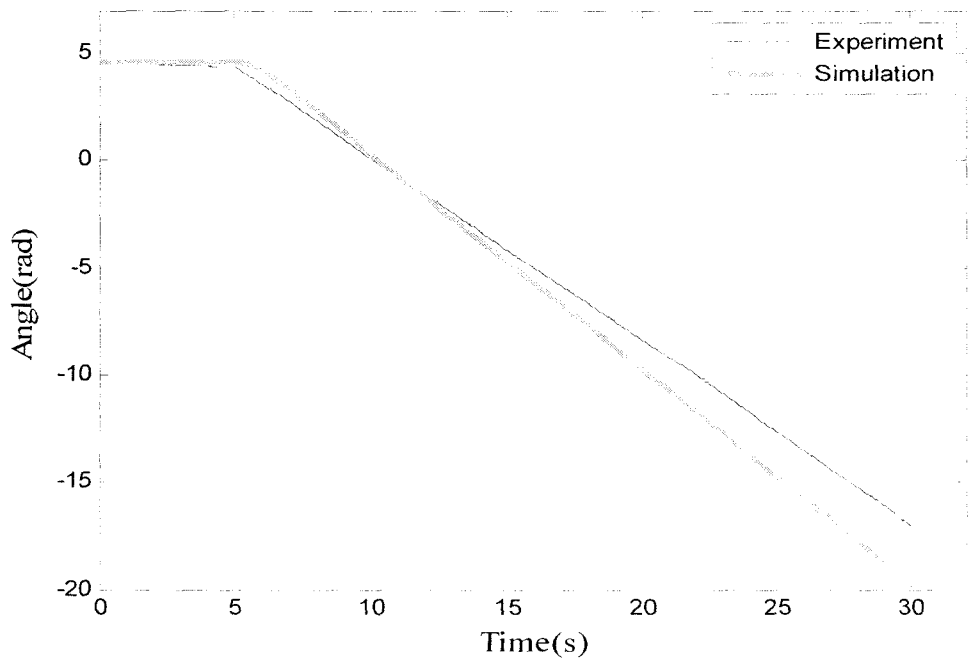

Fig.42. Angle of the WMR for the IC#6

Fig.43 and Fig.44 show the position and path traveled by the WMR for the IC#6 respectively.

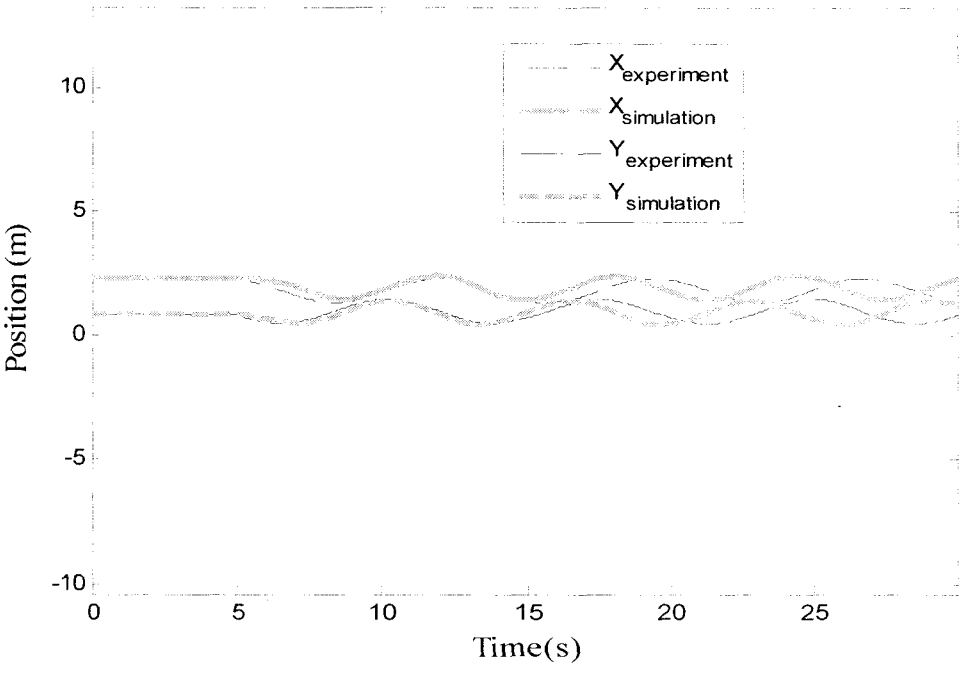

Fig.43. Position of the WMR for the IC#6

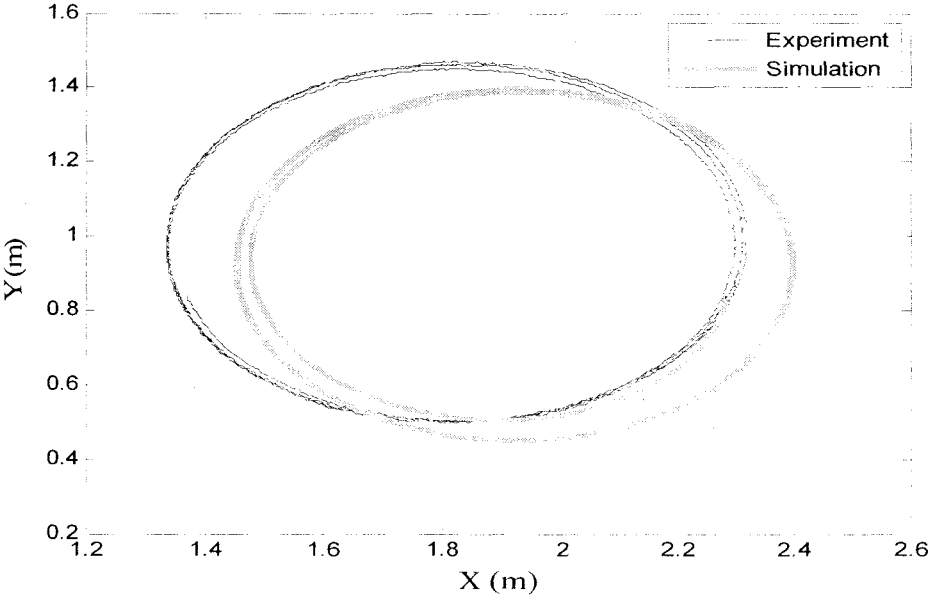

Fig.44. Path followed by WMR for the IC#6

The results show that the calculated values of parameters can be used for the actuator dynamics in the following swarm experiments in chapter 5.

5. Application of Energetic Swarm Control to Wheeled Vehicles

When recent results have been developed on swarm control, most often a point mass dynamics is considered in the literature. But making a swarm of real vehicles and controlling it have not been widely implemented due to a number of challenges such as nonholonomic behavior of vehicles, saturation constraints and uncertainties. There are only few results applicable to the real vehicle applications. On the contrary, a single WMR or hovercraft has been made to follow trajectories or be controlled experimentally but, even controlling a single WMR experimentally needs much attention and rigorous work due to the presence of nonholonomic constraints, saturation constraints of actuators, unmodeled dynamics of vehicles, and disturbances.

This chapter discusses the application of the energetic swarm control with WMRs. Since energetic swarm control is developed for a point mass system, it can not be applied directly to the WMRs. A low level controller is developed with dynamic feedback linearization. As explained previously, many numbers of WMRs can be built in a quick time period to be considered as a swarm. Also, they can be efficiently manipulated over a limited space. Hovercrafts may be replaced with WMRs but they are hard to control over a limited space when they are many vehicles. However, WMRs can be controlled with much ease rather than hovercrafts because of their modeling equations governing the dynamics of the system.

5.1. Low Level Controller Design

In order to implement the energetic swarm with a group of wheeled vehicles experimentally and to get a better tracking performance, inputs from a low level controller are preferred. Here, the high level control input is considered as the $\mathbf{u}_i$ in (88) and high level dynamics is given by (88). Further, low level controllers are successfully applied experimentally to get better tracking performance in [45]-[46] where trajectory tracking of WMRs is considered. When high-level controller inputs are applied directly to a WMR, the trajectory tracking is largely poor and a low level controller is preferred for a better tracking performance.

In the high level layer of energetic swarm dynamics, the point mass is considered. But a WMR consists of vehicle dynamics along with kinematic equations and it is nonholonomic as well. High level control inputs, generated from the control allocation approach, cannot be directly applied to the WMRs. The kinematic equation of WMRs is considered to be the lower level dynamics. As in [45] the dynamic feedback linearization is chosen as the low level controller since this enables the centroid of WMRs to track the desired trajectory. Input output linearization can be done as in section 2.3.2 for the low level dynamics but the proposed low level controller can be used to track the tip of the WMRs which is not desirable. Tracking the centroidal of WMR is preferred and the dynamic feedback linearization closely relates to the form of a PID controller which is used to track trajectories successfully.

Let us consider an i^{th} member of the swarm. Its high level dynamics is given by (88). Let the output of the high level dynamics be

$$\mathbf{X}_{\text{out}} = \begin{bmatrix} x_{r,i} \\ y_{r,i} \end{bmatrix} \tag{163}$$

The lower level dynamics is given by the kinematic equation of the WMR as in (58). The desired reference trajectory $[x_{d,i} \quad y_{d,i}]^T$ that the WMR should track is the output from the high level swarm dynamics. That is

$$\begin{bmatrix} x_{d,i} \\ y_{d,i} \end{bmatrix} = \begin{bmatrix} x_{r,i} \\ y_{r,i} \end{bmatrix} \tag{164}$$

The lower level dynamics can be converted into the linear system as in (87) by dynamic feedback linearization.

Let the lower level dynamics of i^{th} member be

$$\begin{bmatrix} \dot{x}_i \\ \dot{y}_i \\ \dot{\theta}_i \end{bmatrix} = \begin{bmatrix} \cos\theta_i & 0 \\ \sin\theta_i & 0 \\ 0 & 1 \end{bmatrix} \begin{bmatrix} v_i \\ \omega_i \end{bmatrix} \tag{165}$$

Define the output vector $\boldsymbol{\eta}_i$ of the lower level dynamics as

$$\boldsymbol{\eta}_i = \begin{bmatrix} x_i \\ y_i \end{bmatrix} \tag{166}$$

The first differentiation of the output vector $\boldsymbol{\eta}_i$ gives

$$\dot{\boldsymbol{\eta}}_i = \begin{bmatrix} \cos\theta_i & 0 \\ \sin\theta_i & 0 \end{bmatrix} \begin{bmatrix} v_i \\ \omega_i \end{bmatrix} \tag{167}$$

Since the $\dot{\boldsymbol{\eta}}_i$ is not affected by the ω_i, it is necessary to differentiate the output vector until both the inputs appear. In order to avoid differentiation of the original inputs, a new state ξ_i is necessary such that it becomes the integrator for the original input. Define ξ_i as

$$\begin{aligned} &\xi_i = v_i \\ &\Rightarrow \dot{\xi}_i = \tilde{a}_i \end{aligned} \tag{168}$$

Differentiating (167) gives

$$\ddot{\boldsymbol{\eta}}_i = \begin{bmatrix} \cos\theta_i & -\xi_i \sin\theta_i \\ \sin\theta_i & \xi_i \cos\theta_i \end{bmatrix} \begin{bmatrix} \tilde{a}_i \\ \omega_i \end{bmatrix} \tag{169}$$

Define $[\tilde{a}_i \quad \omega_i]^T$ as follows and it is non-singular when $\xi_i \neq 0$

$$\begin{bmatrix} \tilde{a}_i \\ \omega_i \end{bmatrix} = \begin{bmatrix} \cos\theta_i & -\xi_i \sin\theta_i \\ \sin\theta_i & \xi_i \cos\theta_i \end{bmatrix}^{-1} \mathbf{u}_i \tag{170}$$

where $\mathbf{u}_i = [u_{1,i} \quad u_{2,i}]^T$ is the new control input. Then the system (169) becomes

$$\ddot{\boldsymbol{\eta}}_i = \begin{bmatrix} u_{1,i} \\ u_{2,i} \end{bmatrix} \tag{171}$$

Then for the system (171) choose the control law as

$$\begin{bmatrix} u_{1,i} \\ u_{2,i} \end{bmatrix} = \begin{bmatrix} \ddot{x}_{d,i} + k_{p1,i}(x_{d,i} - x_i) + k_{d1,i}(\dot{x}_{d,i} - \dot{x}_i) \\ \ddot{y}_{d,i} + k_{p2,i}(y_{d,i} - y_i) + k_{d2,i}(\dot{y}_{d,i} - \dot{y}_i) \end{bmatrix} \tag{172}$$

where $k_{p1,i} > 0, k_{d1,i} > 0, k_{p2,i} > 0, k_{d2,i} > 0$ *for* $i = 1,2,.....M$

Finally, the dynamic compensator is given by

$$\begin{aligned} \dot{\xi}_i &= u_{1,i} \cos\theta_i + u_{2,i} \sin\theta_i \\ v_i &= \xi_i \\ \omega_i &= \frac{u_{2,i} \cos\theta_i - u_{1,i} \sin\theta_i}{\xi_i} \end{aligned} \tag{173}$$

In terms of control inputs, the angular velocities of the wheels of the WMR are given by

$$\begin{aligned} \omega_{R,i} &= \frac{(2v_i + \omega_i l)}{2R_{R,i}} \\ \omega_{L,i} &= \frac{(2v_i - \omega_i l)}{2R_{L,i}} \end{aligned} \tag{174}$$

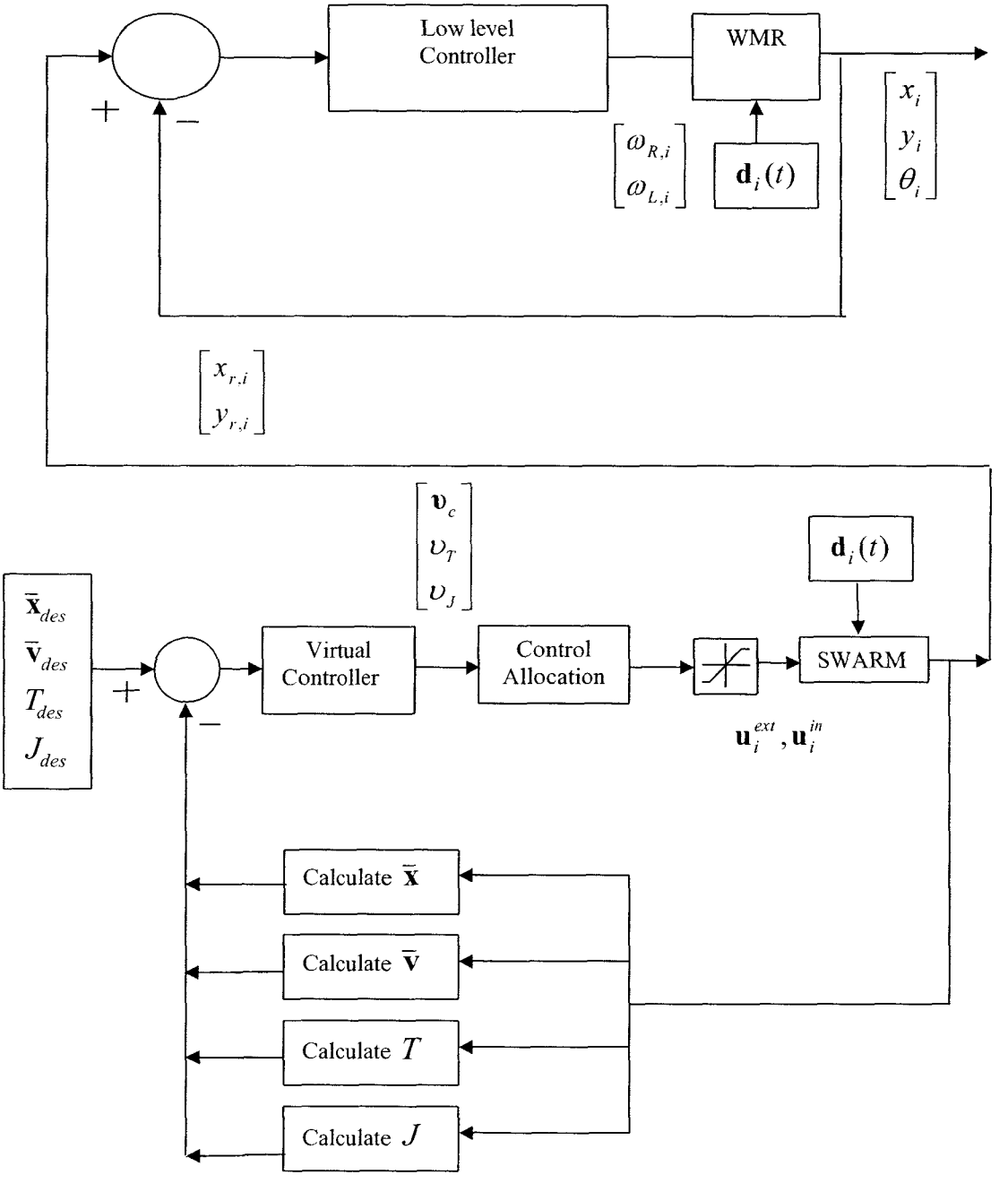

Fig.45. Block diagram of the high level swarm layer and the lower level layer

Fig.45 shows the complete block diagram of the high level swarm layer and how it is combined with the low level layer. The high level layer is the lower part of the Fig.45 and it consists of swarm dynamics, virtual controller and control allocation process. The low level layer is the upper part of the Fig.45 and it consists of WMR dynamics and the low level controller. For the high level swarm controller the inputs are the desired swarm centre trajectory, and the desired temperature and potential values. Based on those desired inputs, the virtual controller that tracks the desired swarm center and regulates desired temperature and potential values will be calculated using the sliding mode control method. Since the system is over actuated, using the control allocation approach, actual inputs that match the necessary virtual inputs will be calculated with saturation constraints.

The output of the swarm dynamics is the trajectories of each individual member. The output of the swarm dynamics will be the desired reference trajectories for the WMRs. The low level controller tracks the desired trajectories of the high level swarm layer and these trajectories are generated online. Further, they are of chaotic type. Here, the dynamic feedback linearization will be used calculate the low level controller since the system (165) is an under actuated one and the inputs to the system (165) are generated online by the high level layer. There is no prior knowledge of these trajectory patterns and the dynamic feedback linearization is preferred than the sliding mode control method. However, in the high level layer, virtual controllers are calculated using the sliding mode control method since, once the virtual controllers are introduced in (104), (114) and (124), the system is neither under actuated nor over actuated. The sliding mode

controllers successfully track the desired swarm centre, desired swarm temperature and desired swarm potential with the presence of disturbance.

5.2. Simulations

In this section, the high level swarm dynamics and the low level dynamics are simulated together. Swarm consists of six members. The desired swarm centre trajectory and the temperature and potential values are chosen as

$$\begin{aligned} \bar{\mathbf{x}}_d &= \begin{bmatrix} 5.0\cos(t) \\ 5.0\sin(t) \end{bmatrix} \\ T_d &= 5.0 \\ J_d &= 5.0 \end{aligned} \tag{175}$$

Table 11 shows the ICs of the swarm members in the high level layer and all other coefficients and positive constants defined in chapter 3. Here, the coefficients are selected such that the members will be homogenous however, different values can be selected if that case is necessary.

ICs	Member 1	Member 2	Member 3	Member 4	Member 5	Member 6
$\mathbf{x}_0$	$\begin{bmatrix}0.0\\0.0\end{bmatrix}$	$\begin{bmatrix}5.0\\5.0\end{bmatrix}$	$\begin{bmatrix}1.0\\1.0\end{bmatrix}$	$\begin{bmatrix}3.0\\-3.0\end{bmatrix}$	$\begin{bmatrix}-2.0\\-2.0\end{bmatrix}$	$\begin{bmatrix}4.0\\2.0\end{bmatrix}$
$\mathbf{v}_0$	$\begin{bmatrix}2.0\\2.0\end{bmatrix}$	$\begin{bmatrix}1.0\\1.0\end{bmatrix}$	$\begin{bmatrix}3.0\\-3.0\end{bmatrix}$	$\begin{bmatrix}-2.0\\0.0\end{bmatrix}$	$\begin{bmatrix}-5.0\\5.0\end{bmatrix}$	$\begin{bmatrix}8.0\\8.0\end{bmatrix}$
m_i	1.0	1.0	1.0	1.0	1.0	1.0
h_i	1.0	1.0	1.0	1.0	1.0	1.0
b_i	1.0	1.0	1.0	1.0	1.0	1.0
$\mathbf{d}_i$	$\begin{bmatrix}1.0\sin(t)\\1.0\sin(t)\end{bmatrix}$	$\begin{bmatrix}1.0\sin(t)\\1.0\sin(t)\end{bmatrix}$	$\begin{bmatrix}1.0\sin(t)\\1.0\sin(t)\end{bmatrix}$	$\begin{bmatrix}1.0\sin(t)\\1.0\sin(t)\end{bmatrix}$	$\begin{bmatrix}1.0\sin(t)\\1.0\sin(t)\end{bmatrix}$	$\begin{bmatrix}1.0\sin(t)\\1.0\sin(t)\end{bmatrix}$
β_i	2.0	2.0	2.0	2.0	2.0	2.0
$g_a(\cdot)$	$\frac{2.0}{\|\mathbf{y}\|}$	$\frac{2.0}{\|\mathbf{y}\|}$	$\frac{2.0}{\|\mathbf{y}\|}$	$\frac{2.0}{\|\mathbf{y}\|}$	$\frac{2.0}{\|\mathbf{y}\|}$	$\frac{2.0}{\|\mathbf{y}\|}$
$g_r(\cdot)$	$\frac{2.0}{\|\mathbf{y}\|^2}$	$\frac{2.0}{\|\mathbf{y}\|^2}$	$\frac{2.0}{\|\mathbf{y}\|^2}$	$\frac{2.0}{\|\mathbf{y}\|^2}$	$\frac{2.0}{\|\mathbf{y}\|^2}$	$\frac{2.0}{\|\mathbf{y}\|^2}$
$\bar{\omega}_i$	1.0	1.0	1.0	1.0	1.0	1.0
$\tilde{\omega}_i$	1.0	1.0	1.0	1.0	1.0	1.0
α_i	1.0	1.0	1.0	1.0	1.0	1.0

Table 11. Initial conditions of the high level swarm layer

Table 12 summarizes the sliding mode parameters defined in section 3.2. Here the parameters $\bar{\boldsymbol{\lambda}}, \lambda_J$ are chosen such that the swarm achieves the steady state in a reasonable time. The parameters η_c, η_T, η_J are chosen such that the disturbance effect is completely removed from the system. The values of the boundary layers are chosen such as the chattering effects are completely eliminated from the system. One can note that the boundary layers ε_T and ε_J are higher than the $\boldsymbol{\varepsilon}_c$. This is because stabilizing the

temperature w.r.t the corresponding potential value needs more room and a control effort. Also these temperature and potential functions are highly nonlinear functions.

Parameters	Value
$\bar{\lambda}$	$\begin{bmatrix} 2.0 \\ 2.0 \end{bmatrix}$
η_c	2.0
ε_c	$\begin{bmatrix} 1.0 \\ 1.0 \end{bmatrix}$
η_T	3.0
ε_T	0.5
λ_J	2.0
η_J	3.0
ε_J	0.5

Table 12. Sliding mode parameters

Table 13 shows the saturation constraints used in the control allocation process in the upper level swarm layer. These constraints are chosen such that these limits are above the minimum allowable values. Again, homogenous bounds are chosen but one can choose different values of saturation constraints based on the required temperature and potential values.

Saturation Constraint	Value
$\mathbf{u}_i^{ext}{}_{\min}$	$\begin{bmatrix} -25.0 \\ -25.0 \end{bmatrix}$
$\mathbf{u}_i^{ext}{}_{\max}$	$\begin{bmatrix} 25.0 \\ 25.0 \end{bmatrix}$

Table 13. Saturation constraint values

Fig.46 shows the trajectory tracking of a WMR by the lower level control inputs. The reference trajectory is generated from the high level swarm dynamics. The initial conditions of the WMR are

$$\begin{bmatrix} x_i \\ y_i \\ \theta_i \end{bmatrix} = \begin{bmatrix} 2.0 \\ 3.0 \\ 0.52 \end{bmatrix} \tag{176}$$

The gains of the lower level controller (172) is selected as

$$\begin{bmatrix} k_{p1} \\ k_{p2} \\ k_{d1} \\ k_{d2} \end{bmatrix} = \begin{bmatrix} 4.0 \\ 4.0 \\ 4.0 \\ 4.0 \end{bmatrix} \tag{177}$$

These gains are chosen such that the error between the desired trajectory and the WMR trajectory is as small as possible and achieves steady state at a reasonable time. The possible potential singularities of the lower level controller are eliminated by resetting ξ_i in (168) as follows, if ξ_i approaches zero.

$$\begin{aligned} &if \|\xi_i\| < 0.01 \\ &\xi_i = 0.01 \; iff \; \xi_i > 0 \\ &\xi_i = -0.01 \; iff \; \xi_i < 0 \end{aligned} \tag{178}$$

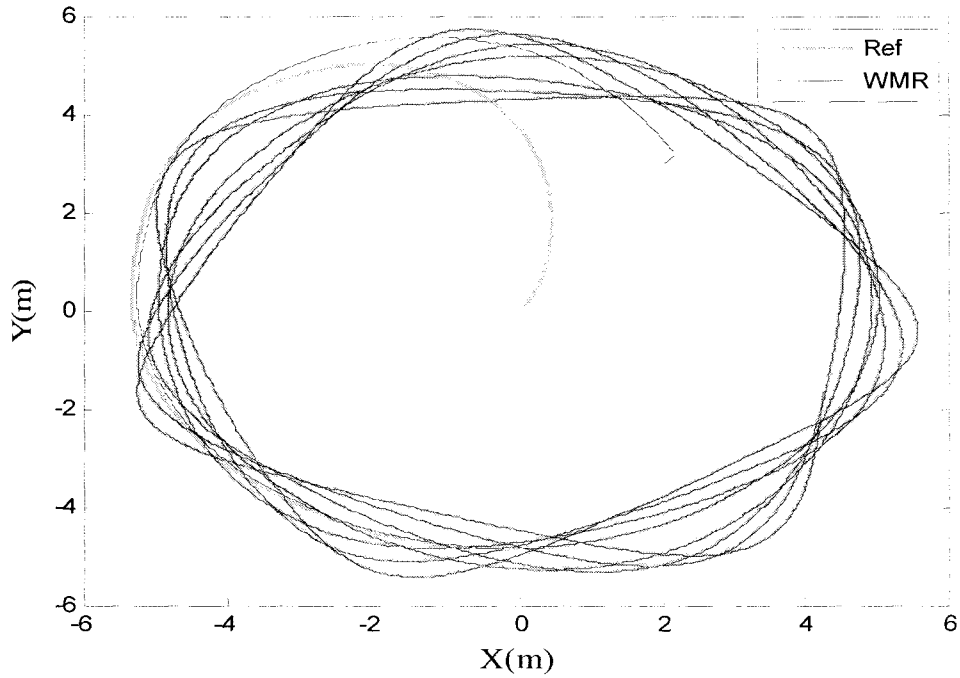

Fig.46. Trajectory tracked by the WMR generated by the high level swarm layer

Fig.47 and Fig.48 show the corresponding lower level control inputs which are $[v_i \quad \omega_i]^T$ in (173)

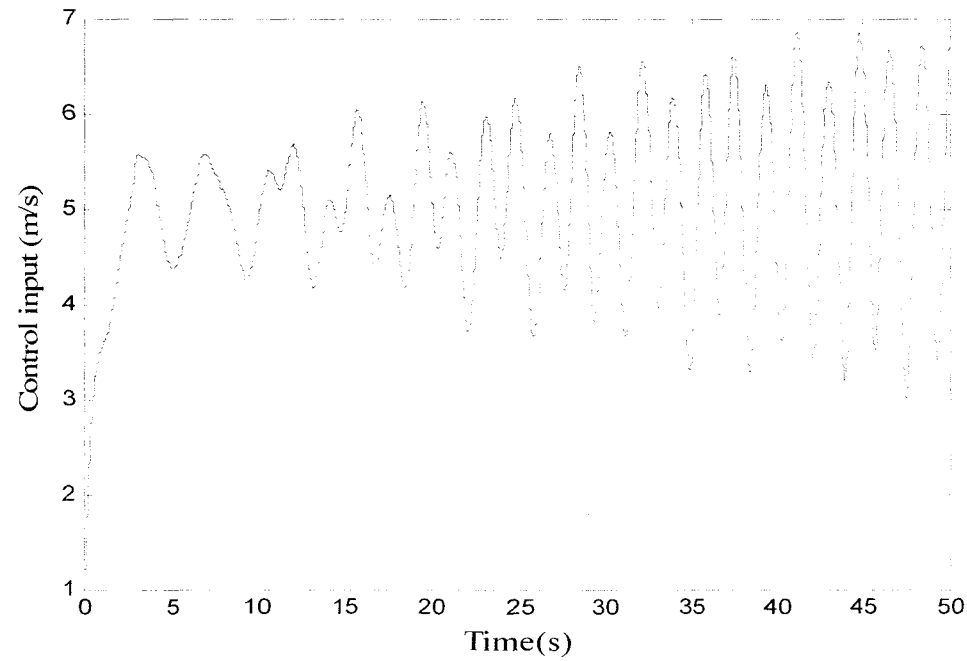

Fig.47. Low level control input

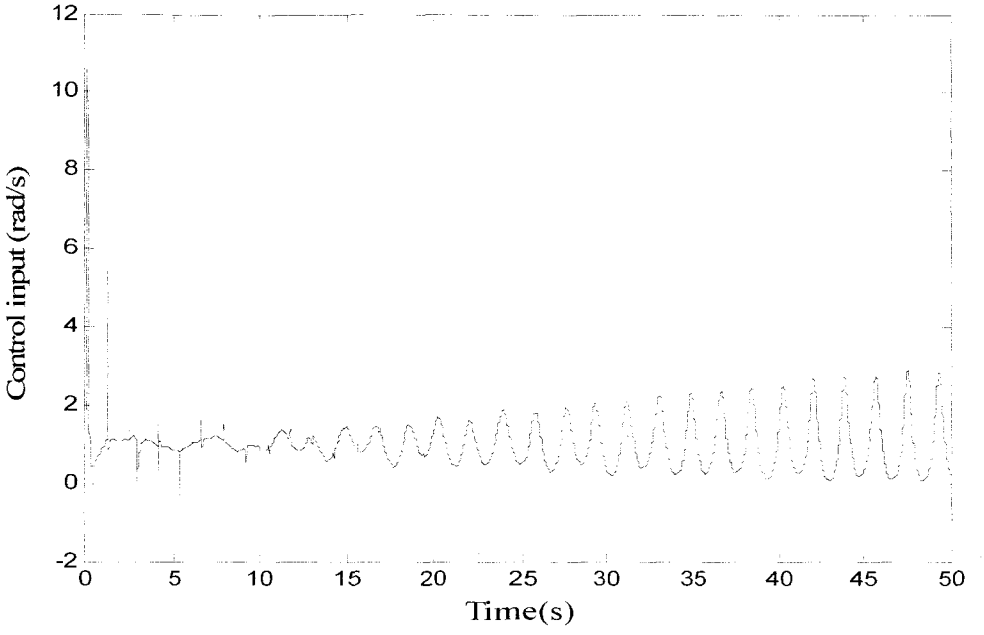

Fig.48. Low level control input

Fig.49 shows the error between the desired trajectory and the trajectory followed by the WMR. The lower level controller achieves the desired objective.

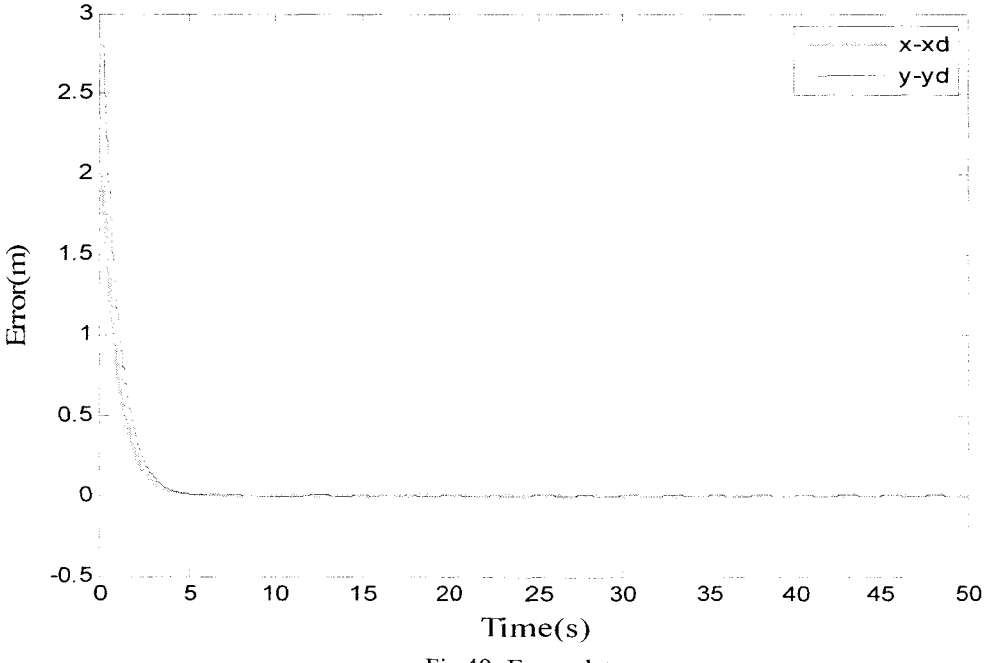

Fig.49. Error plot

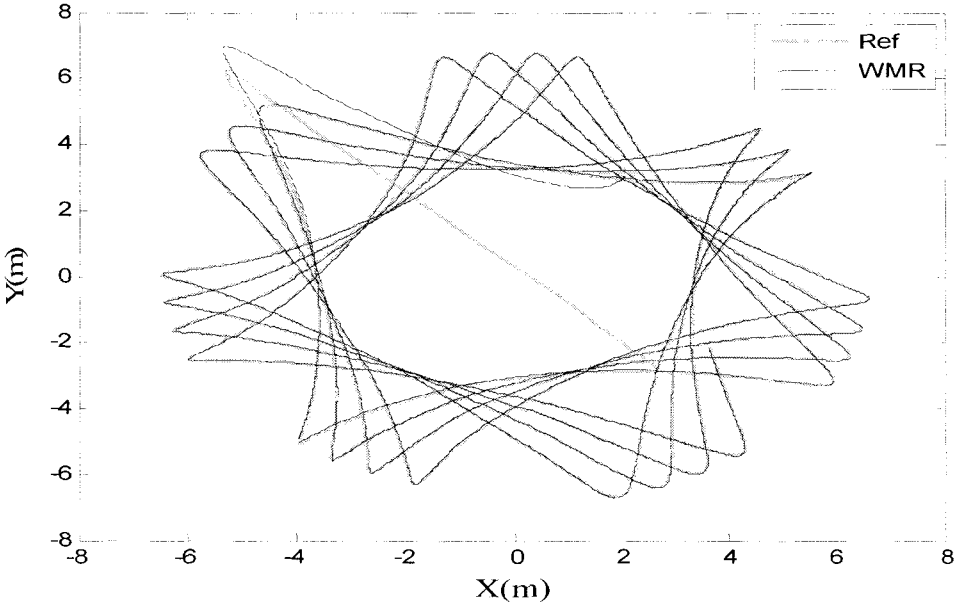

Fig.50. Trajectory tracked by another WMR generated by the high level swarm layer

Fig.50 shows the trajectory followed by another WMR and Fig.51 shows the corresponding error plot.

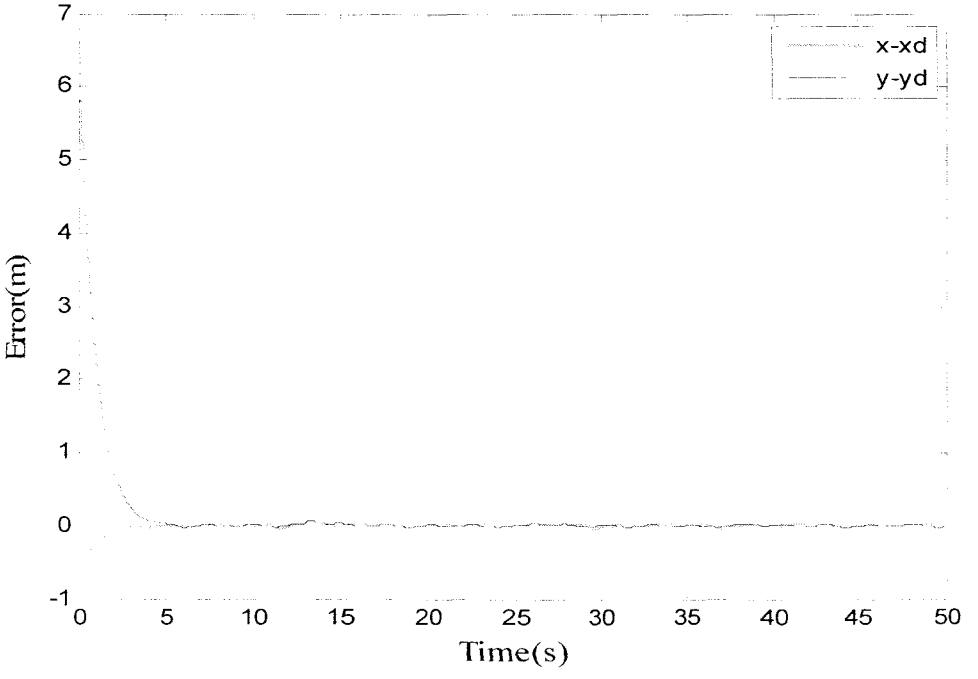

Fig.51. Error plot

5.3. Low Level Controller for Experimental Setup

Although in simulations the lower level controller achieves good tracking performance of the online trajectories generated by the high level layer, in reality, the high level controller and the lower level controller should be synchronized for a practical setup due to disturbances or any other mismatches. In order to get a better tracking performance in a practical implementation, the two loops should be combined together. First, the actual inputs to the high level swarm layer will be found. Next, the high level swarm is allowed to generate the desired trajectories for a certain time period and the outputs of the swarm will be applied to the low level controller. The actual positions and velocities of each WMRs are then computed for the same time period. Finally, the high level swarm states will be updated according to the actual WMRs position and velocities.

The following procedure summarizes the high level and low lever layer synchronization [56].

1) Firstly, the high level swarm is allowed to generate desired trajectories between $t = [t_i, t_i + T_{swarm}]$ where t_i is the initial time and T_{swarm} is the synchronization time between the high level swarm dynamics and the low level dynamics.

2) The desired trajectories for the lower level dynamics are the trajectories generated from the high level dynamics between time $t = [t_i, t_i + T_{swarm}]$. The outputs from the high level dynamics are applied as the inputs to the lower level controller for the time $t = [t_i, t_i + T_{swarm}]$ and the actual positions and velocities of the WMRs are found.

3) In reality there are differences between the trajectory tracked by the WMR and the trajectory generated from the high level swarm dynamics. In order to eliminate the error as much as possible, the states of WMRs are fed back to the high level dynamics. That is, the states of the swarm members in the high level swarm model will be re-initialized with the WMRs positions and velocities found in Step (2).

4) Once the states are fed back, step (1) to step (3) are repeated until the end of the run time.

The above procedure combines the higher and lower level layers at each time interval T_{swarm}. Furthermore, T_{swarm} is the key parameter which determines the tracking performance of WMRs and the stability of high level layer. In an inner loop and outer loop cascaded system, careful adjustment of the gains of both inner loop and outer loop is required. In general, the combined inner and outer loop system shows good tracking performance when the inner loop is significantly faster than the outer loop.

Fig.52 shows the complete block diagram of the high level swarm layer and the low level layer. As explained earlier, two loops will be combined together at every time interval T_{swarm} where the WMRs actual states will be updated at that time. If T_{swarm} is higher than a particular value then the WMR will deviate from the desired trajectory by a certain amount due to the presence of disturbance, but if it is too small then there will not be enough time for the high level layer to adjust the disturbance caused by the state feedback. It may make the high level layer unstable. It is very difficult to regulate the desired temperature in this case due to its nonlinear behavior. Here in the following simulations in section 5.4 it will be found by trial and error.

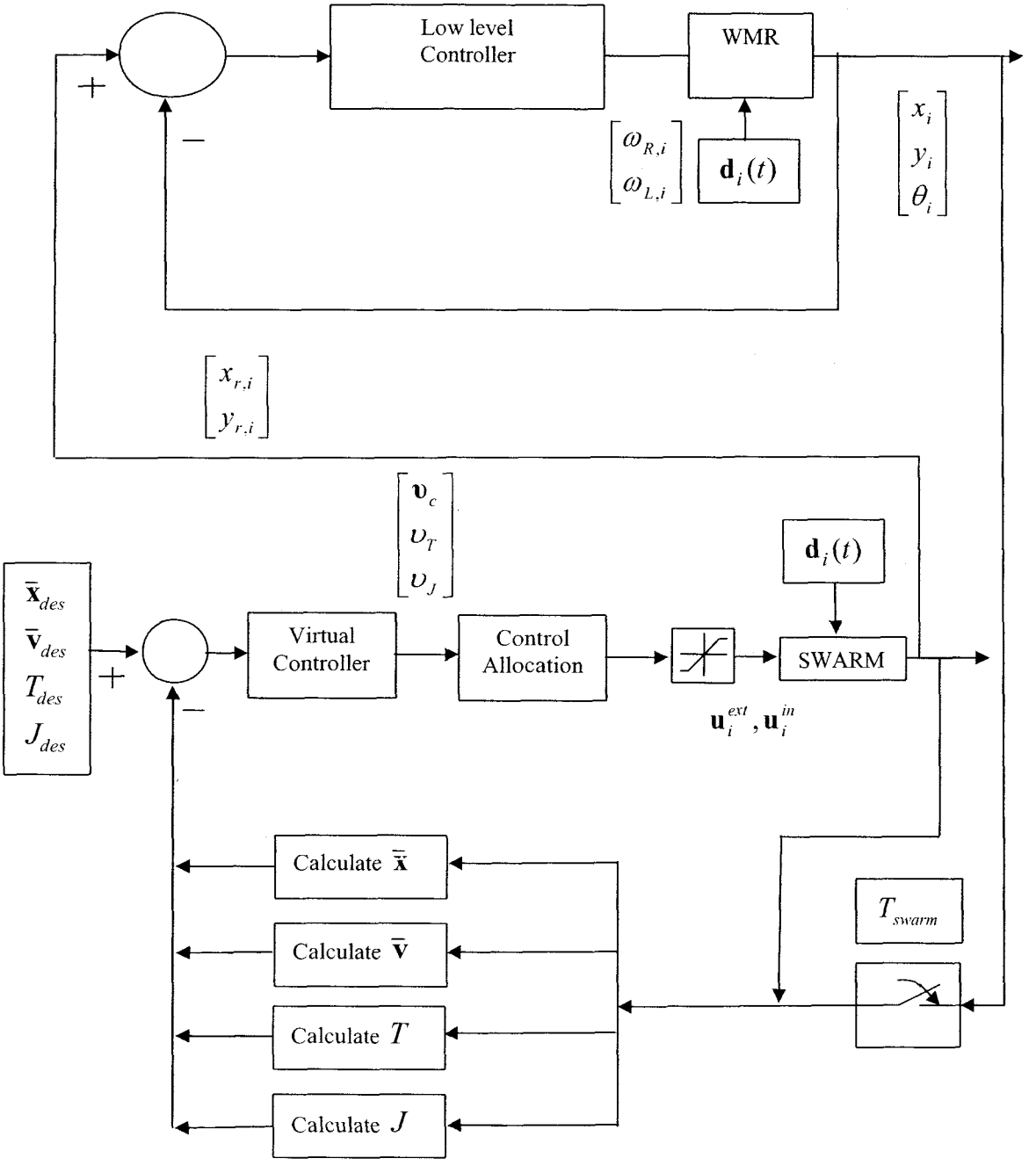

Fig.52. Block diagram of the high level swarm layer and the lower level layer

5.4. Simulation Verification

In this section, simulations are done to verify the synchronization of the high level layer with the low lever layer. As explained previously, the states of the high level layer will be updated with the states of WMRs at a time interval T_{swarm}. The two loops will be closed together. Again the swarm has six members.

The desired swarm centre and the desired temperature and potential values for this case is

$$\begin{aligned} \bar{\mathbf{x}}_d &= \begin{bmatrix} 5.0\cos(t) \\ 5.0\sin(t) \end{bmatrix} \\ T_d &= 10.0 \\ J_d &= 10.0 \end{aligned} \tag{179}$$

The initial positions and velocities of the swarm members in the high level layer will be same as that of in the Table 11. Also, any other coefficients and parameters will be kept the same as that of in the Table 11. However, the sliding mode control parameters will be updated as in Table 14. Since the states are fed back, more control effort is necessary and the parameters will be chosen such that the tracking errors are as small as possible in the high level and low level layers.

Here the parameters $\bar{\lambda}, \lambda_J$ are chosen such that the swarm achieves the steady state in a reasonable time when it gets external disturbance by the state feedback from the low level layer. The parameters η_c, η_T, η_J are chosen such that the disturbance effect is completely removed from the system. The boundary layer values will be selected such that the chattering effects are completely eliminated from the system. However, the price of large boundary layer is the tracking or regulation error at the steady state of the system.

Parameters	Value
$\bar{\boldsymbol{\lambda}}$	$[3.0 \quad 3.0]^T$
η_c	5.0
$\boldsymbol{\varepsilon}_c$	$[0.1 \quad 0.1]^T$
η_T	5.0
ε_T	0.6
λ_J	5.0
η_J	5.0
ε_J	0.6

Table 14. Sliding mode parameters

Further, the saturation constraints will also be relaxed as shown in Table 15.

Saturation Constraint	Value
$\mathbf{u}_{i\ \min}^{ext}$	$\begin{bmatrix} -50.0 \\ -50.0 \end{bmatrix}$
$\mathbf{u}_{i\ \max}^{ext}$	$\begin{bmatrix} 50.0 \\ 50.0 \end{bmatrix}$

Table 15. Saturation constraint values

The T_{swarm} will be selected as 1.0. The value is a good choice as shown in Fig.59 and Fig.63. If the T_{swarm} is beyond this value then the errors will be high due to the disturbance applied to the WMRs. The disturbance will be selected as $[1.0\sin(2t) \quad 1.0\sin(2t)]^T$. However, if the T_{swarm} is reduced further, the high level layer does not have enough time to adjust the disturbance and needs more control effort to track the temperature and potential values and to stabilize the system.

Fig.53 shows the trajectories of each swarm member in the high level layer. Fig.54 shows the swarm centre and the desired swarm centre. Since the WMRs' positions are updated after a certain period of time, the tracking is not smooth but it recovers each time. The swarm centre deviates from the desired one, but it quickly recovers

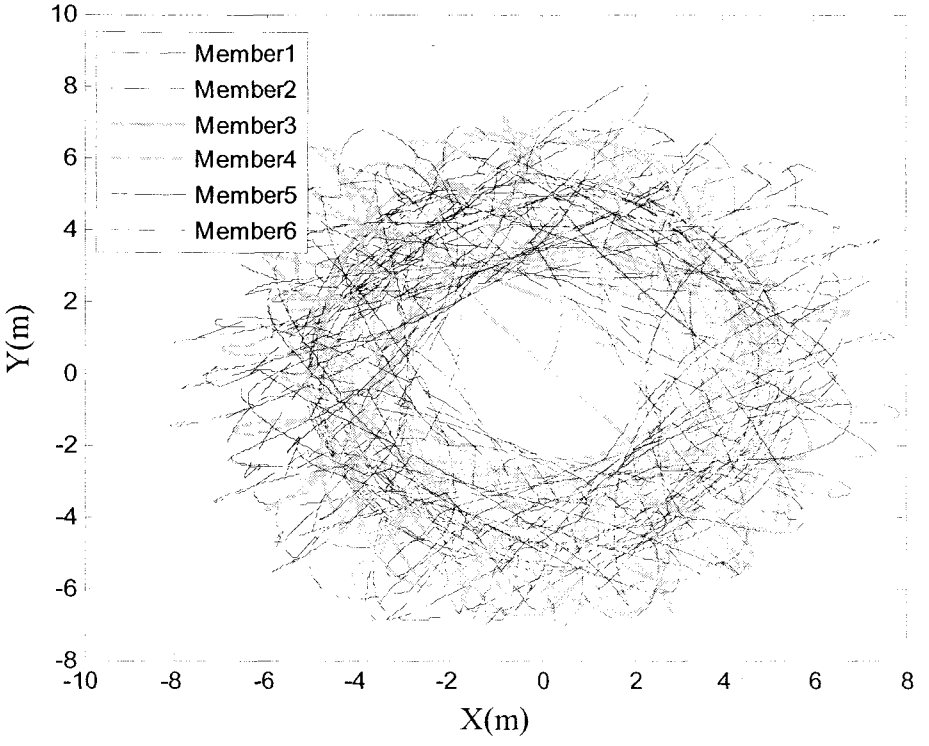

Fig.53. Trajectories of the swarm members

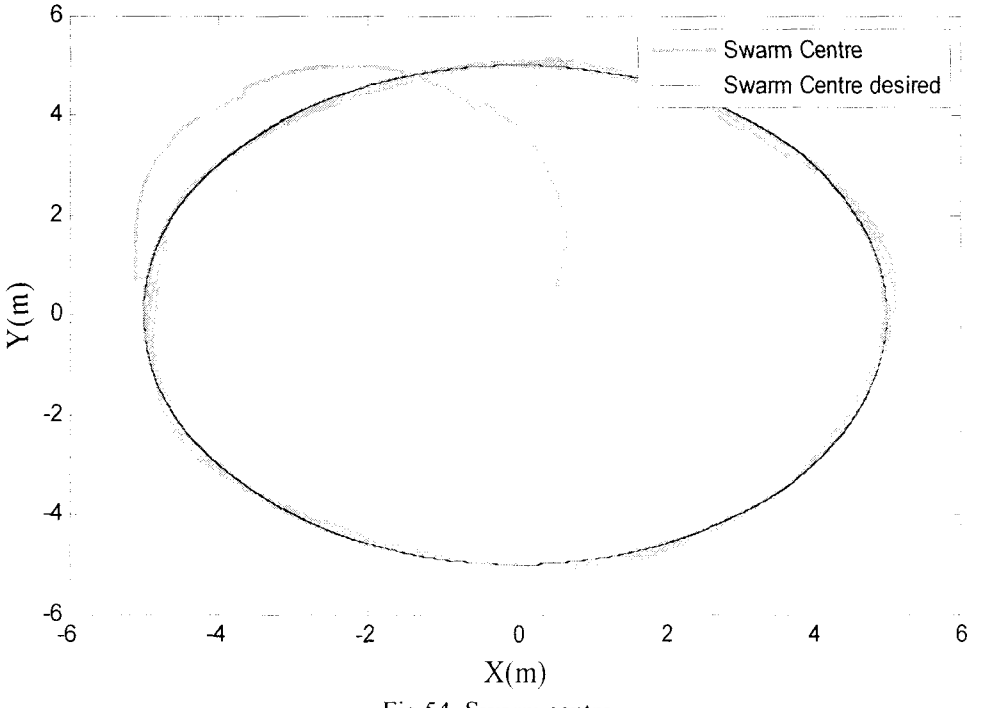

Fig.54. Swarm centre

Fig.55 shows the temperature regulation at the desired value. Since the WMRs' positions are updated, in this graph too, the effects of that are visible.

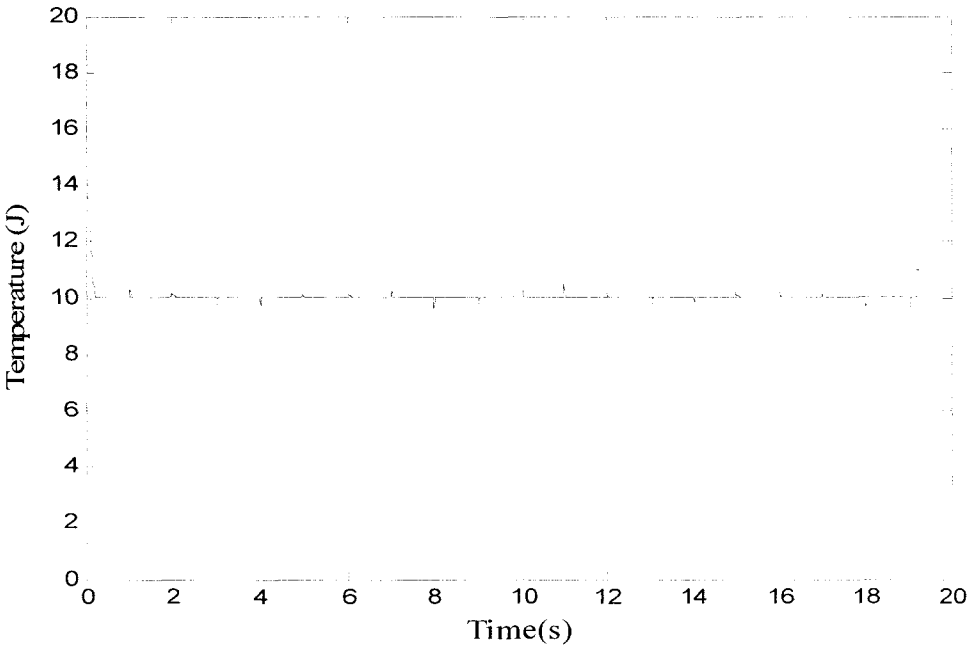

Fig.55. Temperature of the swarm

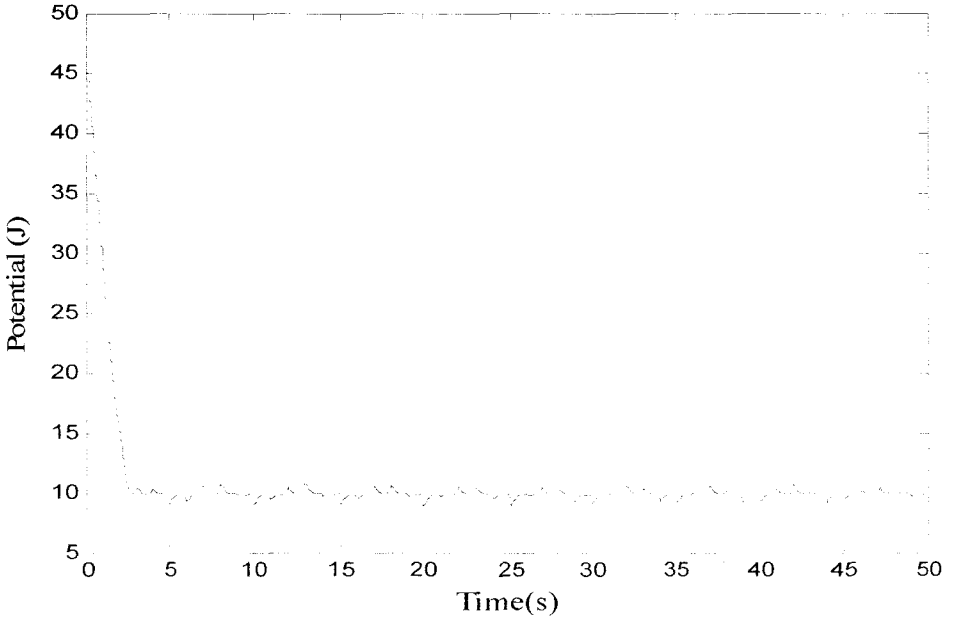

Fig.56. Potential of the swarm

Likewise Fig.56 shows the potential regulation and Fig.57 shows the corresponding swarm size.

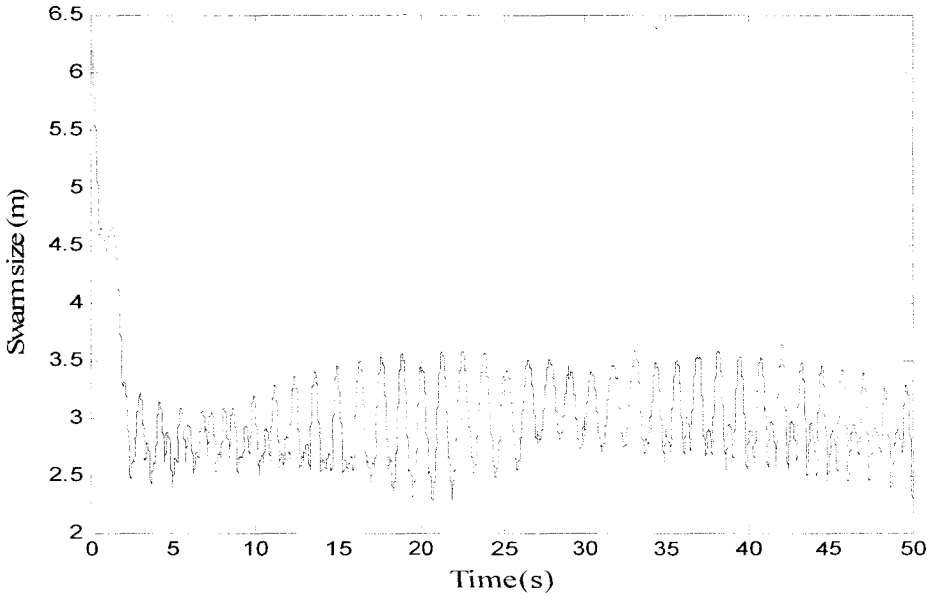

Fig.57. Swarm size

Fig.58 shows the one of the swarm members' high level control input. As mentioned, the saturation limits are set to $+/-50$ during the steady state condition.

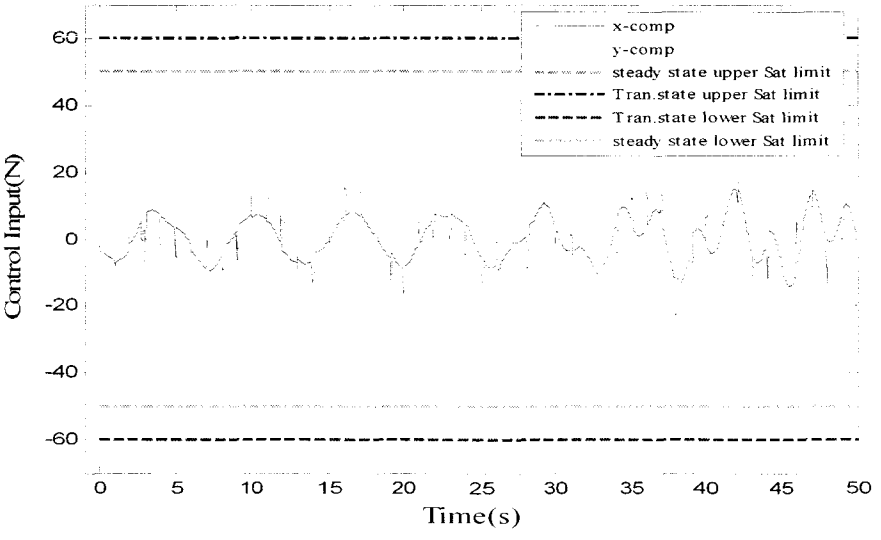

Fig.58. High level control input

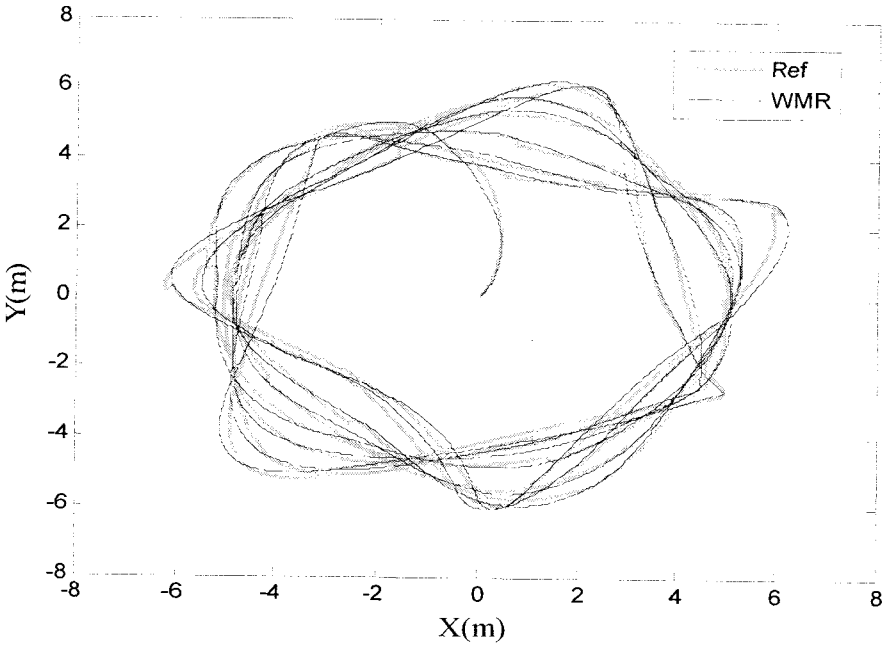

Fig.59. Trajectory followed by a WMR

In Fig.59 the trajectory followed by a WMR is shown and the corresponding tracking error of the trajectory is shown in Fig.60.

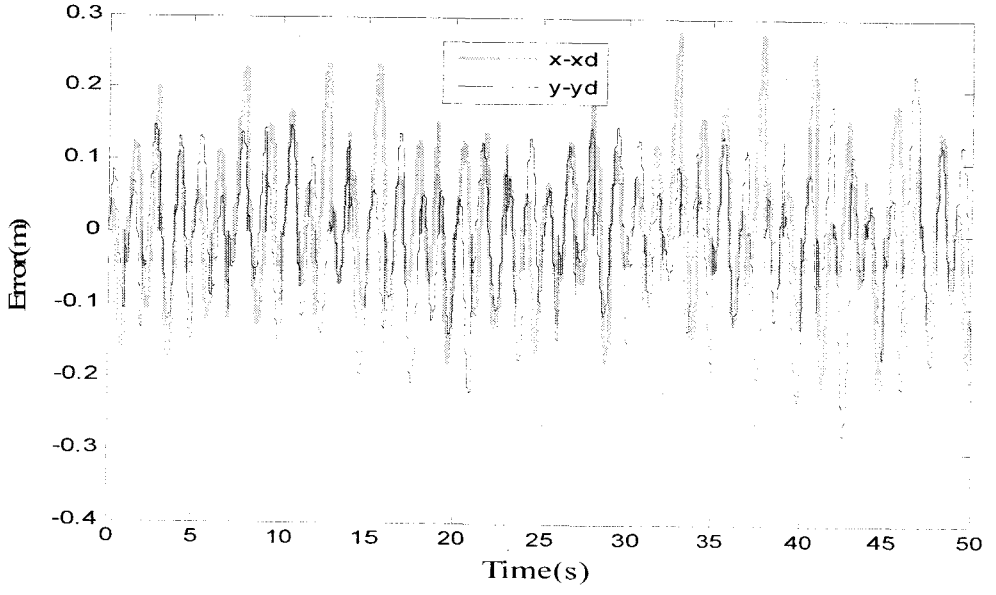

Fig.60. Error plot

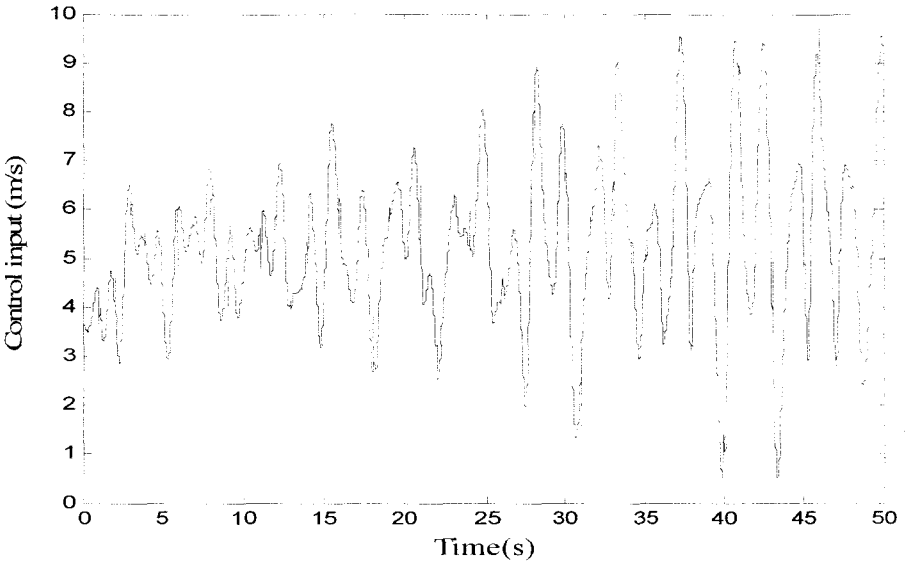

Fig.61. Low level control input

In Fig.61 and Fig.62 the corresponding low level control inputs are shown. Even though there are no saturation constraints directly set for the low level controller, it is obvious from the simulations that the bound on high level swarm controller generates bounded low level control inputs.

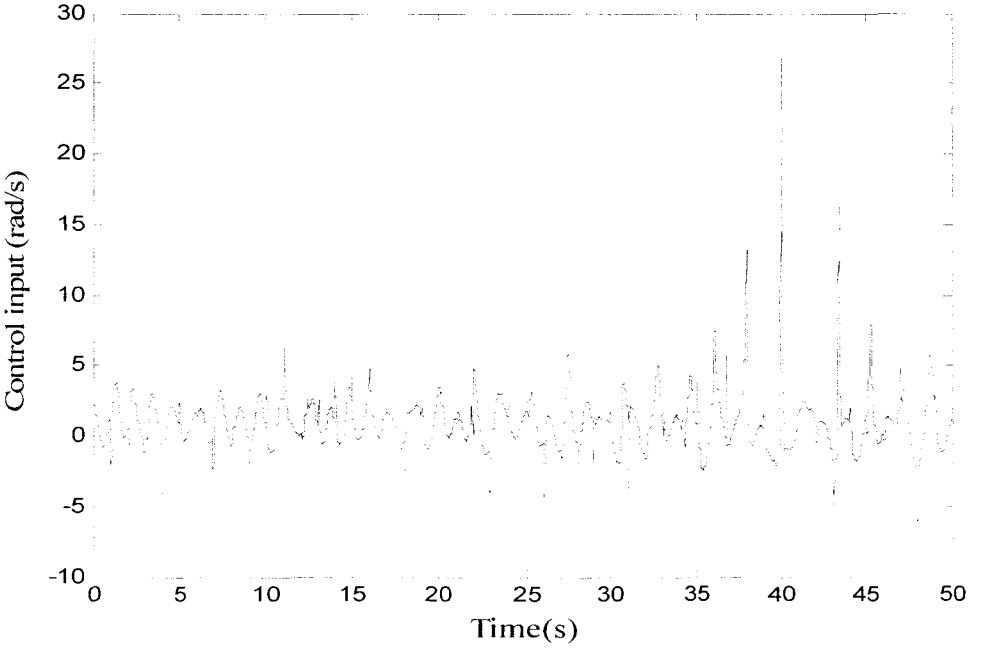

Fig.62. Low level control input

Fig.63 shows the trajectory tracking of another WMR.

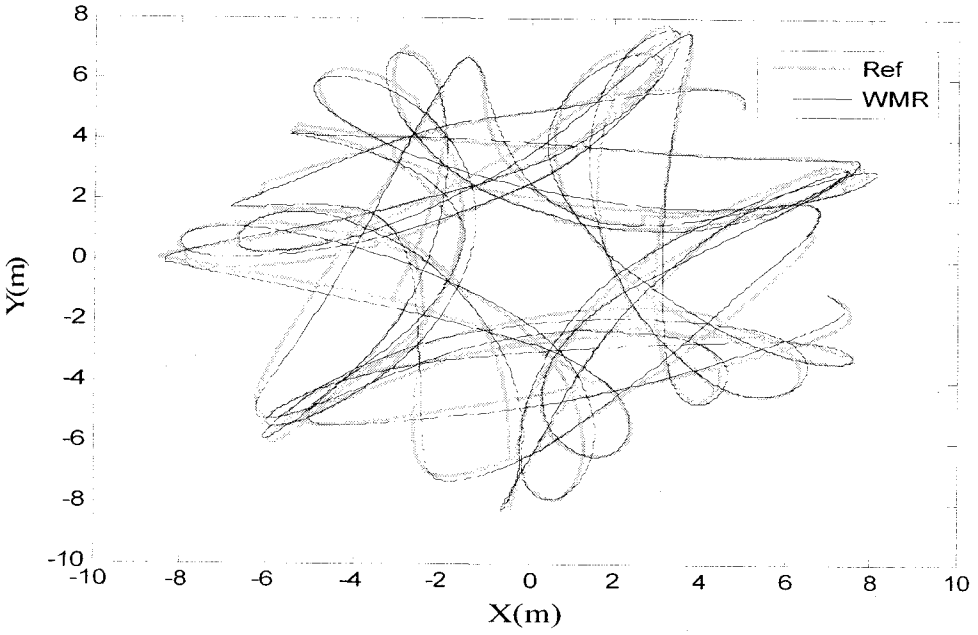

Fig.63. Trajectory followed by another WMR

Fig.64 shows the corresponding error plot of the tracking.

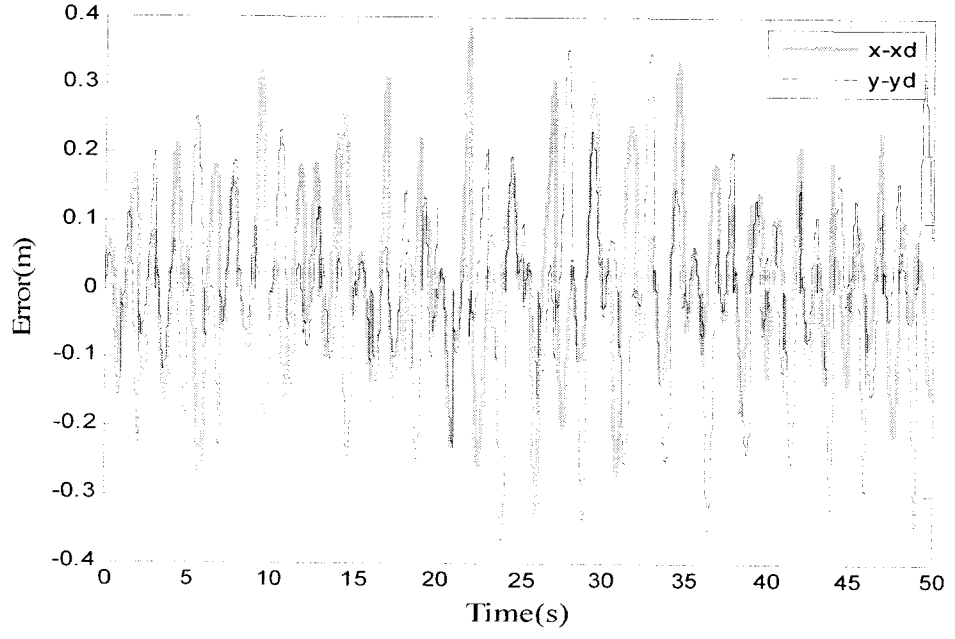

Fig.64. Error plot

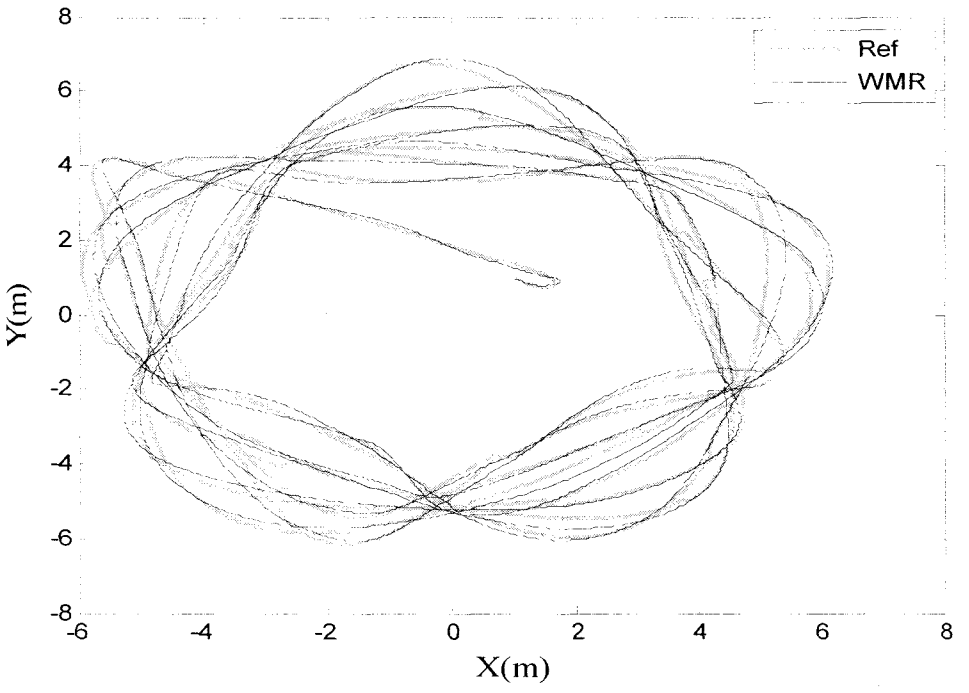

Fig.65. Trajectory followed by a WMR

Finally, Fig.65 shows the trajectory followed by another WMR in the swarm. The error between the desired trajectories and the trajectories followed by any WMR is reasonable one considering the kind of trajectories generated by the high level layer. These are online trajectories of highly chaotic type. There is no prior knowledge of these trajectories. The low level controller successfully follows the trajectories and enables the energetic swarm to be successfully applied to the WMRs.

6. Conclusion and Future Works

In this thesis, the energetic swarm control approach from [36]-[38] is explained and the proposed controllers in [48] are verified through numerous simulations of the high level swarm control system. The main contribution of this thesis is the application of energetic swarm control to WMRs using dynamic feedback linearization as a low level controller. Since the high level energetic swarm layer is a point mass dynamics, the high level inputs cannot be applied directly to the nonholonomic WMRs. Further, the implementation algorithm of the lower level layer enables better trajectory tracking performance while coping with disturbances and keeps the high level controller tracks the desired temperature and potential values.

Also, the saturation constraints on the high level controller are studied numerically for the steady state case. It is found that the pseudo inverse is not adequate enough to handle the control allocation to generate feasible high level control inputs through out the run time. The pseudo inverse is replaced with the SNOPT optimization solver and the actual high level swarm inputs are generated using SNOPT for the control allocation approach. Although SNOPT generates satisfactory high level inputs, there is a minimum allowable limit and below that SNOPT fails to match the virtual inputs. The minimum allowable limits are numerically calculated for the steady state case for a certain operating region. Generally, the minimum allowable limit is a nonlinear function which depends mainly on the temperature and potential values, and their derivatives w.r.t time.

Finally, the modeling parameters of the servo RC motor are identified using various simulations and experiments. RC servo motors are used on WMRs and it is

important to study the modeling parameters of the real actuators in order for the experimental implementation of the energetic swarm.

Future research focuses on modeling the high level swarm dynamics with 2D and 3D rigid body dynamics. It is important to get a mathematical equation that correlates the minimum allowable limits exactly for the steady state case and transient state case. Future research will also investigate the saturation effects on the lower level controller as well. Furthermore, the lower level controller will be expanded such that it is robust to noise and disturbances. Finally, the energetic swarm controller will be applied and tested on various types of vehicles such as hovercrafts, helicopters and robotic fish systems.

7. Reference

[1] V. Gazi and K. M. Passino, "Stability Analysis of Swarms," in *Proc. of the American Control Conference*, vol. 3, pp. 1813–1818, Anchorage, AK, May 2002.

[2] Y.Chen and Z.Wang, "Formation control: a review and a new consideration," *IEEE/RSJ International Conference on Intelligent Robots and Systems*, pp. 3181-3186, August 2005.

[3] V. Gazi and R. Ordóñez, "Target Tracking Using Artificial Potentials and Sliding Mode Control," in *Proc. of the American Control Conference*, vol.6 , pp. 5588-5593, Boston, MA, USA, June-July 2004.

[4] D. Jin and L.Gao, "Stability analysis of a double integrator swarm model related to position and velocity," *Transactions of the Institute of Measurement and Control*, vol. 30, no. 3-4 , pp. 275-293, August 2008.

[5] V. Gazi, "Swarm Aggregations Using Artificial Potentials and Sliding Mode Control," in *Proc. of the 42nd IEEE Conference on Decision and Control*, pp. 2041-2046, Maui, Hawaii, USA, December 2003.

[6] Y.Yang and Y. Tian, "Swarm robots aggregation formation control inspired by fish school," *IEEE International Conference on Robotics and Biomimetics*, pp.805-809, Sanya, China, December 2007.

[7] Z. Liu, R. Jing, X. Ding and J. Li, "Trajectory Tracking Control of Wheeled Mobile Robots Based on the Artificial Potential Field," *Fourth International Conference on Natural Computation*, vol.7, pp.382-387, October 2008.

[8] J. Guldner, V.I. Utkin, H. Hashimoto and F. Harashima, "Tracking gradients of artificial potential fields with non-holonomic mobile robots," in *Proc. of the American Control Conference*, vol.4, pp. 2803-2804, June 1995.

[9] J.Wang, "Multi-agent system tracking using sliding mode control combined with artificial potential," *Chinese Control and Decision Conference*, pp.614-619, June 2009.

[10] E. Rimon and D.E. Koditschek, "Exact robot navigation using artificial potential

functions," *IEEE Transactions on Robotics and Automation,* vol.8, no.5, pp. 501-518, October 1992.

[11] Y.Yongjie and Z.Yan, "Collision avoidance planning in multi-robot based on improved artificial potential field and rules," in *Proc. of the IEEE International Conference on Robotics and Biomimetics*, pp.1026-1031, Bangkok, Thailand, February 2009.

[12] J.Wang, X.Wu, Z.Xu, "Decentralized Formation Control and Obstacles Avoidance Based on Potential Field Method," in *Proc. of the* 5^{th} *International Conference on Machine Learning and Cybernetics*, pp.803-808, August 2006.

[13] V.I. Utkin, S.V. Drakunov, H. Hashimoto and F. Harashima, "Robot path obstacle avoidance control via sliding mode approach," *IEEE/RSJ International Workshop on Intelligent Robots and Systems*, pp.1287-1290, vol.3, November 1991.

[14] J. Guldner and V.I. Utkin, "Sliding mode control for an obstacle avoidance strategy based on an harmonic potential field," in *Proc. of the* 32^{nd} *IEEE Conference on Decision and Control*, pp. 424-429, vol.1, December 1993.

[15] W. Kowalczyk and K. Kozlowski, "Artificial potential based control for a large scale formation of mobile robots," in *Proc. of the Fourth International Workshop on Robot Motion and Control*, pp. 285-291, June 2004.

[16] C.M. Saaj, V. Lappas and V. Gazi, "Spacecraft Swarm Navigation and Control Using Artificial Potential Field and Sliding Mode Control," *IEEE International Conference on Industrial Technology*, pp.2646-2651, December 2006.

[17] H.G. Tanner, A. Jadbabaie, and G.J. Pappas, "Stable flocking of mobile agents, part I: fixed topology," in *Proc. of the 42nd IEEE Conference on Decision and Control*, vol.2, pp. 2010-2015, Maui, Hawaii, USA, December 2003.

[18] D.H. Kim, H.O. Wang, G.Ye, and S. Shin, "Decentralized control of autonomous swarm systems using artificial potential functions: analytical design guidelines," in *Proc. of the 43rd IEEE Conference on Decision and Control*, vol.1, pp. 159-164 , Atlantis, Paradise island, Bahamas, December 2004.

[19] M.C. Lee; M.G. Park, "Artificial potential field based path planning for mobile robots using a virtual obstacle concept," in *Proc. of the IEEE/ASME International Conference on Advanced Intelligent Mechatronics*, pp. 735-740, vol.2, July 2003.

[20] Y. Liu, K.M. Passino, and M. Polycarpou, "Stability analysis of one-dimensional asynchronous mobile swarms," in *Proc. of the 40th IEEE Conference on Decision and Control*, vol.2, pp.1077-1082, Orlando, Florida, USA, December 2001.

[21] V. Gazi and K. M. Passino, "A Class of Attraction/Repulsion Functions for Stable Swarm Aggregations," in *Proc. of the 41st IEEE Conference on Decision and Control*, pp. 2842-2847, Las Vegas, Nevada, USA, December 2002.

[22] S.W. Ekanayake and P.N. Pathirana, "Formations of Robotic Swarm: An Artificial Force Based Approach," *International Journal of Advanced Robotic Systems*, vol. 6, no.1, pp. 7-24, March 2009.

[23] S.W. Ekanayake and P.N. Pathirana, "Artificial Formation Forces for Stable Aggregation of Multi-Agent System," *International Conference on Information and Automation*, pp.129-134, December 2006.

[24] L. Barnes, W. Alvis, M.A. Fields, K. Valavanis, and W. Moreno, "Heterogeneous Swarm Formation Control Using Bivariate Normal Functions to Generate Potential Fields," in *Proc. of the IEEE Workshop on Distributed Intelligent Systems: Collective Intelligence and Its Applications*, pp. 85-94, June 2006.

[25] J.P.Desai, J.P. Ostrowski and V. Kumar, "Modeling and control of formations of nonholonomic mobile robots," *IEEE Transactions on Robotics and Automation*, vol.17, no.6, pp.905-908, December 2001.

[26] J.P. Desai, J. Ostrowski and V. Kumar, "Controlling formations of multiple mobile robots," in *Proc. of the IEEE International Conference on Robotics and Automation*, vol.4, pp.2864-2869, May 1998.

[27] J.R.T. Lawton, R.W. Beard and B.J. Young, "A decentralized approach to formation maneuvers," *IEEE Transactions on Robotics and Automation*, vol.19, no.6, pp. 933-941, December 2003.

[28] T. Balch and R.C. Arkin, "Behavior-based formation control for multirobot teams," *IEEE Transactions on Robotics and Automation*, vol.14, no.6, pp.926-939, December 1998.

[29] L. Chaimowicz, N. Michael, and V. Kumar, "Controlling Swarms of Robots Using Interpolated Implicit Functions," in *Proc. of the IEEE International Conference on Robotics and Automation*, pp. 2487-2492, Barcelona, Spain, April

2005.

[30] L. Barnes, M.A. Fields, and K. Valavanis, "Unmanned ground vehicle swarm formation control using potential fields," *Mediterranean Conference on Control & Automation*, pp.1-8, Athens, Greece, June 2007.

[31] J. Yao, R. Ordonez, and V. Gazi, "Swarm Tracking Using Artificial Potentials and Sliding Mode Control," in *Proc. of the Conference on Decision and Control*, pp. 4670-4675, San Diego, CA, USA, December 2006.

[32] M.I. Koksal, V. Gazi, B. Fidan, and R. Ordonez, "Tracking a maneuvering target with a non-holonomic agent using artificial potentials and sliding mode control," *Mediterranean Conference on Control and Automation*, pp. 1174-1179, June 2008.

[33] V. Gazi and K. M. Passino, "Stability Analysis of Swarms in an Environment with an Attraction/Repulsion Profile," in *Proc. of the American Control Conference*, pp. 1819-1824, Anchorage, AL, May 2002.

[34] V. Gazi and K. M. Passino, "Stability Analysis of Social Foraging Swarms: Combined Effects of Attractant/Repellent Profiles," in *Proc. of the 41st IEEE Conference on Decision and Control*, pp. 2848-2853, Las Vegas, Nevada, USA, December 2002.

[35] H. Hashimoto, S. Aso, S. Yokota, A. Sasaki, Y. Ohyama, and H. Kobayashi, "Cooperative movement of human and swarm robot maintaining stability of swarm," in *Proc. of the 17th IEEE International Symposium on Robot and Human Interactive Communication*, pp. 249-254, Munich, Germany, August 2008.

[36] R. Pedrami and B.W. Gordon, "Control and cohesion of energetic swarms," in *Proc. of the American Control Conference*, pp.129-134, Washington, USA, June 2008.

[37] R. Pedrami and B.W. Gordon, "Control and Analysis of Energetic Swarm Systems," in *Proc. of the American Control Conference*, pp.1894-1899, New York, USA, July 2007.

[38] R. Pedrami and B.W. Gordon, "Temperature Control of Energetic Swarms," *International Conference on Mechatronics and Automation*, pp. 2639-2644, Harbin, China, August 2007.

[39] H. Hashimoto, S. Aso, S. Yokota, A. Sasaki, Y. Ohyama, and H. Kobayashi, "Stability of swarm robot based on local forces of local swarms," *SICE Annual Conference*, pp.1254-1257, August 2008.

[40] N. Michael, C. Belta, and V. Kumar, "Controlling three dimensional swarms of robots," in *Proc. of the IEEE International Conference on Robotics and Automation*, pp. 964-969, Orlando, Florida, USA, May 2006.

[41] V. Gazi, B. Fidan, Y. S. Hanay and M. İ. Köksal, "Aggregation, Foraging, and Formation Control of Swarms with Non-Holonomic Agents Using Potential Functions and Sliding Mode Techniques," Turkish Journal of Electrical Engineering and Computer Sciences (ELEKTRIK), vol. 15, no. 2, pp. 149-168, July 2007.

[42] http://hyperphysics.phy-astr.gsu.edu/hbase/thermo/inteng.html

[43] http://en.wikipedia.org/wiki/Maxwell%E2%80%93Boltzmann_distribution

[44] R. Pedrami and B.W. Gordon, "Control of energetic robotic swarm systems," in *Proc. of the IEEE International Conference on Robotics and Biomimetics*, pp.547-552, Sanya, China, December 2007.

[45] G. Oriolo, A. De Luca, and M. Vendittelli, "WMR control via dynamic feedback linearization: design, implementation and experimental validation," *IEEE Trans. Control Systems Technology*, vol. 10, no. 6, pp.835–852, November 2002.

[46] A. Regmi, R. Sandoval, R. Byrne, H. Tanner, and C. T. Abdallah, "Experimental Implementation of Flocking Algorithms in Wheeled Mobile Robots," in *Proc. of the American Control Conference*, vol. 7, pp.4917-4922, June 2005.

[47] J. Wang and R.G. Longoria, "Coordinated vehicle dynamics control with control distribution," in *Proc. of the American Control Conference*, pp. 5348-5353, Minneapolis, Minnesota, USA, June 2006.

[48] R. Pedrami and B.W. Gordon, "Control allocation for energetic swarms," CIS Technical Report, Concordia University, Montreal, QC, 2008.

[49] S. E. Gill, W. Murray, and M. A. Saunders, "User's Guide for SNOPT Version 7: Software for Large-Scale Nonlinear Programming".

[50] R.M. Murray and S.S. Sastry, "Nonholonomic motion planning: steering using sinusoids," *IEEE Transactions on Automatic Control*, vol.38, no.5, pp.700-716,

May 1993.

[51] D.H. Kim and J.H. Oh, "Tracking control of a two-wheeled mobile robot using input-output linearization," *Control Engineering Practice*, vol. 7, no. 3, pp. 369-373, March 1999.

[52] J.J.E. Slotine and W.Li, *Applied Nonlinear Control*. NJ: Prentice Hall, 1990, pp. 207-275.

[53] M.W. Oppenheimer, D.B. Doman and M.A. Bolender, "Control allocation for over-actuated Systems," *14th Mediterranean Conference on Control and Automation*, pp. 1-6, June 2006.

[54] Y. Zhao, "Decentralized Receding Horizon Control with Application to Multiple Vehicle Systems," M.A.Sc thesis, Dept. Mech. & Ind. Eng., Concordia University, Montreal, Canada, August 2008.

[55] R. Pedrami, S. Wijenddra, J. Baxter and B.W. Gordon, "A control allocation approach for energetic swarm control," in *Proc. of the American Control Conference*, pp.5079-5084, St.Louis, USA, June 2009.

[56] R. Pedrami, W. Sivaram, J. Baxter and B.W. Gordon, "A control allocation approach for energetic swarm control of wheeled mobile robots," in *Proc. of the IEEE International Conference on Robotics and Biomimetics*, pp.1924-1931, February 2009.